



Bio-Engineered Gas Diffusion Electrodes (GDEs) for Proton Exchange Membrane Fuel Cells (PEMFCs)

James Matthew Courtney

A Thesis submitted to The University of Birmingham for
the degree of

Master of Research (MRes)

The Centre for Hydrogen and Fuel Cell Research

PEM Fuel Cell Research group

School of Chemical Engineering

College of Engineering & Physical Sciences

The University of Birmingham

UNIVERSITY OF
BIRMINGHAM

University of Birmingham Research Archive

e-theses repository

This unpublished thesis/dissertation is copyright of the author and/or third parties. The intellectual property rights of the author or third parties in respect of this work are as defined by The Copyright Designs and Patents Act 1988 or as modified by any successor legislation.

Any use made of information contained in this thesis/dissertation must be in accordance with that legislation and must be properly acknowledged. Further distribution or reproduction in any format is prohibited without the permission of the copyright holder.

Abstract

The current cost and finite nature of Platinum Group Metals (PGM) is a barrier to the successful commercialisation of Proton Exchange Membrane Fuel Cells (PEMFCs). Successful mass production of fuel cell components combined with the recovery of PGMs from waste, more efficient PGM use or the replacement of PGMs catalyst is necessary to reduce costs per unit.

Current hydrometallurgy and pyrometallurgy techniques do not provide a 'clean' or economically viable solution to PGM recovery when compared to bio-hydrometallurgy. Bio-catalysts can be manufactured by coupling the oxidation of hydrogen to the reduction of soluble metallic species [e.g. Pd(II), Pt(IV)] *via* Hydrogenase enzymes.

The work presented in this thesis aims to evaluate the incorporation of biohydrometallurgy in producing Gas Diffusion Electrodes (GDEs) for PEM Fuel cell applications. The biomineralisation and subsequent catalytic activity of spin coated engineered biofilms is investigated, as is the use of planktonic cell generated bio-catalysts in traditional GDE fabrication via screen printing.

Although biofilms were found to produce layers containing active PGM particles, the films proved to be nonconductive. As such, it was concluded that although biofilms provide huge potential in the recovery and subsequent use of PGM catalysts, at present, they are unsuitable for Fuel Cell use.

Acknowledgements

The author would like to thank and acknowledge all those who have supported and aided him throughout the MRes course and in completing this thesis. In particular, the author wishes to thank his supervisors Dr Andreas N. Tsoligkas and Dr Bruno G. Pollet of the PEMFC Research group for their continued advice, patience and guidance. He would also like to thank the academic staff, who have contributed greatly during this period, Dr Richard Greenwood, John Hooper MBA, Dr Aman Dhir, Professor Kevin Kendall, Dr Waldemar Bujalski, Dr Rob Hudson, Dr Kevin Deplanche, Professor Lynne Macaskie and many others who have offered help, direction and support.

The author would also like to acknowledge the members of the Centre for Hydrogen and Fuel Cell Research, the Doctoral Training Centre for Hydrogen and Fuel Cells and Advantage West Midlands. He also wishes to thank and acknowledge the following persons for their friendship, discussion and sheer patience which often cleared the path ahead, Tony Meadowcroft, Daniel Symes, Martin Riley, Katie Howe, Tom Pike and Micaela Winter.

The author also gratefully acknowledges the assistance and expertise of the mechanical workshops and the Unit for Functional Bionanomaterials. Finally, he would like to deeply thank his parents and family without whose support he would never have been able to undertake this MRes.

Contents

Table of Contents

Chapter 1 - Introduction.....	1
1.1 Background and Motivation	1
1.2 Aims and Objectives of this Thesis	10
1.3 Thesis Layout.....	11
1.4 Publications (available upon request)	12
1.4.1 Conference Papers, Presentations and Awards.	12
Chapter 2 - Literature review	15
2.1 Chemistry of Proton Exchange Membrane Fuel Cells(PEMFCs)	15
2.2 Current PEM Fuel Cell Design	16
2.3 Catalyst Layers in PEM Fuel Cells	18
2.4 GDE Fabrication Techniques	19
2.5 PGM Production	21
2.6 PGM Recovery.....	22
2.6.1 Pyrometallurgy	22
2.6.2 Hydrometallurgy.....	23
2.7 Bio-hydrometallurgy.....	23

2.8 Use of PGM Bio-Catalysts	25
2.9 Biofilm Formation.....	26
Chapter 3 - Experimental Methods and Materials	29
3.1 Fabrication and Synthesis	29
3.1.1 Biomass Culture.....	29
3.1.2 Biofilm Growth	29
3.2 Biomineralisation	30
3.2.1 Platinum Mineralisation.....	30
3.2.2 Palladium Mineralisation	31
3.3 Recapture of metallic particles ³¹	32
3.4 Supporting Metal catalysts	33
3.5 Ink Formulations (for screen printing).....	33
3.5.1 Commercial catalyst.....	33
3.5.2 Biocatalyst	34
3.5.3 'Mock' Ink.....	34
3.6 Screen printing.....	34
3.7 Analysis.....	35
3.7.1 Assay of Metal content (Pd(II) and Pt(IV)).....	35
3.7.2 SEM	36
3.7.3 STEM	37
3.7.4 Catalytic activity and durability testing.....	37

3.7.5 Conductivity	38
3.7.6 Single cell Electrochemical Evaluation	39
3.7.6.1 Fabrication of test MEA	39
3.7.6.2 Single Test cell set up	39
3.7.6.3 Experimental running	39
Chapter 4 - Biofilm and planktonic cell Metallisation and Reactions	41
4.1 Biomineralisation of Spin Coated Biofilms.....	41
4.2 "Pre-treated" biofilm biomineralisation.	43
4.3 Platinum deposition	48
Chapter 5 - Suitability for Fuel Cell Use.....	51
5.1 Conductivity Experiments.....	51
5.2 Carbon Additives	54
Chapter 6 - Catalytic Activity Testing	58
6.1 Hydrogenation of Dimethyl Itaconate.....	58
6.2 Degradation Characterisation.....	62
Chapter 7 - Screen Printed Bio-Catalyst GDEs for PEM Fuel Cell Use	65
7.2 Commercial Catalyst Screen Printed GDE.....	67
7.3 Bio-Catalyst Screen Printed GDEs	69
7.4 GDE Testing.....	72
Chapter 8 – Conclusion and Further Work.....	75
References.....	Error! Bookmark not defined.

Chapter 10 – Appendix.....	86
10.1 – Supplementary images to Chapter 1	86
10.1.1 – Supplementary images to Chapter 1.4.1	86
10.2 Supplementary Images to Chapter 2	89
10.2.1 Supplementary images to section 2.2 Current PEM Fuel Cell Design.....	89
10.2.2 – Supplementary images to section 2.4 GDE Fabrication Techniques.....	90
10.3 – Supplementary images and tables to chapter 3.....	91
10.3.1 Supplementary images and tables to section 3.6.....	91
10.3.2 – Supplementary images to section 3.7.6.2	93
10.4 Supplementary Images and Tables to Chapter 6	93
10.4.1 Supplementary Images and Tables to Section 6.1.....	93

List of Figures

Figure 1 - Table of the different types of Fuel Cell.	2
Figure 2 - The Allis-Chalmers Fuel cell Tractor circa 1959.....	3
Figure 3 - Current hydrogen demonstration infrastructure.	4
Figure 4 - Cost of hydrogen infrastructure per vehicle (U.S. model)	5
Figure 5 - Running Cost summary, normalised to $\$GJ^{-1}$	5
Figure 6 - Cost breakdown of a 80kw PEMFC unit.....	6
Figure 7 - DoE Fuel Cell price/kW targets.....	7
Figure 8 - Platinum prices since 1992 (per troy ounce).	7
Figure 9 - The HOR reaction and the ORR reaction.	15
Figure 10 - Exploded PEMFC diagram..	17
Figure 11 - Hydrogenation of dimethyl itaconate.	26
Figure 12- ESEM image of a spin-coated biofilm highlighting flow channels.....	27
Figure 13 - Five stages of biofilm growth.	28
Figure 14 - ESEM image of Spin Coated Biofilm.	42
Figure 15 - A. BSE ESEM image of 5% Pd Biofilm, B. ESEM image of the same 5% Pd Biofilm.....	42
Figure 16 - ESEM image of a 5% Pd Biofilm.....	43
Figure 17 - A. BSE image of 5%w/v Pd biofilm showing Pd particles deposited on cells surface, B. BSE image of 5%w/v Pd Biofilm	44
Figure 18 - A. BSE STEM image of 5%w/v Pd biofilm, B. STEM image of 5w/v Pd biofilm.....	45
Figure 19 - EDX spectrum of 5% Pd biofilm.....	45
Figure 20 - BSE ESEM image of 5% Pd planktonic cell bacteria..	46
Figure 21 - A. BSE STEM image of 5%w/v Pd Planktonic cell bacteria, B. STEM image of 5w/v Pd Planktonic cell Bacteria.	47
Figure 22 - Hydrogenase reduction mechanism.....	47
Figure 23 - A. BSE ESEM image of 5%w/v Pt biofilm, B. ESEM image of 5w/v Pt biofilm..	48
Figure 24 - A. BSE ESEM image of 5%w/v Pt biofilm, B. BSE ESEM image of 5%w/v Pt biofilm..	49
Figure 25 - ESEM image of 5% Pt biofilm.	49
Figure 26 - EDX of 5% w/v Pt biofilm.	50
Figure 27 - Diagram of PEM Fuel cell, its components, exploded diagram of catalyst layer, its constituent parts and schematic of the HOR and ORR.	51
Figure 28 - Conductivity measurements of 10% Pt Biofilm.....	52
Figure 29 - Conductivity I/V plot of Pt Biofilms and carbonated Pt biofilms.....	53
Figure 30 – I/V curves for prepared Activated Carbon slide (Vulcan Xc-72) and Toray Paper.	53
Figure 31 - A. ESEM BSE image of 25% w/v Pt carbonated Biofilm, B. Colourised ESEM BSE image of 25%w/v Pt Biofilm.....	54
Figure 32 - A. ESEM BSE image of 25%w/v Pt carbonated Biofilm, B. Colourised ESEM BSE image of 25%w/v Pt Biofilm.....	55
Figure 33 - Resistance Vs Distance plot for Pt Biofilms and Carbonated Pt Biofilms.....	56

Figure 34 - Conversion Vs Time for planktonic cell and Biofilm Bio-Pd catalysts for the Hydrogenation of Dimethyl Itaconate.	59
Figure 35 - Conversion Vs Time for Repeated Reactions for the hydrogenation of Dimethyl Itaconate catalysed by biofilm Bio-Pd catalyst.	60
Figure 36 - Conversion Vs Time for repeated reaction for the hydrogenation of dimethyl itaconate catalysed by planktonic cell bio-Pd catalyst.	61
Figure 37 - Mass of Planktonic supported Biocatalyst Vs No. of repeated reactions.....	62
Figure 38 - ESEM of 5%w/v Biofilm after catalytic cycling.	63
Figure 39 - ESEM BSE image of 5%w/v Pd Biofilm after catalytic cycling.	63
Figure 40 - Concentration of Mock ink Vs mass deposited per centimetre.....	66
Figure 41 - ESEM image of cut commercial catalyst GDE.....	67
Figure 42 - BSE ESEM image of commercial catalyst GDE showing dispersion of Pt particles across catalyst layer surface.	68
Figure 43 - ESEM image of commercial catalyst GDE catalyst layer surface.....	68
Figure 44 BSE ESEM image of a cut Bio-Pd GDE..	69
Figure 45 - BSE ESEM image of bio-Pd GDE showing the even distribution of Pd nanoparticles.....	70
Figure 46 - ESEM image of bio-Pd GDE showing surface of catalyst layer.....	71
Figure 47 - I/V curve and Power curve for screen printed commercial catalyst GDE.....	72
Figure 48 - I/V curve and power curve for commercially obtained GDE.	73
Figure 49 - I/V curve and power curve for screen printed commercial catalyst GDE repeat 2.	74
Figure 50 - Poster presented at the 1st International Fuel Cell Seminar, Yamanashi, Japan, 2010. Courtney, J., Tsoligkas, A.N., Deplanche, K., Macaskie, L.E., 2010	87
Figure 51 - James Courtney receiving poster presentation award at the 1st international Fuel Cell summer seminar, Japan, 2010.....	88
Figure 52 - Presented Poster at the 6th Annual International Conference and Exhibition, Hydrogen & Fuel Cell for Clean Cities.....	88
Figure 53 - Alan Johnson MP, Lab tour, 2009.....	89
Figure 54 - Example PEMFC design.....	89
Figure 55 - Image of painting method for fabrication of GDEs.	90
Figure 56 - Image of the introduction of ink to the screen printer for the fabrication of a GDE.	90
Figure 57 - Table of GDL details.....	91
Figure 58 - Image of Dek 258 screen printer.....	92
Figure 59 - Image of deposited ink within screen printer.	92
Figure 60 - Paxitech FCT - 50s Test station.....	93
Figure 61 - Table of planktonic cell catalyst mass loss during repeated reactions.....	94

Nomenclature and Abbreviations

A – Cross sectional area (m^2)

AFC – Alkaline Fuel Cell

BSE – Back Scattered Electron

CCM – Catalyst Coated Membrane

CCS – Catalyst Coated Substrate

CL – Catalyst Layer

DECC – Department of Energy and Climate Change

DMFC – Direct Methanol Fuel Cell

DoE – Department of Energy

ESEM – Environmental Scanning Electron Microscopy

ETF – Exchange Traded Fund

FFP – Flow Field Plates

GDE – Gas Diffusion Electrode

HOR – Hydrogen Oxidation reaction

I – Current (A)

IAHE – International Association of Hydrogen Energy

kW – Kilowatt

LPG – Liquid Petroleum Gas

MCFC – Molten Carbonate Fuel Cell

MEA – Membrane Electrode Assembly

OFN – Oxygen Free Nitrogen

OPEC – Organisation of the Petroleum Exporting Countries

ORR – Oxygen Reduction Reaction

PAFC – Phosphoric Acid Fuel Cell

PEM – Proton Exchange Membrane

PEMFC – Proton Exchange Membrane Fuel Cell

PGM – Platinum Group Metal

R – Resistance (Ω)

RPM – Revolution per Minute

SCEB – Spin Coated Engineered Biofilms

SEM – Scanning Electron Microscopy

SOFC – Solid Oxide Fuel cell

SX – Solvent Extraction

ρ – Resistivity ($\Omega.m$)

σ – Conductivity ($S.m^{-1}$)

Chapter 1 - Introduction

1.1 Background and Motivation

The popularised view of the Hydrogen Economy was first proposed by Bockris in 1970^{1,2} and several other notable scientists such as Jones.³ It was a proposal written in response to the decreasing price of liquid hydrogen compared to the increasing price of gasoline. Their argument was strengthened by the 1973 OPEC Oil embargo² and the subsequent supply shock leading to the drive for alternative fuels. This eventually resulted in the formation of the International Association for Hydrogen Energy (IAHE, 1974) and the U.S. Department of Energy (DoE, 1977)².

The Hydrogen Economy can be split into several key areas due to the fact that hydrogen is not an energy source but rather an energy carrier⁴⁻⁶. This highlights the processing steps of energy generation, conversion to hydrogen, storage and transportation of hydrogen and conversion of hydrogen to energy.

Fuel cell technology is touted as a highly efficient method to convert hydrogen into usable energy, principally as electricity but in some combined heat and power (CHP) units both heat and power can be generated.⁷ There are several distinctive types of fuel cell, each with specific advantages and disadvantages (as shown in Figure 1).⁸ It can be seen in Figure 1 that PEMFCs are suited for the transport sector. The Department of Energy and Climate Change (DECC) for the U.K. states that 35% of the total energy consumed in the U.K. is used for transport.⁹ PEMFCs could potentially provide a solution to reducing the CO₂ emissions and dependency on oil of the transport sector.

	Low-temperature Fuel Cells			High-temperature Fuel Cells		
	DMFC Direct methanol fuel cell	PEMFC Proton exchange	AFC Alkaline fuel cell	PAFC Phosphoric acid fuel cell	MCFC Molten carbon fuel	SOFC Solid oxide fuel
Electrolyte	Proton-conducting membrane	Proton-conducting membrane	Caustic potash solution	Concentrated phosphoric acid	Molten carbonate	Ceramic
Temperature range	< 100° C	< 100° C	< 100° C	~ 200° C	~ 650° C	800 - 1,000
Fuel	Methanol	Hydrogen	Hydrogen	Hydrogen	Natural gas, coal	Natural gas, coal
Power ranges	Watts/ kilowatts	Watts/ kilowatts	Watts/ kilowatts	Kilowatt	Kilowatts/ megawatts	Kilowatts/ megawatts
Application areas (examples)	Vehicles, small appliances	Vehicles, small generators, domestic supply, block-type heat and power stations	Space	Block-type heat and power stations	Power plants, combined heat and power	Power plants, combined heat and power

Figure 1 - Table of the different types of Fuel Cell.⁸

The first fuel cell was conceived by Swiss chemist Christian Friedrich Schoebein in 1839 and shown on a practical scale by Sir William Grove in 1845^{2,10} naming his demonstration the 'gas battery'. During the 19th century fuel cells remained a scientific curiosity and it was the work conducted by the Royal Navy in the early 20th century that first saw the feasibility of fuel cells for energy conversion. Sir Francis Bacon provided the first significant energy production using fuel cells in 1959, developing a 5 kW unit. Three months later the 'Bacon cell' design was implemented in a tractor by Harry Karl Ihrig, an Allis-Chalmers company engineer (Figure 2).^{2,11}



Figure 2 - The Allis-Chalmers Fuel cell Tractor circa 1959.¹²

However, due to cost and impracticality issues, the technology failed to reach the general public and was only used in the space program by NASA. The technology was dormant to the public interest until the 1970s when the oil crisis highlighted the need for non-oil related energy generation leading to the proposal of the Hydrogen Economy. However, the oil crisis eased, the price of oil reduced and interest waned until the 1990s. During this period environmental issues took a political and cultural significance and as such non-CO₂ producing and more 'environmentally friendly' technologies saw a revival.

Despite the recent interest, not only from the scientific communities but the wider public, there are currently three major obstacles to the success of the Hydrogen Economy:

- Cost and finite nature of natural PGM resources
- Infrastructure
- Public perception

The primary hurdle to the Hydrogen Economy and the deployment of fuel cell technologies use is the high cost.¹³ However, it is worth noting that, without the bridging of both infrastructure and public perception, fuel cell technology will not achieve its full commercial potential. Developing a hydrogen

infrastructure provides a 'chicken and egg' situation, between the supply of hydrogen and the demand for hydrogen. Commercial and governmental incentives are required so that the construction of a hydrogen infrastructure becomes financially viable and develops further than the current demonstration infrastructure (shown in Figure 3). Furthermore, the cost of implementing a European wide hydrogen infrastructure, although significant, is relatively minor compared to its potential impact. With a predicted cost of around 3.5 billion Euros,¹⁴ if compared to the fibre optic broadband infrastructure (estimated to cost £30 billion),¹⁵ the capital cost is not the significant barrier to implementation; more the need for an associated demand for service which must be demonstrated.



Figure 3 - Current hydrogen demonstration infrastructure.¹⁶

The issue of public perception is one of the primary barriers that will need to be overcome. The widely publicised tragedy of the 'Hindenburg' disaster and the Hydrogen Bomb are responsible for a built up perception of danger around all technologies associated with hydrogen. Although the risks associated with hydrogen must not be unduly dismissed, it is not a newly used substance and significant understanding in safety and good practice has already been developed in the food and

space industries. Combining experience with good engineering and practical safety assessments, the risk in certain situations can be compared to current technologies.^{17,18}

The current cost of fuel cell generated power, at present cannot justify the move to a Hydrogen Economy (Figure 4 and Figure 5), even when considering the environmental benefits (e.g. lower CO₂ emissions) and potential localised advantages such as air quality.¹⁹ This is primarily due to the cost when compared to other fuels such as LPG (Liquid Petroleum Gas) (Figure 4) or gasoline (Figure 5). It is also the case that localised issues such as the price of hydrogen and feedback tariffs greatly affect the cost-efficiency of fuel cell systems.²⁰ Instead more work needs to be conducted to reduce the overall unit cost until the product is ready for the market so that any false expectations could be avoided.

Infrastructure costs normalized on a vehicle and kW basis

Alternative fuel	Total infrastructure cost (\$)	Infrastructure cost/vehicle (25 million vehicles) (\$)	Infrastructure cost/kW (40-kW _e powerplant) (\$)
Compressed natural gas	50 billion	2000	50
Methanol	65 billion	2600	65
Hydrogen	95 billion	3800	95

Figure 4 - Cost of hydrogen infrastructure per vehicle (U.S. model)²¹

Fuel cost	2010 (GJ ⁻¹)	2030 Optimistic (GJ ⁻¹)	2030 Pessimistic (GJ ⁻¹)	2030 Average (GJ ⁻¹)	Miles (GJ ⁻¹)	Typical units
Gasoline	\$12.7	\$19	\$38	\$28.5	253	40 mpg
Hydrogen	\$42	\$14	\$56	\$35	506	72 mile kg ⁻¹
Electric	\$36	\$27	\$45	\$36	1013	3.6 miles kWh ⁻¹

Figure 5 - Running Cost summary, normalised to \$GJ⁻¹.²²

There are several main areas that could lead to the reduction in cost of a fuel cell, especially a PEMFC unit. It is not only the cost of the catalyst which is a key area to reducing the overall cost but there are other components of the fuel cell that can be researched/developed to reduce cost. As shown in Figure 6, there are several components used within the PEMFC stack that can be either removed or re-engineered to reduce cost. For example the pressure plates and the bipolar plates (BPPs) could theoretically be altered to reduce the cost.²³

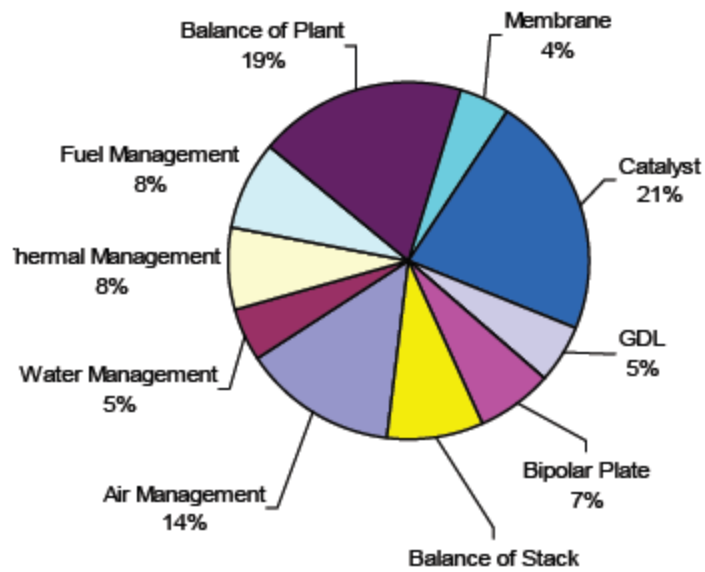


Figure 6 - Cost breakdown of a 80kw PEMFC unit.²⁴

The main area highlighted for the reduction in cost is that of the membrane electrode assembly (MEA) and principally the catalyst and membrane used. Much research is ongoing to replace or reduce the mass of catalyst needed to produce a certain charge per unit area. The U.S. DoE has set a list of principle targets for the reduction of cost needed by certain dates (Figure 7).

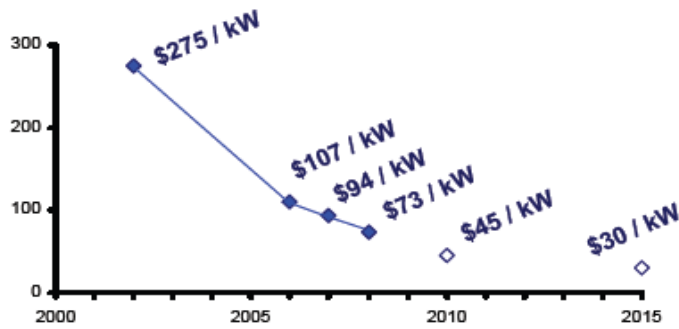


Figure 7 - DoE Fuel Cell price/kW targets.²⁴

The reason for the significant cost of the catalyst within the PEMFC is principally the scarcity and finite nature of the ore. The price of PGM catalysts has consistently risen over the last few decades (Figure 8) and the price is also subject to constant fluctuations due to speculations within the commodities market. For example, in 2006 when, in response to rumours of an ETF (Exchange Traded Fund) being launched for platinum (Pt), the price hit \$1,360 per troy ounce (1 troy ounce = 31.1035 g) on the 22nd of November then returning to \$1,150 per troy ounce the next day.²⁵



Figure 8 - Platinum prices since 1992 (per troy ounce).²⁶

The reason for the finite nature and limited production of PGM catalysts is the scarcity of natural resources. Primarily resources are found in very few geological locations, with 88% of deposits in

South Africa,²⁷ the regional distribution of the reserves negates an often cited argument in favour of fuel cells.

This argument proposes that a move from fossil fuels to a hydrogen based economy will increase the security of energy supply. However, this move would replace a reliance on Middle-Eastern cooperation, to a dependence and susceptibility to South African government policy as well as to market forces and market trends. Therefore, if the strain on Platinum associated raw materials could be reduced this would have a positive impact on the feasibility of a move to PEMFC deployment in the market.

A principle method for reducing this dependence would be to recover platinum from waste and recycle accessible platinum. There are various methods available for this process including hydrometallurgy²⁸ and pyrometallurgy.²⁹ These are both expensive and energy intensive technologies. However, there is a viable alternative method, that of bio-hydrometallurgy, recovering platinum and PGM to produce biocatalysts.

Bio-hydrometallurgy³⁰ is the principle method used and discussed in this project. The method uses the Hydrogenase enzyme to couple the oxidation of hydrogen to the reduction of soluble metal species in raised oxidation states. Despite the availability of the method, its use for PEMFC applications still needs investigation.³¹

This thesis discusses the method which produces nanoparticles 'scaffolded' to the membranes of bacterial cells. The technique investigated enables the *in-situ* recovery of PGM biocatalysts directly into a layer created by the bacteria called a biofilm. Secondly the recapture and preparation of these nanoparticles into the formation of a GDE through more traditional techniques is examined.

The layers produced by the biofilm technique not only exhibit potential for PEMFC use but also for a variety of other applications, showing beneficial properties over alternative catalysts. As such, a catalytic study was conducted of the hydrogenation of dimethyl itaconate to collect data on the 'catalytic' activity of the catalyst and as a proof of concept for a variety of industrial catalytic reactions.

Previous studies have highlighted the possibilities of recapturing the nanoparticles produced for fuel cell use, however the fabrication techniques used led to the possibility of large experimental errors.³¹ As such, the screen printing method for the fabrication of Gas Diffusion Electrodes (GDEs) was developed as a 'potentially' more reliable method.

1.2 Aims and Objectives of this Thesis

The aims and objectives of the work presented in this thesis are as follows:

1. – To biomineralise, spin coated engineered biofilms previously produced by Tsoligkas *et. al.*³².
 - a. To investigate the effect of biomineralisation on biofilms. Analysing biofilm formation and structure using ESEM and STEM.
 - b. To characterise Pd and Pt deposits on biofilms and planktonic cells.
2. – To evaluate the use of the biomineralised films for PEMFC use
 - a. To evaluate the biofilms conductivity
 - b. To investigate whether carbon additives can be used to increase the biofilms conductivity.
3. – To evaluate the catalytic activity of the biofilms compared to the planktonic cell prepared catalysts.
 - a. To investigate whether the films are catalytically active using the hydrogenation of Dimethyl Itaconate as a test reaction of industrial importance.
 - b. To compare the catalytic activity of the biofilm with the catalytic activity of the planktonic cell catalysts.
 - c. To investigate the degradation of the catalytic activity with repeated reactions cycling.
4. - To develop the screen printing technique of GDE fabrication with commercial fuel cell catalyst and obtain GDEs made from planktonic cell bio-catalysts.
 - a. To investigate the screen printing process
 - b. To produce GDEs fabricated using the process and commercial fuel cell catalyst
 - c. To produce GDEs fabricated using the screen printing process and utilising bio-catalyst.
 - d. To compare Bio-catalyst GDEs with commercial catalyst GDEs.
 - e. To evaluate the performance of the commercial catalyst GDE using a single test station and compare with commercially produced GDEs.

1.3 Thesis Layout

Chapter 1 has introduced the work included in this thesis. A literature review is presented in Chapter 2 covering the concept of fuel cells, the 'chemistry' and 'engineering' of the PEM fuel cell, the current fuel cell design, the catalyst layer (CL) in PEM fuel cells, the GDE fabrication methods currently used, the problems with current techniques and materials, the methods relating to the recovery of PGM metals, previous and relevant studies on the bio-hydrometallurgy technique, work on biofilm formation and previous investigations on the use of recovered PGM bio-catalysts.

Chapter 3 covers the experimental set-up and procedures used during testing and fabrication of the biofilms, planktonic cell recovered PGMs and GDE fabrication as well as the analytical methods used.

Chapter 4 discusses the results obtained for the fabrication of spin coated biofilms, the biomineralisation of the films with Pd and Pt and the comparison with the biomineralised planktonic cell catalyst. Chapter 5 discusses results obtained relating to the suitability for the biofilms use as fuel cell catalyst layers. This chapter also discusses the conductivity of the films and the effect of additives to the films' characteristics and conductivity.

A discussion of the results obtained for the catalytic activity testing of the Pd-mineralised biofilms is presented in Chapter 6. A comparison with planktonic cell obtained bio-catalysts and the ability to catalyse the hydrogenation of dimethyl itaconate is also presented. The chapter also discusses the degradation of the biofilm immobilised catalysts and the issues with planktonic cell supported catalysts.

Chapter 7 discusses the results obtained for the production of screen printed GDEs and the recapture and processing of PGM catalysts from planktonic cell obtained deposits.

Chapter 8 presents the conclusions from this investigation and recommendations for further work.

1.4 Publications (available upon request)

Biomineralisation of Biofilms. Tsoligkas, A. N., Pollet, B.G., Courtney, J. M., – submitted, in Biotech Letters.

1.4.1 Conference Papers, Presentations and Awards.

Conference Posters

1st International Fuel cell summer Seminar, Yamanashi, Japan, 2010

Bio-Engineered Catalyst Layers for PEM Fuel Cells – From Waste to Riches. Courtney, J.M., Tsoligkas, A.N., Deplanche, K., Macaskie, L.E., Pollet, B.G., (appendix section 10.1.1)

6th Annual International Conference and Exhibition, Hydrogen & Fuel Cells for Clean Cities, Vehicles and Buildings.

Novel Fabrication Techniques for Catalyst Layer production, Courtney, J.M., Pollet, B.G.,

2nd CARISMA MEA conference, La Grande-Motte, France, 2010

Bio-Engineered Catalyst Layers for PEM Fuel Cells – From Waste to Riches. Tsoligkas, A.N., Courtney, J.M., Deplanche, K., Macaskie, L. E., Pollet, B.G.,

Presentations

1st International summer seminar, Yamanashi, Japan, 2010

Led Group Discussion – Catalysts in PEM Fuel Cells, Courtney, J.M.

British Science Festival, Aston University, Birmingham, 2010

Hydrogen and Fuel Cells, Birmingham and Science City, Courtney, J.M., Hudson, R.

Cambridge University, Professor Tim Burnstein and the Electrochemistry group, 2010

Fabrication techniques for PEM fuel cell catalyst layers, Courtney, J.M., Pollet, B.G.

Awards

1st International Summer Seminar, Yamanashi, Japan, 2010

Best Poster Presentation Award

2nd CARISMA MEA conference, La Grande-Motte, France, 2010

Best Poster Presentation Award

Media and Miscellaneous

BBC Frontiers programme, BBC radio 4, Interview and Lab tour, broadcast July 2010.

BBC News, liaison, logistics and lab tour, broadcast September 2010, available online - <http://www.bbc.co.uk/news/business-11297410>

Alan Johnson MP, Lab. tour and logistics

Lord Peter Mandelson, Lab. tour and logistics

David Willets MP, Lab. tour and hydrogen vehicle demonstration

Community day and open days – Lab. tours, hydrogen vehicle demonstrations, various 2010

Chapter 2 - Literature review

2.1 'Chemistry' of Proton Exchange Membrane Fuel Cells (PEMFCs)

Fuel cells are a promising technology for the production of energy in the Hydrogen Economy. Fuel cell stacks are 20-30 % more efficient than combustion of fossil fuels³³ with an operating efficiency of 40-60 %³⁴⁻³⁶ and for that reason, they pose an energy gain over conventional combustion processes.

The chemical reaction for producing energy from hydrogen is:



This is the same reaction that, through a combustion process, took the shuttle to the moon. However in a fuel cell the reaction is split into two sub reactions separated by a Proton Exchange Membrane (PEM), the Hydrogen Oxidation Reaction (HOR shown in Figure 9) and the Oxygen Reduction Reaction (ORR shown in Figure 9) connected through an external circuit.

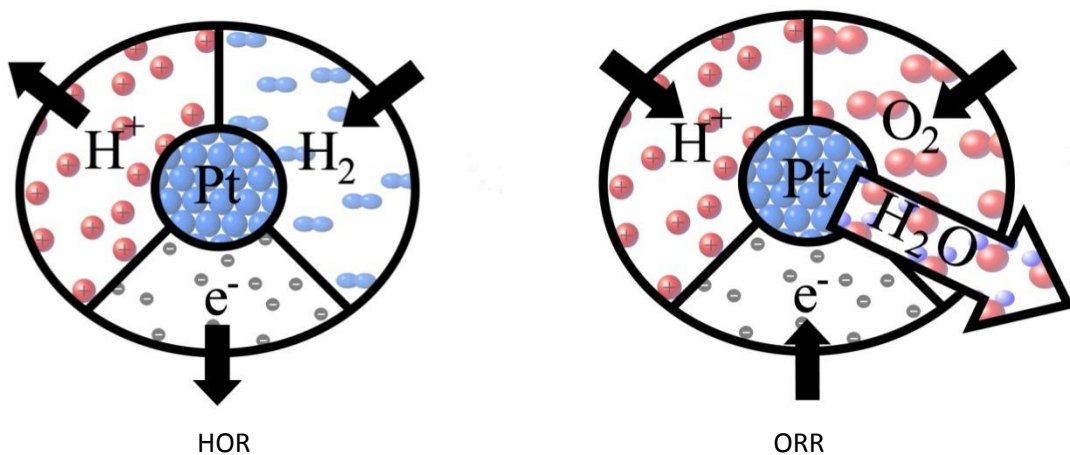


Figure 9 - The HOR reaction and the ORR reaction. James Courtney©

The hydrogen is split into protons (H^+) and electrons (e^-) on a catalyst surface with protons transferred from the anodic to the cathodic side of the cell through a proton exchange membrane and along an ionomer matrix. The electrons produced travel through an external circuit to the cathodic side of the fuel cell. There the electrons and protons are combined with oxygen to form water on a catalyst surface.

Of the two reactions, the splitting of hydrogen is a relatively labile reaction and occurs swiftly on a platinum catalyst with other catalysts being developed to reduce the content of platinum in the cell, including palladium and Pt/Ru alloys. However, the ORR reaction is slow in comparison and a larger concentration of platinum is required in the cathodic side of the cell to produce the required current density.

There are various proposed explanations for the slow nature of the ORR reaction and it is still under debate as to which intermediates are formed during the process. Currently the favoured catalytic intermediary is surface oxidation of the platinum catalyst forming a Pt-O intermediate with both α and β -Pt-O₂ species detected during in-situ XRD (x-ray diffraction) and XAS (x-ray absorption spectroscopy) experiments.³⁷ Although several ORR catalysts have been demonstrated including Iron-Nitrogen (Fe-N) complexes,³⁸ nano-silicon carbide (Si-C),³⁹ Pt-Co/C,⁴⁰ tantalum oxide (TaO),⁴¹ there has not yet been a catalyst which can match the performance of platinum in current density per unit of cost or current density per unit of weight.

2.2 Current PEM Fuel Cell Design

The PEM cell was first developed by General Electric in the early 1960s⁴² through the development of Nafion® perfluorinated membranes by Dupont⁴³. PEMFCs have slowly increased in efficiency and current density leading to the current design as shown in Figure 10.

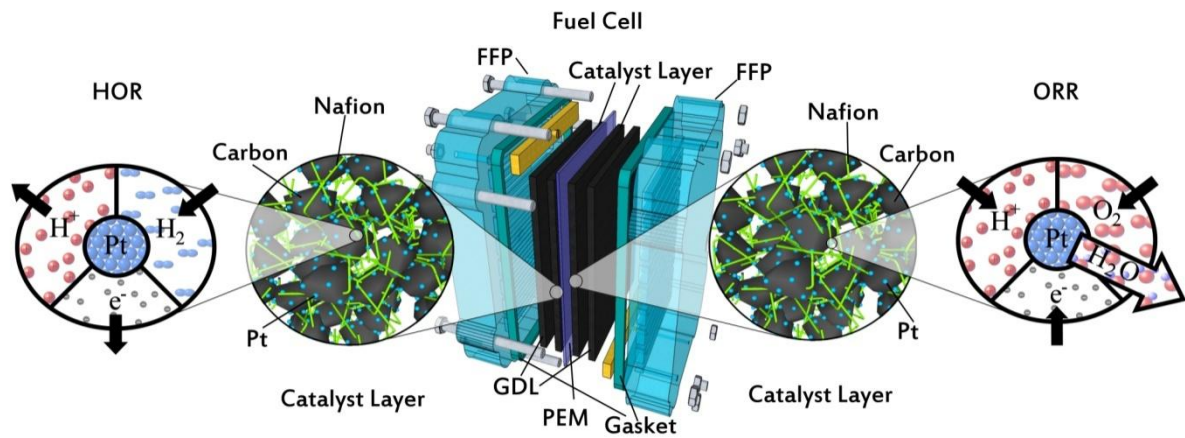


Figure 10 - Exploded PEMFC diagram. James Courtney©.

The gases are first distributed throughout the cell by the use of bipolar plates (BPPs), also known as Flow Field Plates (FFPs). The design of BPPs and flow fields are an intense area of research with the size, shape and orientation affecting the performance of the cell.⁴⁴ The main research area and focus for improving the fuel cell is the Membrane Electrode Assembly (MEA). This is the ‘heart’ of the fuel cell and, as shown in Figure 10, consists of two gas diffusion layers (GDLs), two catalyst layers (CLs) and a proton exchange membrane (PEM).

The role of the gas diffusion layer (GDL) is to hold the catalyst layer and to distribute gases evenly throughout the fuel cell, conduct electrons to and from the reaction sites to the flow field collection plate and, on the cathode side of fuel cell to aid the removal of water from the catalytic sites. There are numerous GDL materials, mostly derived from carbon cloth or carbon paper impregnated or sprayed with Teflon. The GDL thickness ranges from 100-330 μm .⁴⁴ There is some disagreement in the literature as to which GDL material provides the highest current density within the fuel cell. There is some evidence that carbon cloth aids water removal and reduces mass transport limitation in the plateau region of I/V curves (high current densities).⁴⁵ However, the simplest design of GDL is

Toray Paper with 5% w/v Teflon. So as to reduce possible external effects on the fabrication technique being investigated, it was decided to use Toray Paper with 5%w/v of impregnated Teflon as the experimental GDL.

2.3 Catalyst Layers in PEM Fuel Cells

Catalyst layers (CLs) are designed to maximise the catalytic activity and current density from a minimum amount of PGM catalyst. As previously discussed, the anodic and cathodic catalysts are similar although slightly different (e.g. loadings, sizes etc) due to the different kinetics of the two reactions. The base of both catalyst layers is Pt nanoparticles supported on carbon mixed with Nafion ionomer.⁴⁴ The carbon particles form a porous layer and a Nafion ionomer matrix allows for Proton conductivity throughout the layer.

Due to the faster kinetics of the HOR reaction, a lower loading of Pt or a different catalyst can be used for the anodic catalyst layer. For example, loadings of 0.2-0.4 mg Pt.cm⁻² are typically used⁴⁶ with the U.S. DoE highlighting an eventual move to a loading of 0.05 mg Pt.cm⁻². There are a large number of Pt, Pt-alloy or non-Pt catalysts which have been investigated for use as the anode catalyst within PEM fuel cells.^{44,46}

The main issue for anodic catalysts is the CO poisoning due to non-high purity hydrogen.⁴⁷ This leads to the success use of Pt-Ru alloys as anode catalysts, as they show a greater tolerance to CO-poisoning.^{48,49} Another promising possibility is to replace the Pt based anode catalyst with more cost-effective and much more widely available palladium based catalysts. Pd nanoparticles⁵⁰⁻⁵², Pd-Pt bimetallics^{50,51,53} and Pd alloys⁵⁰ have all been investigated. The results showed that Pd could replace Pt as the primary anode catalyst demonstrating a maximum power density of up to 0.75 W.cm⁻² with a Pt/C based cathode catalyst in single cell tests.⁵³

Not only has palladium been tested as a replacement for platinum as an anode catalyst but also as a cathode catalyst.⁵² It was shown that palladium is a feasible cathode electrocatalyst, however, so far palladium has not exhibited the performance of traditional Platinum based catalysts. Several Pd alloys such as Pd-Co⁵⁴ and Pd-Cu⁵⁵ have shown improved performance but Platinum still remains the principle electrocatalyst.

This is because, unlike the HOR, the ORR incurs not just additional mass transportation limitations (due to the need to remove water from the active catalyst sites) but also kinetic limitations. This leads to the need for higher loadings of Platinum catalyst within the cathodic catalyst layer and subsequently, is the main barrier to the use of fuel cells representing 70% of the cost of the cell. The potential use of both palladium and platinum for fuel cell applications leads this study to investigate the recovery of palladium and platinum.

2.4 GDE Fabrication Techniques

There are two main groupings for catalyst layer fabrication techniques. The production of catalyst coated membranes (CCM)^{56,57} involves printing or painting the catalyst layer onto the PEM membrane directly, whereas the production of catalyst coated substrates [CCS or GDE (gas diffusion electrodes)]⁵⁶ involves printing the catalyst layer onto the gas diffusion layer. There is debate as to which method produces the highest performance fuel cell and there are merits to both production techniques.

There are many methods for depositing the catalyst layer including, InkJet printing,^{58,59} various decal methods,^{60,61} spraying,⁵⁶ doctor blading⁶², direct chemical vapour deposition,⁶³ painting,^{64,65} screen printing^{66,67} and many more.⁴⁴ As previously discussed, cost is a major issue with the uptake of fuel cells and as such, the manufacturing process needs to be relatively low cost and rapid. It is also important that the manufacturing process can be scaled up to mass production volumes.⁶⁸ Each

method has reported benefits to the performance of the MEA within the PEM fuel cell. For example, Decal processes produce catalyst layers with reduced surface roughness allowing for better contact between the catalyst layer and the proton exchange membrane and, therefore, less resistance to proton migration through the cell.⁶¹ However, the development of these processes is lengthy and without adequate industrial 'know-how' most lab groups resort to testing using the painting and hand spraying method.

Previous studies in the use of bio-catalysts have been limited by using the painting technique.³¹ This is due to its unreliability and dependence on individual parameters. For example, the painting technique results in an uneven surface profile,⁶⁹ the nature of which is determined by the individual 'painter'. Therefore, the screen printing technique was chosen as the method to develop. This is due to the high repeatability, the reported high current densities achieved from low Platinum loadings,^{61,66,70} the high levels of adaptability of the process using different inks⁶⁶ and catalysts coupled with the ease of scale up of the process.^{61,67}

The screen printing fabrication process starts with the production of a suitable ink to be printed. The ink consists of Nafion®, the catalyst (on a carbon support e.g. carbon black) of choice and a solvent selected for task. There are a range of solvents which are suitable to use with the screen printing technique such as ethylene glycol,⁶² Iso-propanol,^{71,72} *n*-butyl acetate⁷¹, water,^{57,66,73} and glycerol.^{66,72} The inks are sonicated to ensure good mixing and then introduced onto the screen within the screen printer. *For full instruction and demonstration see video on attached CD.*

Work conducted previously has shown that burning the biomass from bio-catalysts and re-supporting the catalyst on activated carbon could be used to produce working GDEs.³¹ However, the work was brought to an end due to the unreliable technique used to prepare the catalyst layers leading to potentially large experimental errors. As such, it was decided to develop the screen printing method of GDE production in order to produce bio-catalyst, GDEs for PEM fuel cell use.

2.5 PGM Production

Platinum was discovered in the 16th century by Spaniards exploring the pre-Inca sources in Columbia believing it to be 'unripe' gold.^{27,74} Platinum was found in the alluvium and river beds and was seen more as an annoyance than a resource. Currently the largest known deposits of platinum are in South Africa (63million kg), Russia (6.2million kg) and Canada (310,000kg) although the US has reserves and deposits totalling around 900,000 kg⁷⁵. The natural abundance of Platinum is around 0.01ppm⁷⁶ although it is found in higher amounts on the moon, asteroids and in asteroid impact zones such as the Sudbury Basin in Canada.⁷⁷

The largest reserve is the Bushveld Complex in South Africa⁷⁵ with one deposit with a strike length of over 100 km (the Merensky Reef) and total mass of 5.76 million kg of Platinum and 3.29 million kg of Palladium substantiating the claim to be around 88% of the World's Platinum reserves.²⁷ South African production accounts for around 77% of world production and in 2006, 239,000 kg of platinum was traded worldwide.²⁵

By far the largest user of PGMs is the automotive industry, accounting for ca. 55% of platinum sales in the US for domestic autocatalysts.²⁵ In an average vehicle, 2.4 g of PGM are required for the catalytic converter (ratio of 67:26:7/Pt:Pd:Rh)⁷⁴ and this is expected to rise as further emission legislations are brought in. A steady rise in demand for platinum catalysts has been seen year-on-year and in 2006 alone there was an 11% rise.^{25,75}

2.6 PGM Recovery

Due to the high cost and finite nature of platinum reserves and the drive towards environmentally friendly catalysts⁷⁸ the method of platinum recovery for catalyst use has become a popular research topic which is essential to the chemical industry. In 2006, platinum recovery increased by 11% reaching 26,600 kg being recovered globally from Autocatalysts alone.²⁵ In addition, in 2009, 17,000kg of PGM catalysts were recovered in the US alone.⁷⁵

There is a wide range of methods for the recapture of PGM catalysts, from hydrometallurgy, pyrometallurgy, electrochemical to biological methods. Hydrometallurgy is the extraction of the metal via aqueous solutions of a salt and the recovery of the metal from solutions.²⁸ Pyrometallurgy is the recovery or purification of metals through the use of heat and often includes processes such as 'roasting' or refining.²⁹ The biological process either, uses microbes to alter the oxidation state of the metal being extracted to produce a more soluble⁷⁹ metallic species, or utilises a biomineralisation³¹ process to directly recapture PGMs onto the surface of bacteria through a technique known as biohydrometallurgy.³⁰

2.6.1 Pyrometallurgy

Pyrometallurgical techniques are essentially based on smelting processes which use the density differences in metals to separate the bulk materials. The main problem with pyrometallurgic techniques is that they need to be over 90 % efficient at recovering metals to become cost effective.⁸⁰ This is due to the large energy input required to operate them. A plasma ARC reactor is used to heat the input material in a crucible to around 1,300 °C and the heavier PGM metals settle to the bottom of the crucible where they are tapped and poured away to form 'bullions'.⁸¹ A secondary method combines pyrometallurgy and hydrometallurgy. The material is roasted at a high

temperature in the presence of sulphuric acid and one or more halogen salts, which then allows less harsh chemicals to be used in the dissolution of metals in a hydrometallurgical step.⁸²

2.6.2 Hydrometallurgy

Hydrometallurgy techniques are usually based on the selective dissolution of the PGM.⁸³ The first step in the process is to use a variety of oxidising agents and complexing agents to oxidise the PGM to an ionic form that can then form stable complexes. Ion exchanges are then used to remove and replace the complex ions either with ion exchange resin,^{84,85} solvent extraction(SX),^{86,87} ion exchange membranes⁸⁸ or to precipitate the platinum salt^{86,89}. Various oxidising agents have been developed such as fluorides⁹⁰, super critical water⁹¹, cyanide⁹², aqua-regia⁹³ as well as many more.

There are many issues with the hydrometallurgical techniques. For example, using cyanide as the principal complexing and oxidising species leads to high cost in materials as well as financial and environmental costs when dealing with the disposal of wastes.⁹² Iodides and bromides might reduce cost but have just as high an environmental impact⁸³ whereas aqua-regia, although ensuring complete dissolution of PGMs, has economic disadvantages.^{92,93} This is due to the poor kinetics associated with the oxidation process,⁹³ the high reagent use and the material cost.⁹²

2.7 Bio-hydrometallurgy

Bio-hydrometallurgy first became a reality with the discovery of sulphur and iron-oxidising Acidophilic Archea in 1965⁹⁴ and their subsequent isolation from acidic natural springs in Yellowstone national park. Although some writers cite the first instance as the bioleaching process developed by the Kennecott Copper Corporation in the 1950s.⁹⁵ Many processes have been reported utilising bio-hydrometallurgy such as bio-oxidation of refractory gold, extraction of copper from sulphide, metal

removal from effluents by active sulphate reduction and metal removal by the use of wetlands.⁹⁶ It is argued in the literature that the method of bio-hydrometallurgy possesses a more environmentally friendly method to recover metals, as well as possessing the ability to economically process low-grade ores and waste materials,⁹⁷ reducing demand on ores, energy or landfill sites.⁹⁸ However, there is some debate surrounding reactor designs and the power requirement which might affect the economic price competitiveness when compared to pyrometallurgy.⁹⁹

Microorganisms affect the cycling of metals in the environment by assimilation/adsorption, precipitation and dissolution, oxidation and reduction, and methylation and dealkylation reactions.¹⁰⁰ Metals have multiple functions within microbial cells and a variety of functional groups exist within biomolecules that occur on the cell walls including carboxylates and phosphates. These can confer a net negative charge on the surface of most microorganisms affected by the pH of the solution. Oxidation and reduction occur when the metals are involved in energy conservation and act as direct or indirect electron donors and/or acceptors in microbial metabolism.¹⁰⁰

Biosorption¹⁰¹ or biomineralisation³⁰ can effectively increase the concentration of PGM by binding the metal to the surface of active or dead biomass.¹⁰² Many different strains of bacteria can be used such as *Desulfovibrio desulfuricans*, *Desulfovibrio fructosivorans* and *Desulfovibrio vilgaris*.¹⁰³ In 1998, studies showed that Hydrogenase enzymes can be used by the bacteria strain *Desulfovibrio desulfuricans* to convert $\text{Pd}(\text{NH}_3)_4\text{Cl}$ a form of Pd(II) to deposit particles of Pd(0), 50nm in diameter, on the surface of cells.¹⁰⁴ Recovery of Pd, Pt and Rh from automotive catalyst wastes was demonstrated in 2003 with *Desulfovibrio desulfuricans*, using an electrobioreactor with electrochemically produced hydrogen fed directly to bacteria. The bacteria formed a biofilm on the Pd/Ag alloy membrane electrode which produced hydrogen directly. The bacteria then produced deposits of Pd, Pt and Rh from pre-treated aqua-regia leachates.¹⁰⁵ A different approach showed that the same process

occurred for waste circuit board leachates when hydrogen gas was bubbled through the reactor eliminating the need for electrodes.¹⁰⁶

The Hydrogenase enabled reduction of metals is still relatively unknown although it has been shown that the reduction of Pt(IV) to Pt(0) occurs via two different Hydrogenase enzymes. It was proposed that the octahedral Pt(IV) was sterically inhibited from binding to the active site of the Hydrogenase enzyme and unable to pass through the membranes of the bacteria. It was shown that a cytoplasmic, oxygen-sensitive Hydrogenase was responsible for reducing Pt(IV) to Pt(II) via a 2-electron donation process. Secondly, a periplasmic Hydrogenase used hydrogen donors to reduce Pt(II) to Pt(0). This allowed for Pt(0) deposits to form in the periplasmic space between bacterial membranes.¹⁰⁷

The use of these bacterially produced PGM nanodeposits is of keen interest for use in various catalysed reactions and as environmental recovery and production of PGM resources.

2.8 Use of PGM Bio-Catalysts

Many applications have already been investigated for the planktonic cell produced bio-catalysts. Such as the Hydrogenation of 2-butyne-1,4-diol^{108,109}, the Hydrogenation of 2-pentyne¹¹⁰ and preliminary studies into the use of bio-Pd for Fuel cell use as anode catalysts³¹. This investigation into catalysts generated biologically is led by the suggested advantages, principally the possible economic incentives. Such as, reducing demand on reserves due to the recovery techniques used, the possible reduction in cost of the catalysts, the environmental implications as well as the benefits the use of biofilms could present. Biofilms present an opportunity to overcome some of the issues associated with each of these applications, such as catalyst recapture.

The Hydrogenation of dimethyl itaconate (Figure 11) is of importance due to the use of succinic acid derivatives as key intermediates in the pharmaceutical industry, in particular for the production of potent rennin inhibitors.

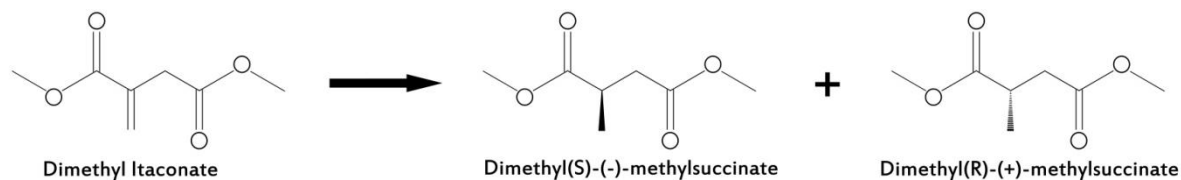


Figure 11 - Hydrogenation of dimethyl itaconate. James Courtney©

The olefin reacts with hydrogen to form two isomeric products, dimethyl(S)-(-)-methylsuccinate and dimethyl(R)-(+)-methylsuccinate. It has been shown that biocatalysts have managed some degree of increased selectivity for the Hydrogenation of 2-pentyne when compared against a commercially available Pd/Al₂O₃ catalyst.¹¹⁰ Spin coated biofilms have recently been employed to achieve a 20% increase in reaction yield compared to planktonic cell supported catalysts for the biotransformation of three different halotryptophans³².

2.9 Biofilm Formation

Highlighted for PEM fuel cell use, biofilms potentially remove the need to process the bio-PGM catalyst and fabricate a GDE by a mechanical means such as screen printing⁶⁶ or spraying techniques.¹¹¹ Instead directly recapturing the bio-catalyst into the biofilm could provide a 'one pot' synthesis of the catalyst and catalyst layer from a GDL substrate and PGM waste stream. This has the potential to reduce the susceptibility of PEM fuel cells to issues associated with PGM reserves by directly recycling the resource from waste streams, reducing the manufacturing cost by removing

many processing and fabrication steps as well as reducing the potential chemical wastes produced when fabricating catalysts from raw materials.

Biofilm formation has been extensively researched due to the implications to the food and health industries, however the exact genes and enzymes involved are not fully understood. What is currently known is that biofilms form through several distinct phases before maturing with a distinctive and characteristic three dimensional structure. This structure provides an open and porous structure with interconnected flow channels running throughout the film (shown in Figure 12) presenting an attractive feature for PEM Fuel cell catalyst layers.

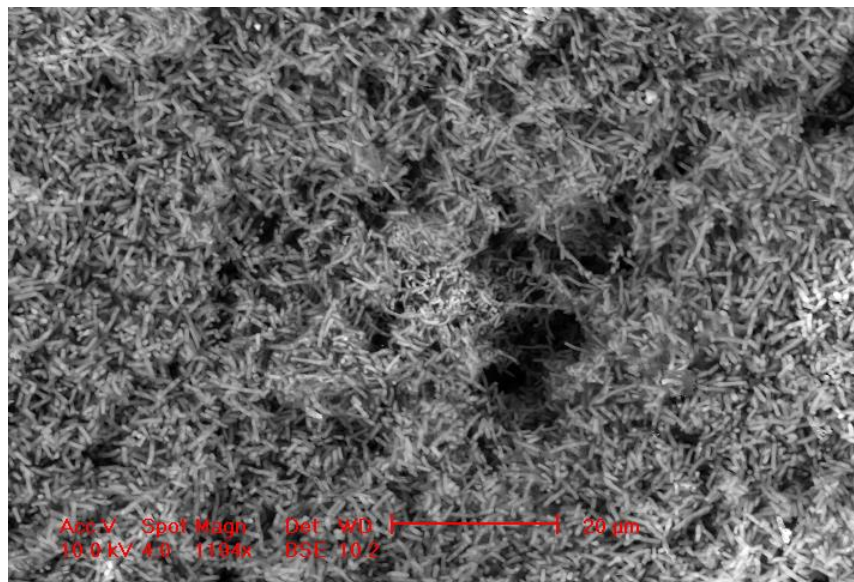


Figure 12- ESEM image of a spin-coated biofilm highlighting flow channels

This structure is obtained due to the five stages of growth shown by the bacteria during biofilm formation (Figure 13), which has evolved to generate the best dispersion of media throughout the film in order for every cell to receive nutrients and as a method to protect the overall cell colony. The biofilm grows through five distinctive growth phases; initial attachment, irreversible attachment maturation I, maturation II and dispersion. It is thought that if this interconnected flow channel

structure can be maintained after the bacteria have recaptured the Nano-particle catalysts then an enhanced distribution of gases throughout the catalyst layer could be observed. Combined with the fact that nano-particles will only be produced on cells that are exposed to the solution within the flow channel structure, only producing catalyst particles in active areas of the biofilm, it is hoped that biofilms could potentially provide a cost-effective, sustainable and effective method for the production of PEM fuel cell catalyst layers.

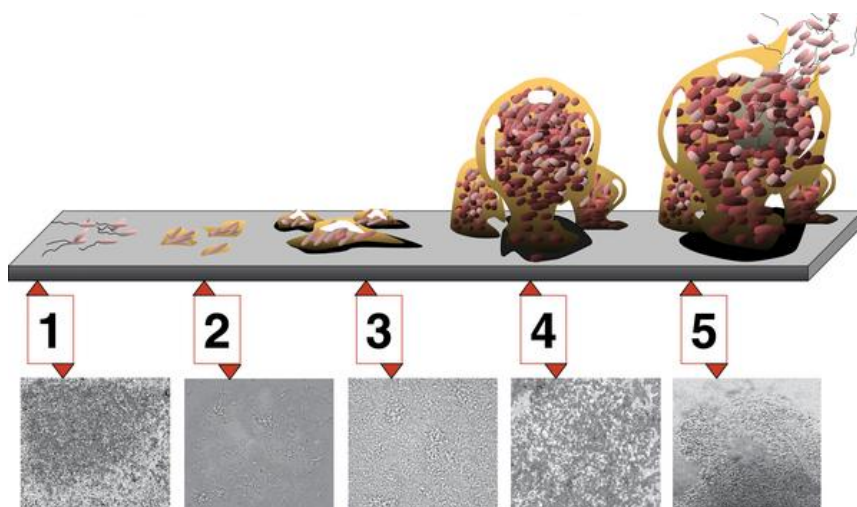


Figure 13 - Five stages of biofilm growth. ¹¹²

Chapter 3 - Experimental Methods and Materials

3.1 Fabrication and Synthesis

3.1.1 Biomass Culture

The strain used was *E.coli* strain PHL644 (MC4100 *malA-Kan ompR234*) and was previously reported by Vidal *et al.*¹¹³ It was kindly supplied for use by the authors. The strain was transformed using the heat-shock method as described by Tsiglikas *et al.*³² Transformants were grown in Luria-Bertani (LB) broth (10 g.L⁻¹ tryptone, 5g.L⁻¹ yeast extract, 10 g.L⁻¹ NaCl) with the addition of ampicillin (100 µg.mL⁻¹) or Half-Luria-Bertani (1/2 LB) broth (5 g.L⁻¹ tryptone, 2.5 g.L⁻¹ yeast extract, 5 g.L⁻¹ NaCl) with the addition of ampicillin (100 µg.mL⁻¹).

3.1.2 Biofilm Growth

Surface-adhered biofilms were matured and curli expression was promoted in M63 medium as described by Vidal *et al.*¹¹³ (100 mM KH₂PO₄, 15 mM (NH₄)₂SO₄, 0.8 mM MgSO₄.7H₂O, 17 mM K-succinate 1 mM Glucose, adjusted to pH 7.0) with the addition of ampicillin (100 µg.mL⁻¹). Prior to biofilm formation, glass slides were coated with approximately 4 mL of 0.1% (w/v) Poly (L-lysine) (PLL) in water (sigma), then dried overnight in an oven at 60°C. Single colonies were picked from a day old agar plates (plate supplemented with ampicillin) and used to inoculate 200 mL of ½ LB (tryptone, yeast extract, NaCl – as above) supplemented with ampicillin (100 µg mL⁻¹). The cultures were incubated in an orbital shaker at 30°C and at 180 rpm. Following the incubation, cultures were transferred aseptically into a sterile 750 mL

polypropylene centrifuge bottle (Beckman Coulter UK Ltd.) containing the PLL-coated glass slides supported on a bed of glass beads (200 g, soda-glass beads, 4mm diameter) to provide a flat surface to prevent cracking during centrifugation and were centrifuged at 851 *g* for 10 minutes in a centrifuge fitted with a swinging bucket rotor. After centrifugation, the glass slides were gently placed in 500 mL sterilised wide necked Erlenmyer flasks (fischer scientific) containing 70 mL of M63 medium supplemented with ampicillin (100 µg.mL⁻¹). The spin coated biofilms were incubated in an orbital shaker incubator at 30°C at 70 rpm and set with a throw of 19 mm (set to a low speed to minimise bacteria shearing) for a maturation period of 7 days. The slide was further incubated for 7 days at 30°C at 70 rpm.

3. 2. Biomineralisation

3.2.1 Platinum Mineralisation

Bio-Pt was manufactured by growing cells under anaerobic respiratory mode (LB supplemented with 0.4 % w/v sodium fumarate and 0.5 % glycerol) in 2 L Durham bottles inoculated using overnight preculture ((10 % v/v) grown in the same way). Mid-Logarithmic phase cultures (OD₆₀₀ = 0.5-0.7) were harvested by centrifugation (12,000 *g*, 15 min), washed three times in 100 mL of MOPS-NaOH buffer (20 mM, pH 7.2) re-suspended in 50 mL of the same buffer and stored at 4°C as concentrated cell suspensions until use, usually the next day. Cell concentration was determined by correlation to a pre-determined OD₆₀₀ to dry weight conversion.

A known volume of concentrated resting cell suspension was transferred under oxygen free nitrogen (OFN) conditions into 200 mL serum bottles and an appropriate volume of degassed 2 mM Pt (IV) solution (hexachloroplatinate salt, 0.01 M nitric acid, water) was added so that the final ratio (weight

of Pt:dry weight of cells) was 1:19, to give a final loading of 5 % Pt on biomass. Pt/Cells were left to stand for 30 min at 30⁰C with occasional shaking to promote biosorption of Pt(IV) complexes³¹ before H₂ was sparged through the suspension (200 mL/min, 20 min) to reduce cell surface-bound Pt(IV) to Pt(0). The Pt(0) coated biomass was harvested by centrifugation (3000 g, 10 min, 25⁰C) and washed three times in distilled water (dH₂O). Following a final acetone wash, the black precipitate was re-suspended in 5 mL of acetone and left to dry in air overnight. Black Pt/cell powder was finely ground and passed through a size selective sieve (100 µm then 38 µm) producing the bio-Pt/cell catalyst.

Immobilised bio-Pt/cell catalysts were prepared in the same way but the pre-prepared biofilms on glass were removed from the Pt(0) solution following the anaerobic biosorption step to avoid chemical reduction of Pt(IV). Reduction of the adsorbed Pt(IV) species was carried out using H₂ as the electron donor in MOPS-NaOH buffer (20 mM, pH 2.3). Following H₂ sparging (200 mL/min, 20 min), slides were kept overnight in buffer under H₂ atmosphere. Slides were rinsed gently under distilled H₂O stream and kept in air until use.

3.2.2 Palladium Mineralisation

A known volume of concentrated resting cell suspension (as prepared for Platinum, section 3.2.1) was transferred under oxygen free nitrogen (OFN) conditions into 200 mL serum bottles and an appropriate volume of degassed 2 mM Pd(II) solution (sodium tetrachloropalladate, 0.01 M Nitric acid, water) was added so that the final ratio (weight of Pd:dry weight of cells) was 1:19, to give a final loading of 5 % Pd on biomass. Pd/Cell were left to stand for 30 min at 30⁰C with occasional shaking to promote biosorption of Pd(II) complexes³¹ before H₂ was sparged through the suspension (200 mL/min, 20 min) to reduce cell surface-bound Pd(II) to Pd(0). The Pd(0) coated biomass was harvested by centrifugation (3000 g, 10 min, 25⁰C) and washed three times in distilled water (dH₂O).

Following a final acetone wash, the black precipitate was re-suspended in 5 mL of acetone and left to dry in air overnight. Black Pd/cell powder was finely ground and passed through a size selective sieve producing the bio-Pd/cell catalyst.

Immobilised bio-Pd/cell catalysts were prepared in the same way but the pre-prepared biofilms on glass were removed from the Pd(0) solution following the anaerobic biosorption step to avoid chemical reduction of Pd(II). Reduction of the adsorbed Pd(II) species was carried out using H₂ as the electron donor in MOPS-NaOH buffer (20 mM, pH 2.3). Following H₂ sparging (200 mL/min, 20 min), slides were kept overnight in buffer under H₂ atmosphere. Slides were rinsed gently under distilled H₂O stream and kept in air until used.

3.3 Recapture of metallic particles³¹

The free-cell bio-metal/cell catalysts were produced as described above, cells were harvested by centrifugation (3,000 *g*, 10 min, 25⁰C) and washed three times with deionised water followed by three washings with acetone. The samples were dried at 60⁰C, finely ground with pestle and mortar and then transferred to 10 mL alumina ceramic crucibles. The samples were then ramped to 700⁰C over 4 hours and kept at 700⁰C for an additional 4 hours (oven at normal pressure and atmospheric content). The samples were cooled to room temperature using natural oven cooling. The Samples were then finely ground using pestle and mortar and passes through a selectivity sieve, first stage 100 µm, second stage 38 µm to obtain small particle sizes for further processing.

3.4 Supporting Metal catalysts

To support Bio-catalysts, two methods were used. The first preparation procedure followed work previously conducted by Yong³¹. 20 mg of bio-metal catalyst were mixed with 80 mg of activated carbon (XC-72 Vulcan black, Fuel Cell Store) and suspended in 1 mL of distilled water and 0.2 mL of 10 % w/v Nafion in water (Sigma-Aldrich, Germany). The mixture was sonicated for two hours and left overnight before further use.

In the second method, 20 mg of bio-metal catalyst was mixed with 80 mg of activated carbon (XC-72 Vulcan Black, Fuel Cell Store) and suspended in 1 mL of Glycerol and 0.2 mL of 10 %w/v Nafion in water (Sigma-Aldrich, Germany). The mixture was sonicated for two hours and left overnight before further use.

3.5 Ink Formulations (for Screen Printing)

3.5.1 Commercial catalyst

Commercial catalyst based inks were produced by mixing 0.04 g of 20 % w/v Pt/C (E-tek, HP catalysts, Fuelcellstore.com) in a 5 mL vial, introducing 100 μ L of 10 % Nafion Solution (10 % Nafion in deionised water and alcohols, Fuelcellstore.com) and 0.8 mL of Glycerol (Sigma-Aldrich). This mixture was sonicated for two hours and left for 24 hours before use. To achieve a variety of concentrations the overall volume of solution was kept constant and values adjusted accordingly.

3.5.2 Biocatalyst

Bio-catalyst based inks were produced by weighing 0.04 g of 20 % w/v Bio-Pt/C or 20 % w/v Bio-Pd/C (fabricated as shown above) in a 5 mL vial, introducing 100 μ l of 10 % Nafion Solution (10 % Nafion in deionised water and alcohols, Fuelcellstore.com) and 0.8 mL of Glycerol (Sigma-Aldrich). This mixture was sonicated for two hours and left for 24 hours before use.

3.5.3 'Mock' Ink

A variety of 'mock' inks were used to assess the properties of the ink needed to achieve successful screen printing of the catalyst layer. Primarily a carbon black based ink was used to reduce cost of experimentation by removing the expensive platinum catalyst. 0.4 g of activated carbon (Vulcan XC-R72, fuelcellstore.com) was, mixed with 200 μ l of 10 % Nafion solution (10 % Nafion in deionised water and alcohols, Fuelcellstore.com) and 0.8 mL of Glycerol (Sigma-Aldrich). This mixture was sonicated for two hours and left for 24 hours before use. A variety of concentrations were used and obtained by keeping the total volume of ink constant and altering Nafion, carbon and glycerol values accordingly. A few different mock inks were tried using IPA (isopropanol Alcohol), 1:1 acetone:water, ethanol and THF as the solvent used instead of Glycerol.

3.6 Screen printing

For a full demonstration of the screen printing technique, *see attached CD for a full video demonstration*. Numerous GDLs and catalyst inks were trialled for this technique and for the ink that was used. Toray paper H-060, Freudenberg H2315I6, Freudenberg H2315C2, SGL 10BC and SGL 10AA were all trialled (see appendix 10.3.1 for all the GDL properties used in this work). Unless otherwise stated, Toray paper H-060 was the substrate used in this work. The substrate was cut into 5x5 cm

pieces and masked to show a 4×4 cm section (the eventual active area) and adhered to a piece of filter paper. The substrate was then placed on the vacuum table of the screen printer (DEK 258) and aligned with position markings. The screen printer was either set to automated or manually used. For the experiments the first sample was conducted manually, setting the height of table and distance of squeegee passes. The table height was adjusted to bring the substrate in contact with the mesh screen; the squeegee was set to pass from 2.5cm either side of the mesh opening. Subsequent repeats were automated to use the first's printer settings. 0.8 mL of ink was introduced in a consistent line at the leading edge of the uncovered mesh on the screen (see appendix 10.3.1 for image). The first squeegee was passed over the mesh in one direction and the second was brought back in the opposite direction. The substrate was removed, turned to 90° and the process repeated without the addition of more ink. The substrate and printed catalyst layer were removed and placed into a vacuum oven at 120 °C and left at atmospheric pressure for one hour, and then at 0.8 mPa overnight. The newly produced GDE was weighed and added mass calculated. The process was repeated until a desired loading was reached.

3.7 Analysis

3.7.1 Assay of Metal content [Pd(II) and Pt(IV)]

To assess the metal content of the metal/cell catalysts, the free Pd(II) and free Pt(IV) ion content in solution was monitored at all stages of the bio-metal/cell preparation using the spectrophotometry method of Charlot (1978).¹¹⁴ Timed samples (1 mL) were withdrawn, centrifuged (12,000 *g* , 4 min, IEC Centra bench centrifuge) and supernatants were assayed to estimate the residual metal ion concentration. The Sn(II) reagent was prepared by dissolving 29.9 g of SnCl₂ powder into 500 mL of concentrated HCl. For assay, a 200 µL sample was added to 800 µL of SnCl₂ solution in a 1.5 mL plastic

cuvette and the absorbance at the wavelength of 463nm was determined after one hour of incubation at 30°C against a blank prepared in the same way. The assay method was validated by analysis of reference and selected test sample by a commercial laboratory (H2B, Capenhurst U.K.).

3.7.2 SEM

Several preparation techniques were used to analyse samples via SEM. Primarily the biological cell samples were prepared using the following technique. The samples were immersed in 2.5 % gluteraldehyde for one day to preserve structure of living tissue with no alteration from the living state and then dehydrated using 50 %, 70 %, 90 % and 100 % ethanol for 15 mins at each concentration and repeated twice. After fixation and rinsing the samples were critical point dried using a critical point dryer (agar scientific) and mounted onto microscope stubs for carbon coating using an Cemscope SC 500 sputter coater (Cemscope, Ashford, UK) and examined using a XL-30 FEG ESEM (Cambridge Instruments, Cambridge, UK).

A secondary preparation technique was used for some 'free-cell' bio-metal/cell catalysts where the dehydration procedure was skipped and the sample directly mounted onto microscope stubs using carbon tape. If the sample was seen to be charging when viewed, the sample was removed and carbon coated using the same procedure as above. It was then observed using the same equipment as above.

For non-biological samples (commercial catalysts, GDEs), the samples were cut to required size (2.5 cm × 0.5 cm) or selected (if powder) and mounted onto microscope stubs using carbon tape and super glue. For thickness measurements and side views of GDEs the samples were mounted perpendicular to the microscope stub. The samples were then analysed using the same equipment as above.

3.7.3 STEM

In preparation for scanning transmission electron microscopy (STEM) and transmission electron microscopy (TEM), the Pd-SCEBs and Pd-planktonic cell samples were immersed in a 2.5% glutaraldehyde solution for one day. A secondary fixation was conducted in 1 % Osmium Tetroxide for 1 hour in order to 'dye' the sample (if precise EDX spectra were required this step was skipped). The samples were then dehydrated using 50 %, 70 %, 90 % and 100 % alcohol in 2×15 mins steps for each concentration. Two further 15 minute dehydration steps were taken in Propylene Oxide. Following dehydration, the samples were embedded in a 1:1 mixture of propylene oxide / resin for 45 min (on a rotator in a fume hood) followed by pure resin for 1 hour (on a rotator in a fume hood). The samples were placed just under the surface of the resin in embedding moulds, a vacuum was pulled for 30 min and then the sample was allowed to return to atmospheric pressure (if necessary the samples were orientated accordingly). The resin was cured at 60⁰C for at least 16 hours. The blocks produced were trimmed with a glass knife. A microtome was used to take 1µm sections for light microscope examination. The slides were mounted and stained with toluidine blue. For STEM use, the samples were cut into ultra thin section. A diamond knife was used to obtain ultra thin sections (50-150nm) and the sections were collected on Electron microscope grids (Formvar film/ carbon coat). A stain of uranyl acetate and lead citrate was then added. The samples were examined using the Jeol JSM-7000f FE-SEM with Oxford Inca EDS, wave WDS and crystal EBSD.

3.7.4 Catalytic activity and durability testing

The catalytic activity and durability of the planktonic cell and immobilised bio-Pd/cell catalysts were assessed using the hydrogenation of dimethylitaconate (DMI) to dimethyl methylsuccinate. A custom made shake flask of 25 mL volume was used to hold 15 mL of 0.08 M DMI solution. The 36 mg of immobilised bio-Pd/cell (mounted on glass slides following preparation procedure shown

earlier), 36 mg of 2.5 % planktonic cell bio-Pd/Cell and 18 mg of 5 % planktonic cell bio-Pd/cell were added to the separate solutions and reaction vessels. The reactor was purged with Nitrogen (20 mins) and hydrogen was introduced at 100 mL.min⁻¹ (constant through reaction). The reactor was shaken by a rotary shaker to apply gentle agitation and the temperature was kept constant at 25 °C. Samples of 0.5 µL were taken at regular intervals (initial experiments of ½ hour intervals, catalytic degradation tests 1.5 hours) throughout the course of the reaction. Gas Chromatography was used to assess the change in DMI concentration and the emergence of the two isomeric products. The samples were injected into a 30 m×0.25 mm×0.25 µm film thickness Gamma DEX™ 225 capillary column. (injection port: 175°C: detector 180°C; column oven: initial temperature 80°C, ramp at 3°C.min⁻¹ to 140°C.min⁻¹, head pressure 15 psig, split ratio – 90/1).

3.7.5 Conductivity

The conductivity of immobilised catalyst films was assessed for suitability to PEM fuel cell applications. Numerous samples were tested with or without additives as fabricated via procedures shown earlier. A Solartron (1400 cell test system) potentiostat was used to produce I/V plots in view to obtain resistance values at distances of 2.5 cm, 2 cm, 1.5 cm, 1 cm and 0.5 cm between electrical connections whereby the temperature was kept constant (25°C). The scan rate was 0.1 V every 30 seconds with a 30 second resting period between voltage steps over a potential range of 0-1 V. The plots produced were analysed and compared to blanks (such as Toray paper). Resistance values were obtained ($R = V / I$) at each distance. Resistivity (ρ) was then calculated using the Equations below and conductivity (σ) values were obtained.

$$\rho = R \times (A / l) \quad (2)$$

$$\sigma = 1 / \rho \quad (3)$$

3.7.6 Single cell Electrochemical Evaluation

3.7.6.1 Fabrication of test MEA

4×4 cm² section of samples, commercial (0.5 mg Pt.cm⁻² E-tek) GDEs and 5×5cm section of Nafion[®] membranes 212 were cut by using a craft knife. The three sections were positioned so that the Nafion[®] membrane was sandwiched between the two GDEs with the catalyst layers turned inward to the Nafion[®] Membrane. The three sections were hot pressed together using a hydraulic hot press at 500 psi with a temperature of 120⁰C for 1 minute. This produced an MEA with anodic and cathodic active area of 16 cm².

3.7.6.2 Single Test cell set up

The pre-prepared MEA was positioned inside a single cell hardware [Paxitech FCT-50s (see appendix section 10.3.2 for images)] with the anodic GDE orientated to the hydrogen inlet. A thin polymeric gasket was positioned between the MEA and bipolar plate on either side of the MEA. The tension bolts were tightened to a torque of 5 N.m. The hydrogen inlet was set to a pressure of 2 bar with a humidifier temperature of 55⁰C and a line temperature of 55⁰C. The Oxygen inlet was set to a pressure of 2 bar with a humidifier temperature of 55⁰C and a line temperature of 55⁰C. The stoichiometry was set to 2:1 (H₂:O₂). The cell was left so gas pressure settled and the cell was also inspected for gas leaks. The MEA was then activated by holding at a constant cell voltage of 0.6 V (with a variable load) overnight or until current produced became stable.

3.7.6.3 Experimental running

In this experiment, cell voltage (V_{cell}) vs. current density (i) and power (P) curves were obtained. The system (Paxitech FCT-50s, as described in section 3.7.6.2) was set to a voltage scan rate of $1 \text{ mV}\cdot\text{s}^{-1}$ with data points collected every 0.003 V over a range on $0\text{-}1 \text{ V}$.

Chapter 4 - Biofilm and Planktonic cell Metallisation and Reactions

4.1 Biomineralisation of Spin Coated Biofilms

The first objective of this investigation was to produce biofilms *via* the spin coated fabrication technique³² and analyse the films under environmental scanning electron microscopy (ESEM). Figure 14 shows that the spin coated biofilms retain the same characteristic flow channels (highlighted by the black arrows) that are seen in naturally grown biofilms. The importance of using the spin coated biofilms is due to the time constraint during manufacture. Naturally grown Biofilms can take up to 21 days to mature, a time length which is simply unfeasible in commercial applications. However, spin coated biofilm can reach maturity within 7 days. This is due to the drastically reduced time associated with initial surface attachment. This reduced growth time allows for the use of biofilms to be used commercially and it was therefore essential they exhibited the same flow channel structure as shown in Figure 14.

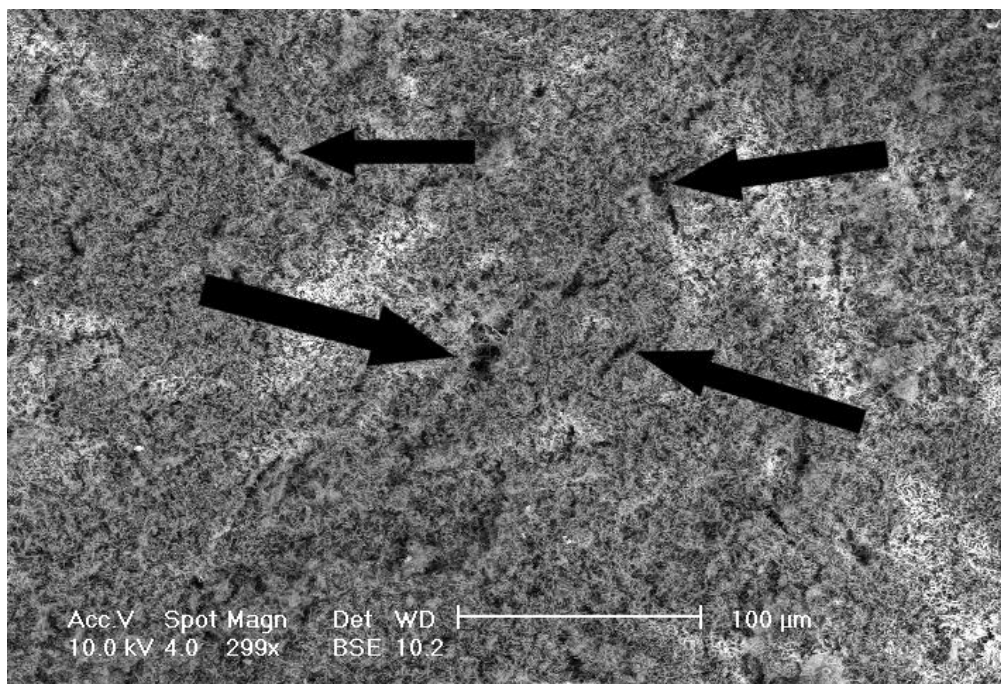


Figure 14 - ESEM image of Spin Coated Biofilm. Black arrows show Flow channels.

The next step in the experimental work was to investigate whether the same biomineralisation could be demonstrated in Biofilms as for that in planktonic cell bacteria. The first experiments concentrated on the biological production of Pd nanoparticles. Figure 15 shows a 5 % bio-Pd w/v biofilm. The image clearly shows the deposition of Pd within the film. However, it can also be seen that the deposition occurs on the extracellular polymeric substance (EPS) rather than on the membranes of the bacteria.

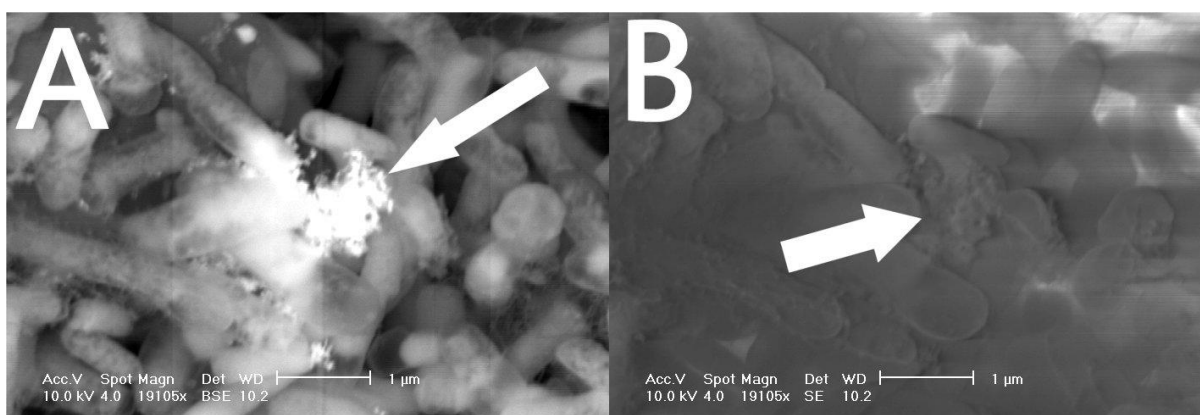


Figure 15 - A. BSE ESEM image of 5% Pd Biofilm, white vector shows Pd particle formation. B. ESEM image of the same 5% Pd Biofilm, white vector shows the area of Pd deposition to be on the EPS.

The deposition on the EPS produced by the cells can be seen by comparing the BSE ESEM (Figure 15, A) and the normal ESEM images (Figure 15, B). In the BSE ESEM Image (Figure 15, A) the Pd particles are highlighted due to the greater scattering effect of the Pd atoms. The normal ESEM image (Figure 15, B) shows the surrounding environment without the highlighting effect and by comparing the images it can be seen that the particles form on the EPS. The EPS is generated by the cells and physically stabilises the cells to the biofilm¹¹⁵. These images show that Pd deposition had not occurred throughout the film (Figure 15). It is also important to note that the deposition of Pd has not affected the flow channel structure of the biofilm as is observed in Figure 16.

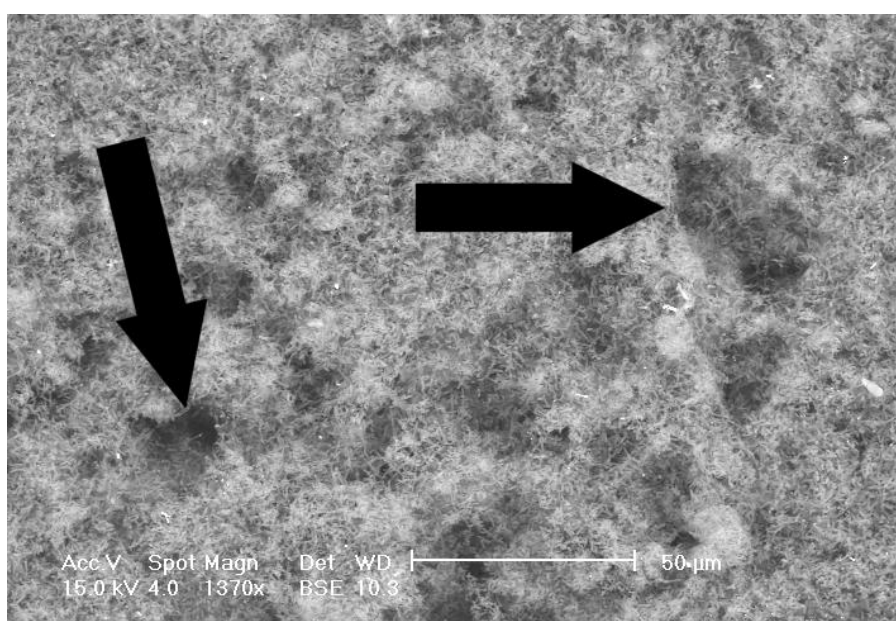


Figure 16 - ESEM image of a 5% Pd Biofilm, Black vectors point to Flow Channels.

4.2 “Pre-treated” biofilm biomineralisation.

To overcome the problem of the Pd deposition occurring on the EPS and therefore leading to an uneven distribution and aggregation of particles (Figure 15), it was decided to pre-treat the cells. The cells were ‘pre-treated’ with a small amount of Pd before biofilm formation providing nucleation

points for further biomineralisation. These films were then analysed via ESEM and as shown in Figure 17. From the figure, it can be observed that the deposition occurs on the membrane of the cells and not in the EPS.

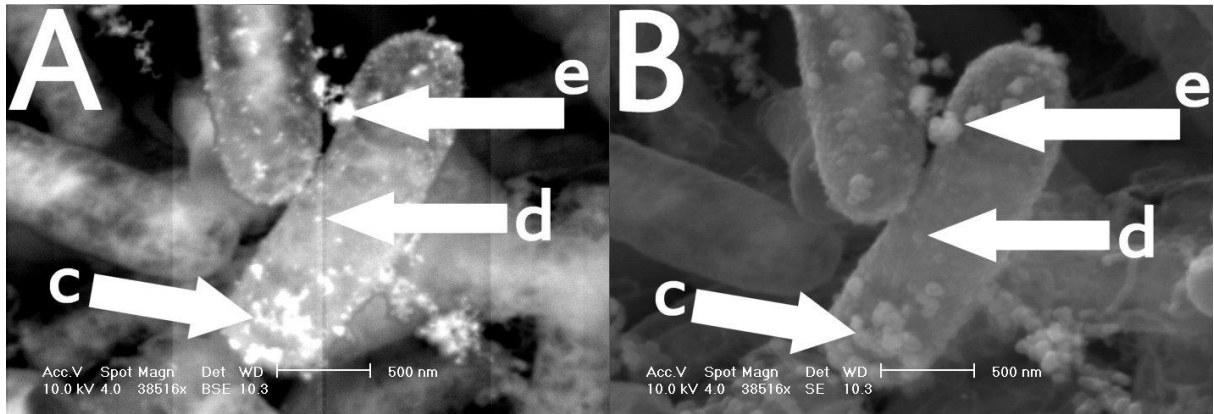


Figure 17 - A. BSE image of 5%w/v Pd biofilm showing Pd particles deposited on cells surface, white vectors show Pd deposits (c, d & e). B. BSE image of 5%w/v Pd Biofilm showing position of Pd particle deposits, white vectors show particle position (c, d & e).

It can also be observed from Figure 17 that a variety of particles sizes are produced on the surface of cells. Deposit (e) shows the largest particle size with the smallest identifiable particle highlighted as (d).

To locate exactly where the particles are deposited and to gain further information on the particle size, scanning transmission electron microscopy (STEM) was used to produce exact images of single cells. Figure 18 A shows the BSE STEM image and Figure 18 B the normal STEM image of the cells and deposited palladium nanoparticles.

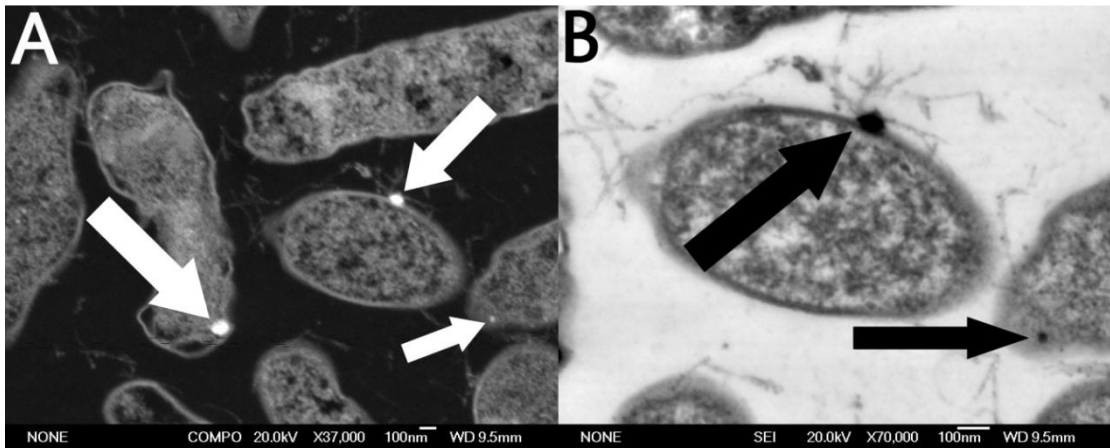


Figure 18 - A. BSE STEM image of 5%w/v Pd biofilm. White arrows show Pd particle deposits on surface of cells. B. STEM image of 5w/v Pd biofilm. Black arrows show position of deposits on surface of cell.

It can be observed that the particles size varied between approximately 20 nm and 50 nm in diameter, agreeing with previously reported work.¹⁰⁴ *In situ* EDX spectra were then produced (Figure 19) to show the exact make up of the nanoparticles. Unfortunately the lead staining used to provide clear images of the particles and biomass means that the EDX spectrum is dominated by its signature. However, the presence of palladium can still be detected. These images and spectra combined clearly show the deposition of palladium nanoparticles on the surface of the bacterial cells within the biofilm.

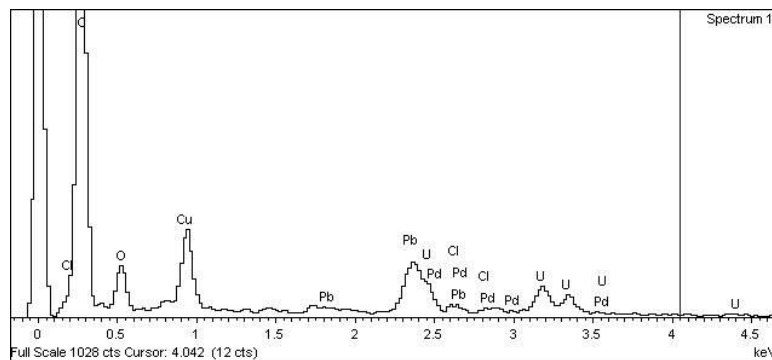


Figure 19 - EDX spectrum of 5% Pd biofilm

For comparison purposes, STEM and ESEM were also conducted on Pd particles produced by planktonic cells. It can clearly be seen by comparing Figures 20 and 21 with Figures 17 and 18 that the crystals formed in planktonic cell and biofilm conditions are of similar size and are deposited within the same periplasmic space and surface of the cells.

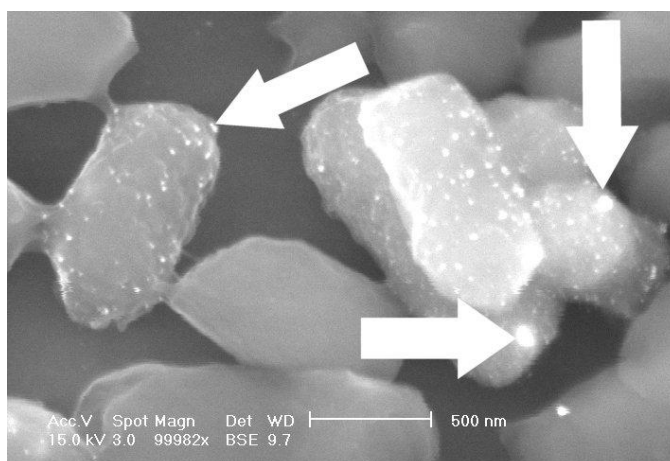


Figure 20 - BSE ESEM image of 5% Pd planktonic cell bacteria. White arrows show Pd deposits.

With a similar particle size of around 20 nm, it is expected that the catalytic behaviour seen in planktonic cell supported bio-catalysts will also be seen in biofilm supported catalysts. Although this particle size is much larger than commercial catalytic nanoparticles used for PEM fuel cells it is thought that the size of particles deposited can be controlled through the time scales used for biomineralisation. For example, it is thought that shortening the time allowed for the reduction of Pd may produce smaller Pd particles.

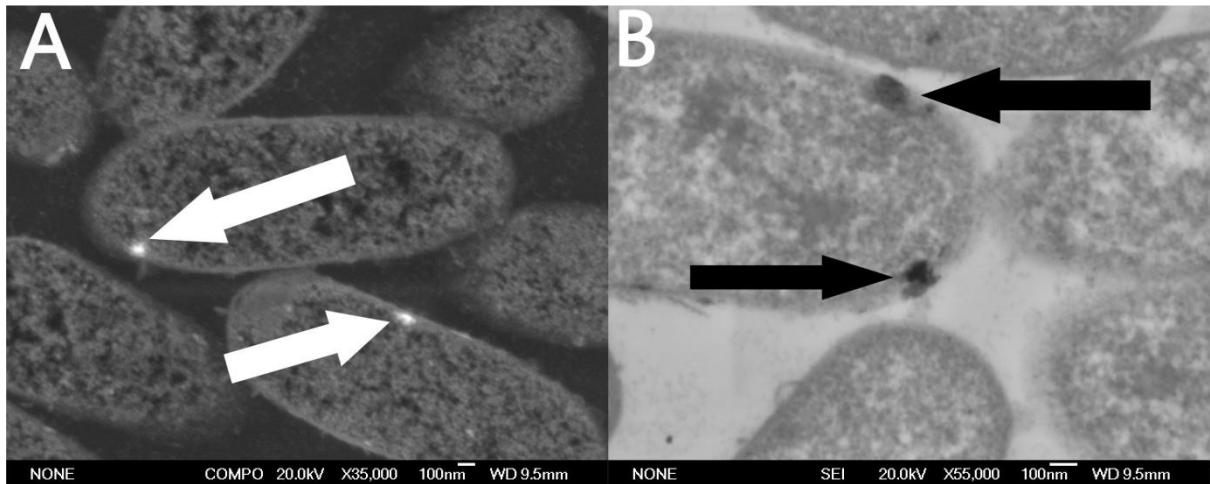


Figure 21 - A. BSE STEM image of 5%w/v Pd Planktonic cell bacteria. White vectors show Pd particle deposits on surface of cells. B. STEM image of 5w/v Pd Planktonic cell Bacteria. Black vectors show position of deposits on surface of cells.

It is interesting to note that little change in the characteristics of palladium biomineralisation between the planktonic cell and biofilm bacteria. When undergoing biofilm formation, bacterial cells behave differently from planktonic cells of the same strain. Biofilm formation is normally due to a response to environmental pressures which normally causes a phenotypic shift in cell behaviour and different gene responses.¹¹⁶ It appears that the gene response producing the specific Hydrogenase enzyme involved in PGM biomineralisation is unaffected by the formation of biofilm and the phenotypic shift in this strain of *E.coli*.

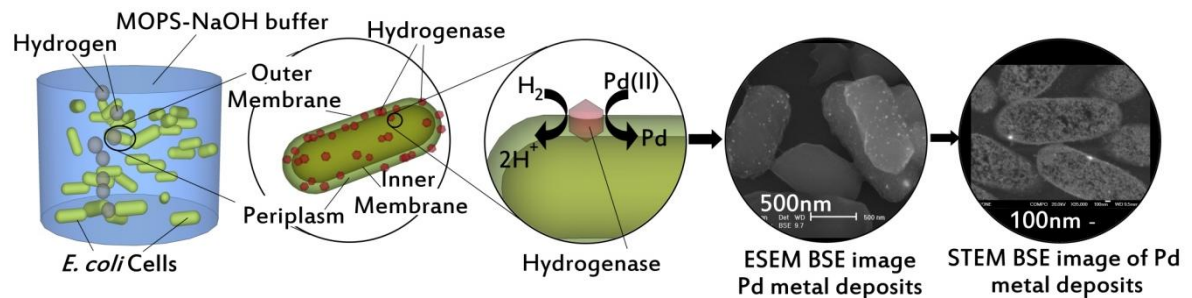


Figure 22 - Hydrogenase reduction mechanism. James Courtney©

The lack of significant change in the deposited particles (both in dispersion and particle size) shows that the mechanism for biomineralisation (shown in Figure 22) for planktonic cell bacteria is unaffected by the formation of biofilms. Of primary importance is that the biomineralisation of bacteria can occur in both planktonic cells and biofilms.

4.2 Platinum deposition

Pt deposition is of much keener interest for PEM fuel cell applications due to its much higher catalytic activity and higher exchange current densities generated then for Pd based systems. Figures 23 and 24 show the deposition of Pt nanoparticles within the biofilm.

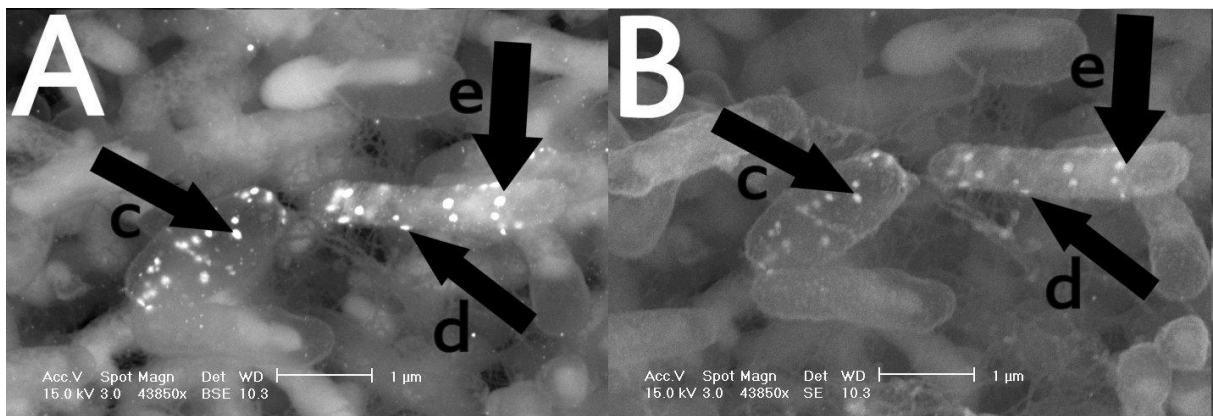


Figure 23 - A. BSE ESEM image of 5%w/v Pt biofilm. Black arrows show Pt particle deposits on surface of cells (c, d & e). B. ESEM image of 5w/v Pt biofilm. Black arrows show position of deposits on surface of cell (c, d & e).

Figure 24 also shows a protrusion into a flow channel which has significant deposits of Pt, highlighted in white due to the BSE image. Figure 25 shows that the characteristic structure of the biofilm is unchanged from the natural, or Pd biofilm and the existence of interconnected flow channels remain.

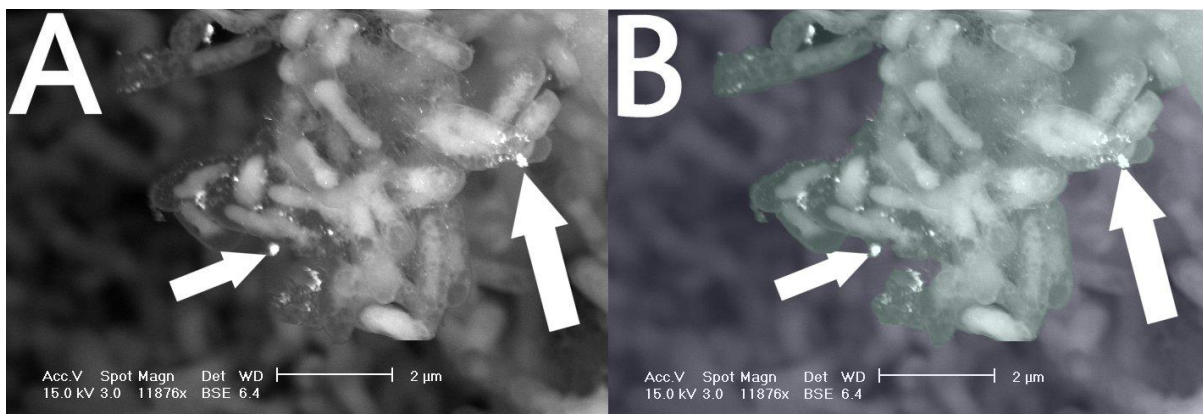


Figure 24 - A. BSE ESEM image of 5%w/v Pt biofilm. White arrows show Pt deposits. B. BSE ESEM image of 5%w/v Pt biofilm. White arrows highlight position of Pt particles. A. Additional colouration has been added so that the protrusion into the flow channel can be observed.

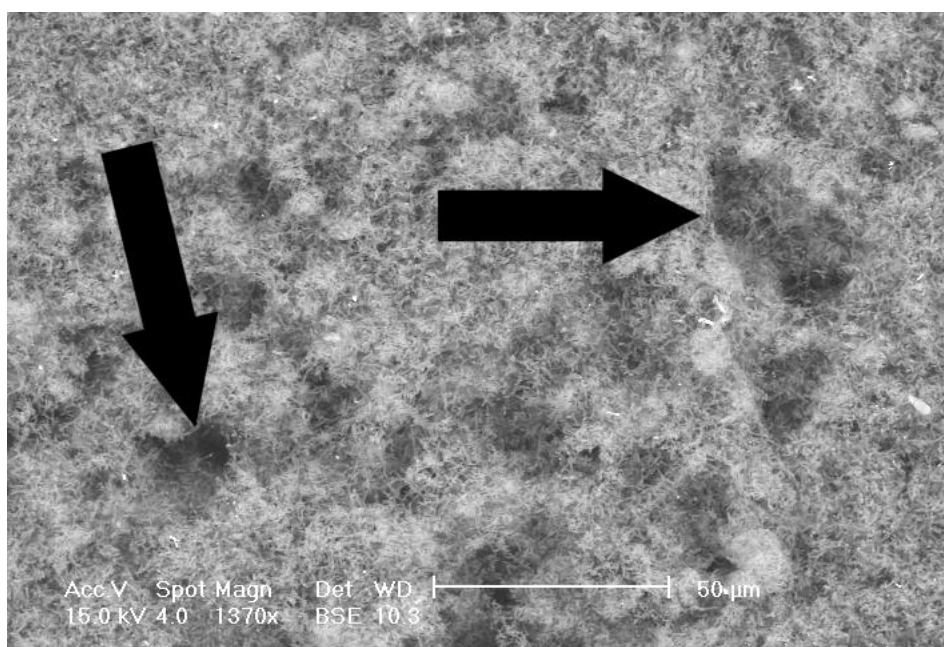


Figure 25 - ESEM image of 5% Pt biofilm. Black arrows highlight Flow channels within the biofilm structure.

In situ EDX spectra were taken under areas of observation in ESEM investigations (Figure 26) showing that Pt(0) was deposited on the surface of bacterial cells within the biofilm.

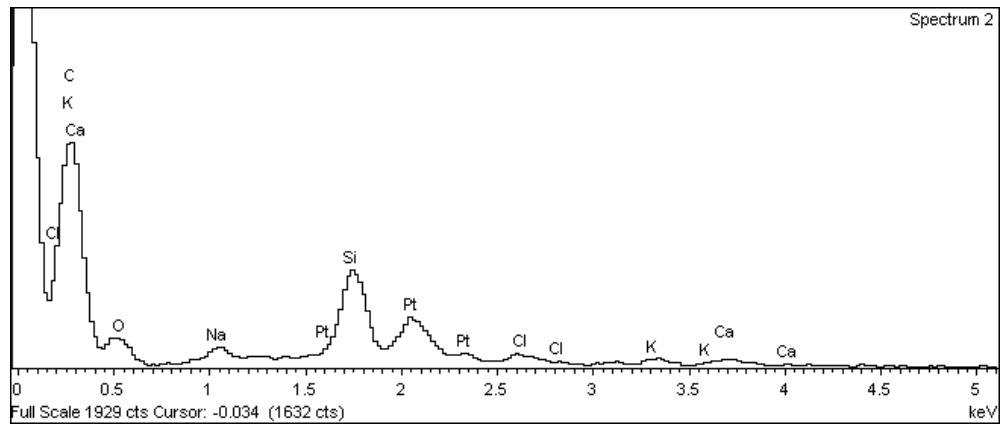


Figure 26 - EDX of 5% w/v Pt biofilm.

Thus, it has been clearly shown that both Pt and Pd can be deposited on the surface of bacterial cells within the biofilms in a similar way to that of planktonic cell bacteria using a slightly adapted technique. It has also been observed that the biofilms retain their flow field structure when either PGM is deposited.

Chapter 5 - Suitability for Fuel Cell Use

5.1 Conductivity Experiments

Having demonstrated that biofilms can be produced with an even dispersion of PGM nanoparticles, the films were tested for suitability as PEM Fuel cell catalyst layers. A high proton conductivity could hopefully be achieved with the introduction of Nafion[®] forming an ionomer matrix within the film using the same technique used to promote proton conductivity in plasma aided spray deposition where the layers are dip coated or soaked in Nafion solution.¹¹⁷ This produces catalyst layers similar to that shown in the diagram (Figure 27) of fuel cell construction shown below.

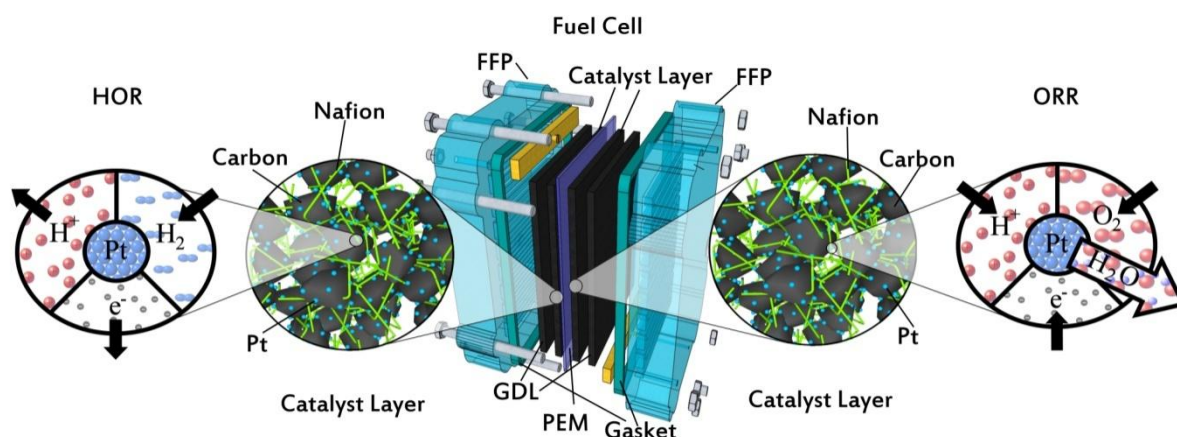


Figure 27 - Diagram of PEM Fuel cell, its components, exploded diagram of catalyst layer, its constituent parts and schematic of the HOR and ORR. James Courtney©

Unfortunately during the experiments, it was found that the biofilms were not conductive, as shown in Figure 28. The measurement technique used was designed to provide simple data on the conductivity of the slides. By recording data the current response to a voltage change, at several

different distances this data could be used to calculate a resistance value at variable distances. This could then be combined with cross sectional area to give conductivity values for the material.

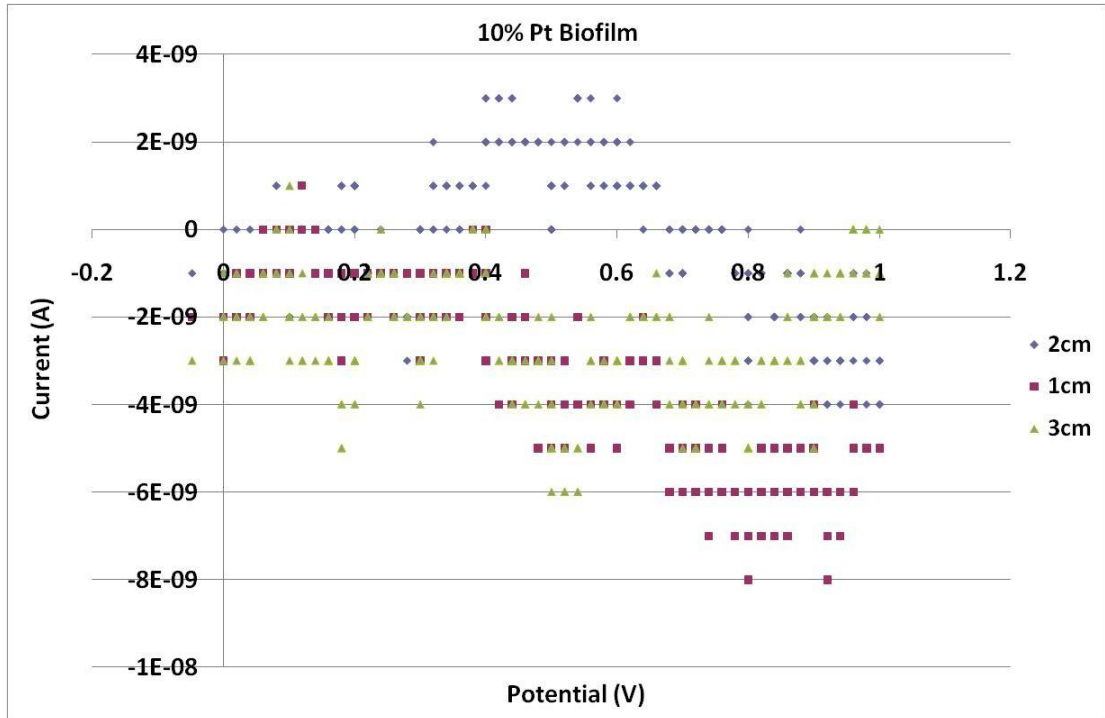


Figure 28 - Conductivity measurements of 10% Pt Biofilm.

However, the only current response observed was due to the internal 'noise' generated by the experimental equipment used in the measurement (Figure 28). Because of this, the films were placed in a humidified atmosphere 'mimicking' real case scenarios in a PEM fuel cell environment. A slight increase in conductivity was observed (Figure 29) but the value of the current response was small and due to the presence of surface water.

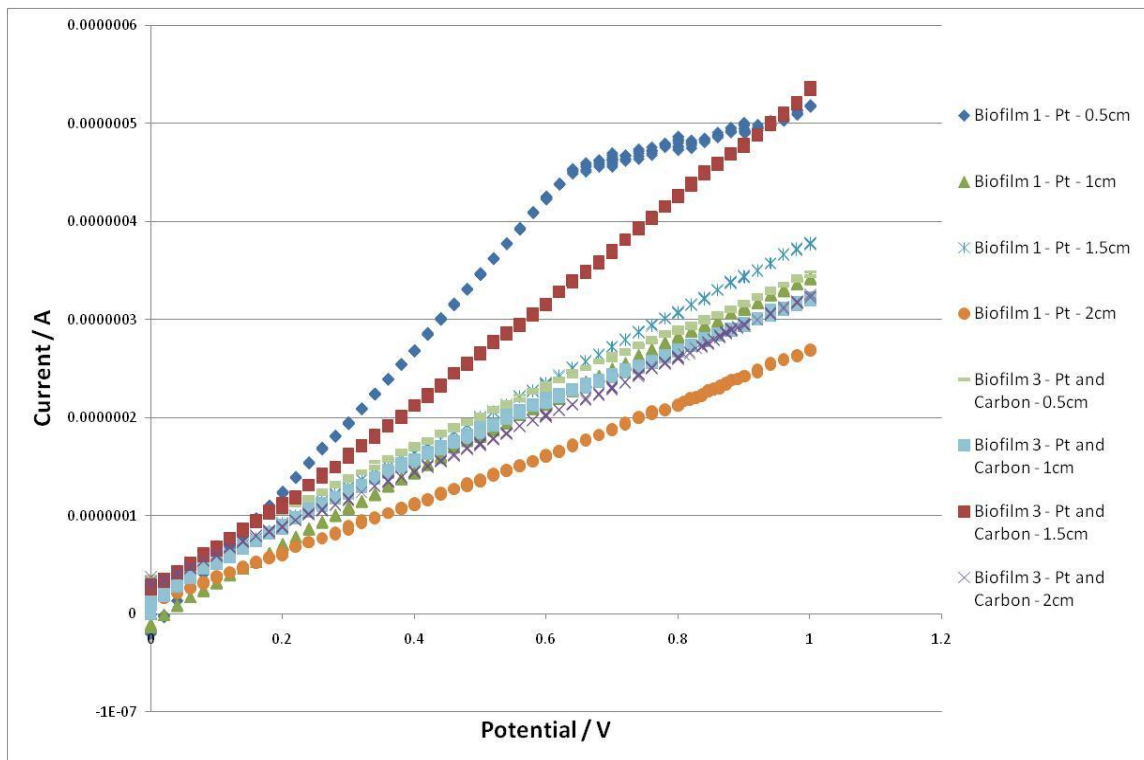


Figure 29 - Conductivity I/V plot of Pt Biofilms and carbonated Pt biofilms.

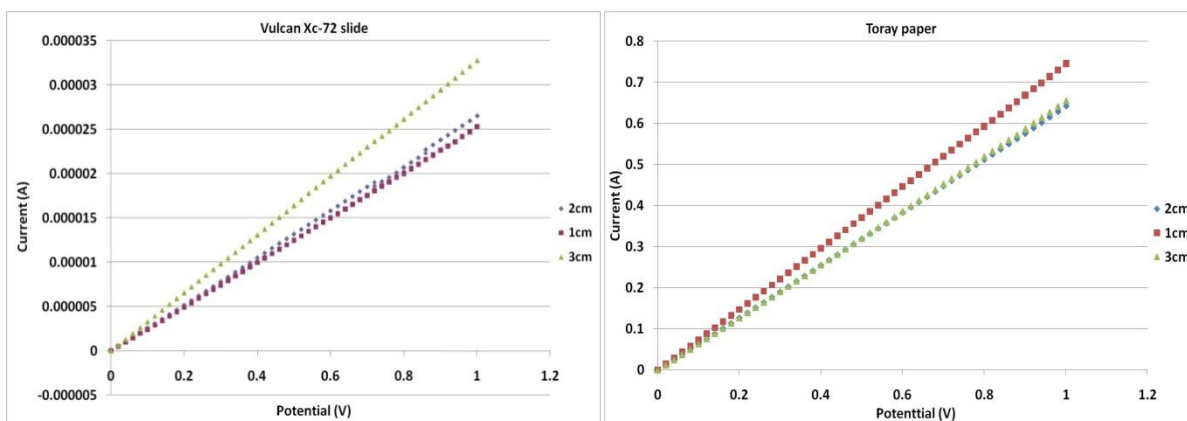


Figure 30 – I/V curves for prepared Activated Carbon slide (Vulcan Xc-72) and Toray Paper.

To verify that our observations were not due to experimental errors, a slide was prepared from activated carbon (Vulcan Xc-72) and I/V curves were generated (Figure 30). Sections of Toray paper (Carbon Paper) were also cut to sizes of the films and tested (Figure 30). These slides and sections of Toray paper generated almost ideal I/V curves for conductive materials, demonstrating our experimental set up was accurate. The observed nature of the biofilms was expected as it has been

shown previously that the biomass left when the bacteria are processed is non-conductive. For PEM fuel cell applications, the biomass would really need to be conductive. There are several reported methods to increase the conductivity of bacterial biomass, the primary method is the use of conductive additives.

5.2 Carbon additives

The first objective of this work was to observe whether additives would inhibit the formation of biofilms or the deposition of PGM nanoparticles. As such, carbon black (Vulcan XC-72R) was used as a potentially conductive additive. Various concentrations of carbon black in water were added to the initial growing media of the biofilms to demonstrate if incorporation into the films could be achieved. Figure 31 shows the incorporation of carbon particles within the biofilms.

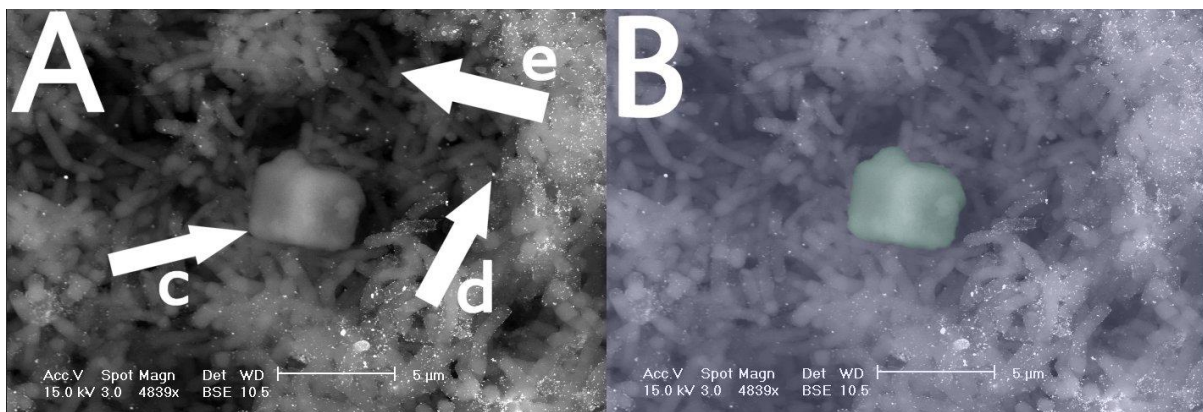


Figure 31 - A. ESEM BSE image of 25% w/v Pt carbonated Biofilm. White arrow c shows carbon particle. White arrow d shows Pt particle. White arrow e shows existence of Flow Channels. B. Colourised ESEM BSE image of 25%w/v Pt Biofilm to highlight carbon particle position.

It can be observed in the ESEM images [Figure 31, white arrow (e) and Figure 32] that the overall structure of the biofilm is unaffected and the interconnected flow channels can still be seen and have not collapsed. It can also be seen in Figure 31 [white arrow (d)] that the deposition of Pt nanoparticles still occurs at the surface of the cells and not on the carbon particles.

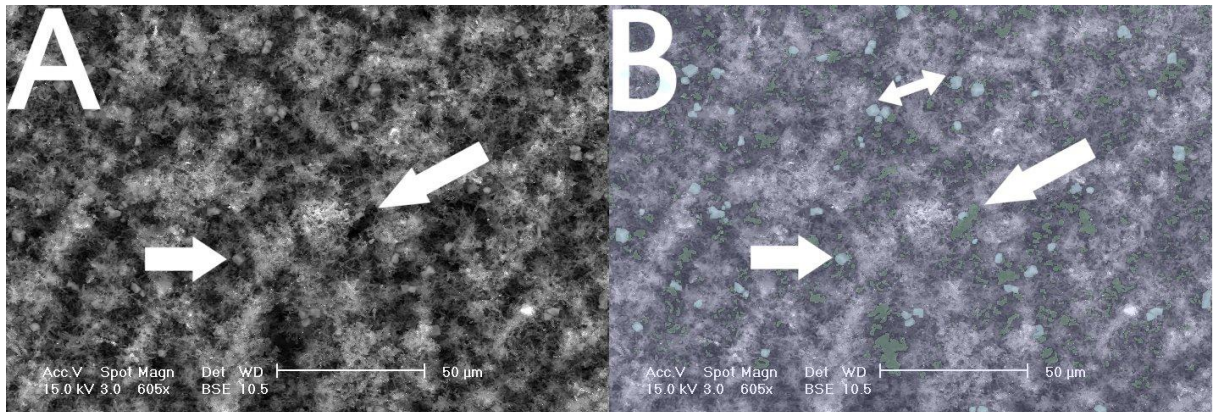


Figure 32 - A. ESEM BSE image of 25%w/v Pt carbonated Biofilm. White arrows highlight position of carbon particle and flow channel. **B.** Colourised ESEM BSE image of 25%w/v Pt Biofilm to highlight carbon particle position (highlighted blue) and flow channel existence (highlighted green) White Vectors show position of carbon particle, flow channels and distance between carbon particles.

However, when the conductivity of the films was tested, the films were not conductive (Figure 29 and 33) and no improvement was observed over the original biofilms, again this is not surprising. It can clearly be seen from the ESEM images (Figures 31 and 32) that the carbon particles are not evenly distributed throughout the film in high enough concentration to provide conductive pathways throughout the layer. At higher concentrations of carbon black, whilst in the biofilm growth phase, the carbon particles simply inhibited the attachment of bacteria to the substrate, either by blocking 'adhesion' of cells to the surface or by impacts between particles dislodging cells already attached.

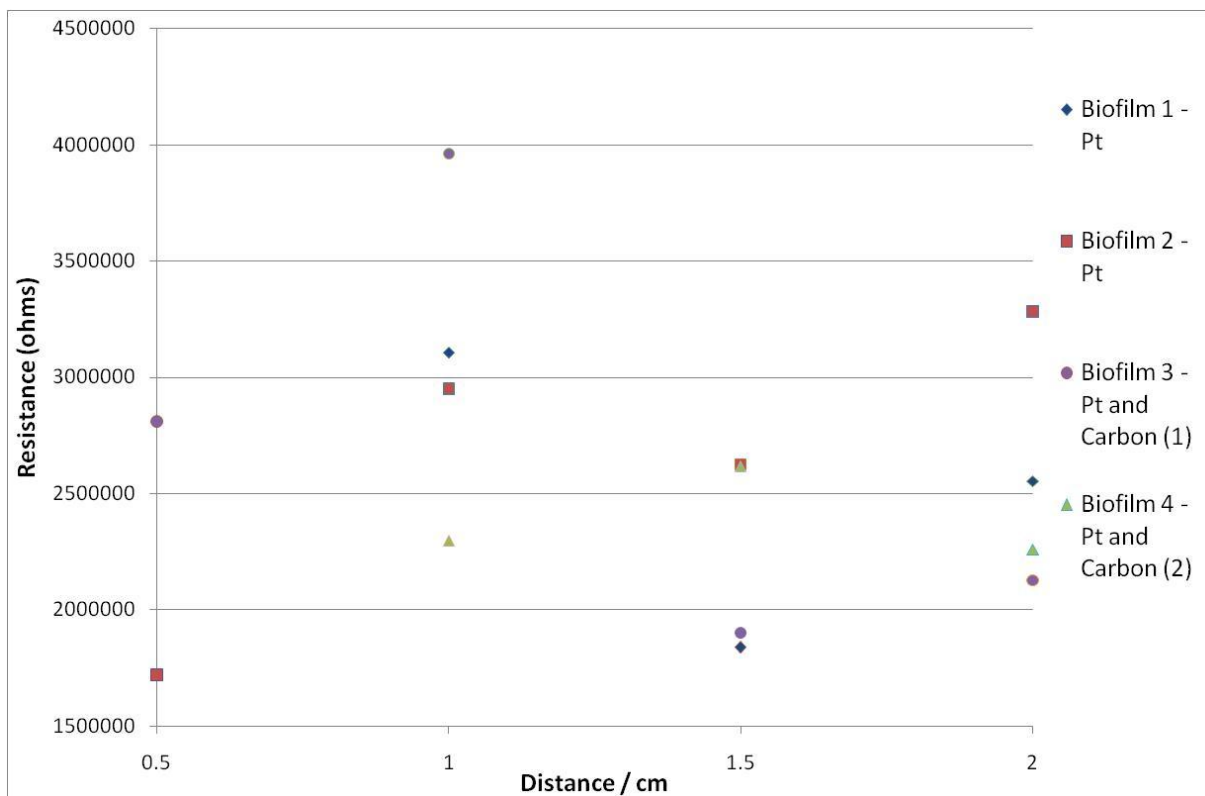


Figure 33 - Resistance Vs Distance plot for Pt Biofilms and Carbonated Pt Biofilms.

It has been reported that with the addition of carbon nanotubes (CNTs) the conductivity of biomass can be increased.¹¹⁸ As such, it was decided to use and include CNTs within the biofilms. Unfortunately suspending the CNTs whilst also growing biofilms proved to be difficult due to the aggregation of the CNTs in the absence of sonication and films incorporating CNTs were unable to be produced for testing.

The non-conducting properties of the biofilms present a major obstacle to their application as catalyst layers for PEM Fuel Cells. However, the demonstrated ability to directly recover PGM bio-catalysts directly into a layer structured with interconnected flow channels has many potential applications and is still very appealing for use within the fuel cell sector.

The use of additives introduced into biofilms requires further research and development. One of the primary advantages of biofilm use is the reduction in processing required and the reduced cost. The use of additives increases the steps required in fabrication and depending on the additive used, could vastly increase the cost. However, the benefit of catalyst recovery and reduced processing over planktonic cell recovery processes still holds vast potential especially for PEM fuel cell use.

Chapter 6 - Catalytic Activity Testing

6.1 Hydrogenation of Dimethyl Itaconate

After initial investigations into the application as PEM fuel cell catalyst layers, it was decided to investigate whether the Pd nanoparticles retain their catalytic activity inside the biofilm. The difference in catalytic activity compared to the planktonic cell supported Pd and whether another application could be seen was of significant interest. The hydrogenation of dimethyl itaconate is a reaction of high industrial importance due to the use of succinic acid derivatives as key intermediates in the pharmaceutical industry, in particular for the production of potent rennin inhibitors.

The hydrogenation of dimethyl itaconate was first used to investigate the different catalytic activity of two 5 % w/v Pd biofilms and two loadings of Bio-pd on planktonic cells (2.5 % w/v and 5 % w/v). The data was used to compare between planktonic cell supported and biofilm bio-catalysts. Figure 34 shows the % conversion vs. time graph for the reaction with the concentration of product increasing. It can clearly be seen that the rate of reaction for the planktonic cell supported catalyst was much higher than that of the biofilm supported catalyst. It is also demonstrated that that both concentrations of planktonic cell catalyst achieve significantly higher rates of reaction than that of the biofilm catalyst.

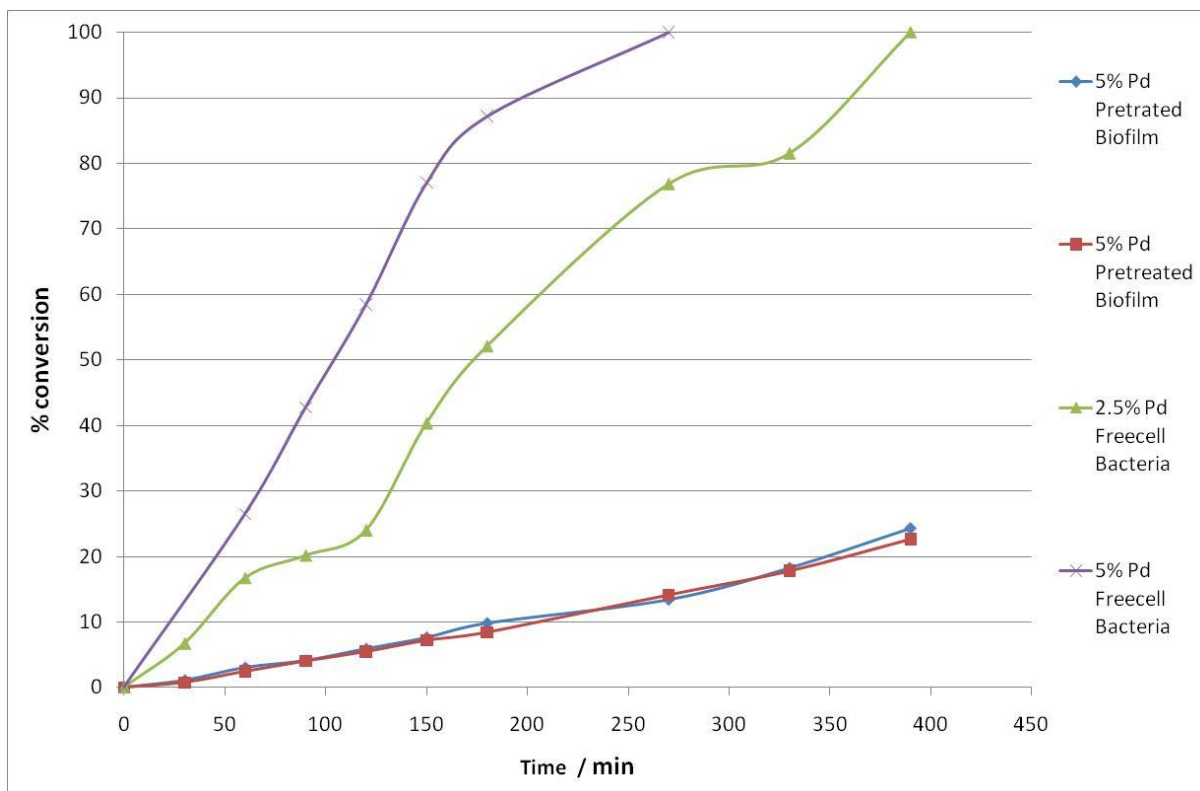


Figure 34 - Conversion Vs Time for planktonic cell and Biofilm Bio-Pd catalysts for the Hydrogenation of Dimethyl Itaconate.

The difference in reaction rates could possibly be due to mass transport effects. In the case of planktonic cell bacteria, there are no significant mass transport limitations, with diffusion through the solution contributing little to the overall rate of reaction. The rate of reaction is rather determined by concentration (as shown by the different rates for different concentration in Figure 34) and the kinetics. However, in the case of biofilms there are significant mass transport limitations that reduce the rate of reaction. As previously described, large amounts of the active catalyst particles are distributed within the biofilm and not just on the surface. This means that the reactants must first diffuse through the biofilm in order to reach the catalytic sites and react. This leads to a significant diffusion limitation on the reaction rate.

However, after the reaction had finished and the biofilms removed and the planktonic cell catalyst recaptured, it was observed that the biofilms were unaffected whereas significant loss had occurred in the mass of planktonic cell suspended catalyst. It was decided to conduct long term catalytic durability tests on the biofilms compared to the planktonic cell supported catalysts. Figure 35 shows that over a series of reactions lasting a total reaction time of 60 hours with 10 reaction batches that the catalytic conversion was maintained between 30 and 36 % for the biofilm supported catalyst. Furthermore, it can be seen that the biofilm has the potential to be used much longer than the implemented test period and batch number but the planktonic cell supported catalyst had a very limited run time due to the catalyst lost during separation (Figure 36). In fact to carry out repeated runs on the same batch of planktonic cell catalyst, the substrate amount had to be adjusted accordingly to keep the same catalyst:reactant ratio.

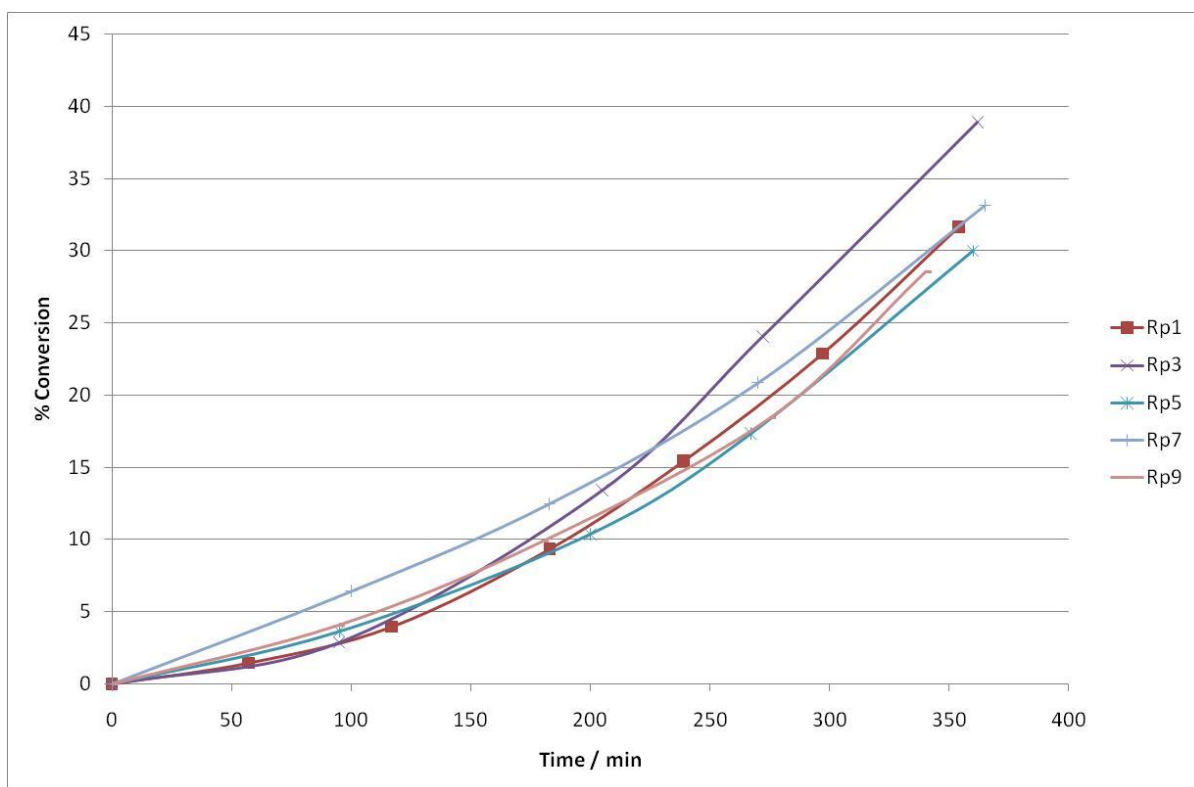


Figure 35 - Conversion Vs Time for Repeated Reactions for the hydrogenation of Dimethyl Itaconate catalysed by biofilm Bio-Pd catalyst.

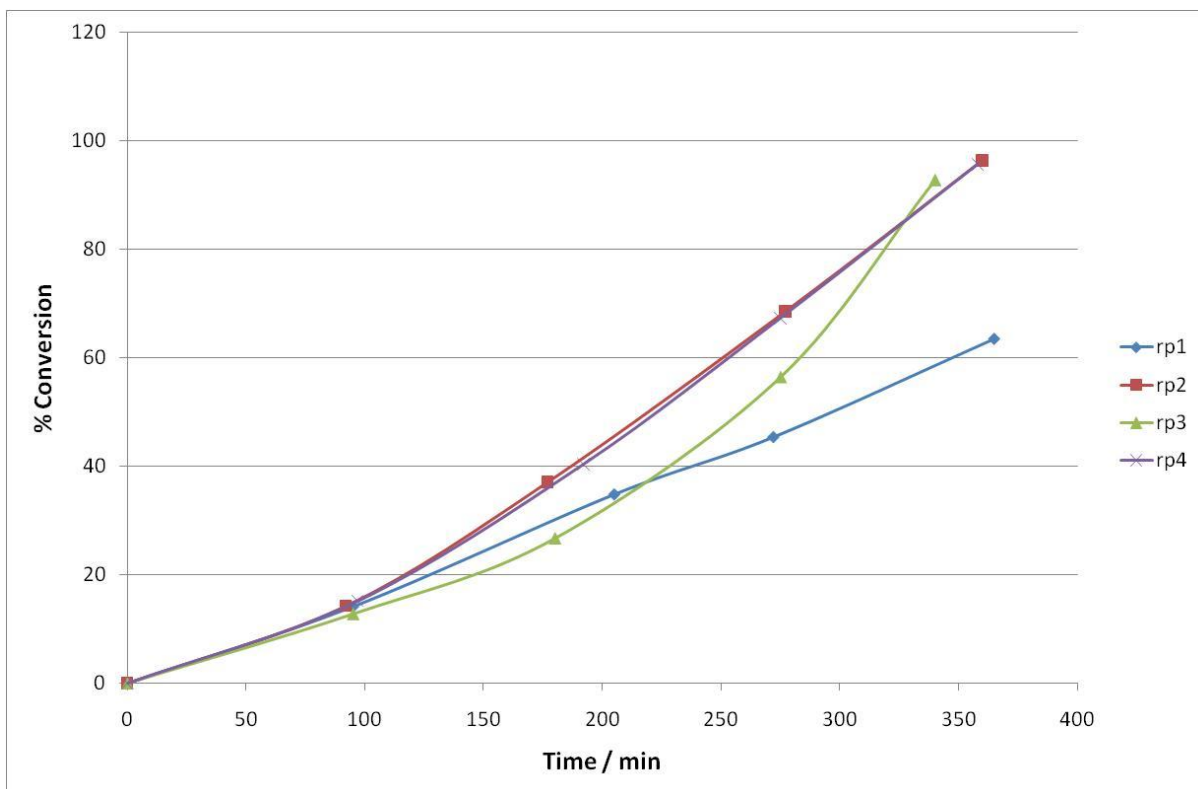


Figure 36 - Conversion Vs Time for repeated reaction for the hydrogenation of dimethyl itaconate catalysed by planktonic cell bio-Pd catalyst.

It is clear from both Figures 35 and 36 that the catalytic activity of both the planktonic cell and biofilm supported bio-Pd catalysts was not reduced during the repeated runs. It can be seen that the Biofilm maintained a steady reaction rate that was relatively low compared to the reaction rate of the planktonic cell supported catalyst. However, it was also shown that there was a large loss of catalyst when separating planktonic cell supported catalysts from the substrate between each reaction run that was not seen with the Biofilm supported catalyst (Figure 37). On average the 5 % w/v planktonic cell biocatalyst lost 12 % mass per reaction and the 2.5 % w/v planktonic cell biocatalyst lost 34 % mass per reaction (see appendix section 10.4.1 for further details). This indicates that, although the biofilm had a lower starting reaction rate, repeated reaction runs could be maintained with the same effective catalyst for longer than planktonic cell supported catalysts. Whereas with the use of planktonic cell supported catalysts complicated separation procedures

would be required and possibly a large amount of fresh catalyst added for each reaction run. This could result in higher cost when utilising the planktonic cell supported catalyst when compared with establishing recycling routes for unused reactants when utilising the biofilm catalysts.

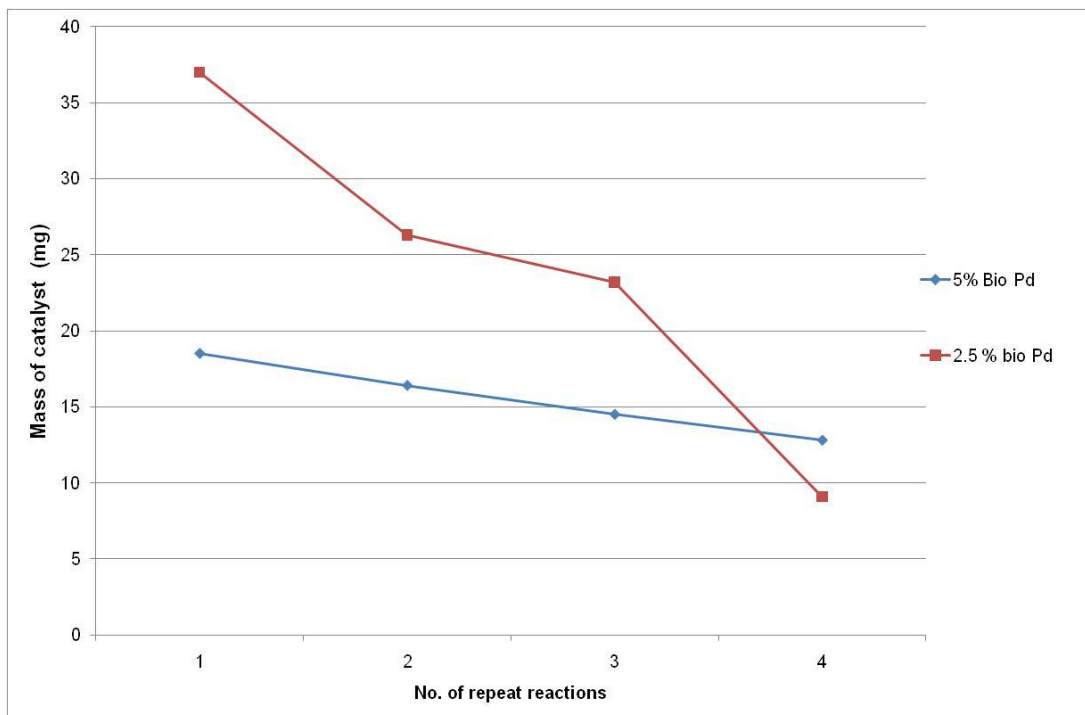


Figure 37 - Mass of Planktonic supported Biocatalyst Vs No. of repeated reactions

6.2 Degradation Characterisation

Having conducted experiments into the catalytic activity degradation of the biofilms and the planktonic cell supported biocatalysts, it was decided to investigate whether any changes had been caused to the structure of the films or the planktonic cell biocatalysts.

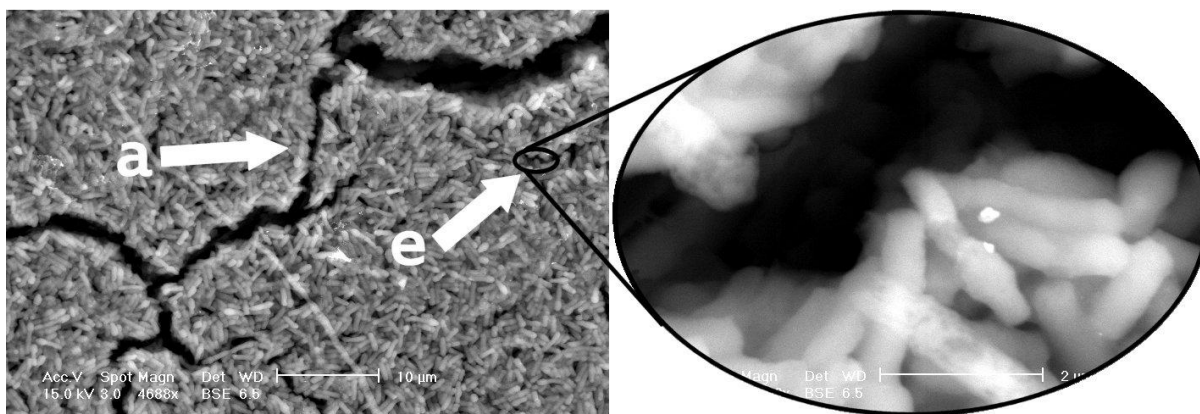


Figure 38 - ESEM of 5%w/v Biofilm after catalytic cycling. Arrow a shows the cracking caused by dehydration. Arrow e shows the retention of flow channels.

Figure 38 shows ESEM images of the biofilms catalysts after use, the figure suggests that although the biofilms have dried and cracked, the overall interconnected flow channel structure of the biofilms remained. It is also shown that the Pd particles have not aggregated or moved from the surface of the bacterial cells (Figures 38 and 39). However, the images produced are not conclusive enough due to their non-pristine nature and due to the cracking thought to be caused by the dehydration step in preparation for the ESEM.

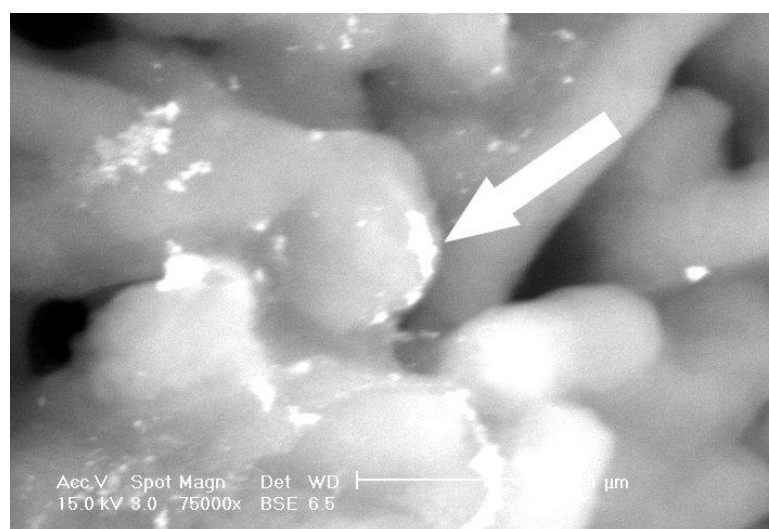


Figure 39 - ESEM BSE image of 5%w/v Pd Biofilm after catalytic cycling. The white arrow shows the Pd deposits intact.

The apparent long term catalytic activity and durability of the biofilms highlight again their potential use as PEM fuel cell catalyst layers as degradation of fuel cell catalyst layers is still one of the main obstacles needed to be overcome for the success of the technology. It also shows that there is an attractive proposition for commercial hydrogenation reactions. Although the overall catalytic rate of reaction is reduced compared to suspended catalysts the removal of the need for a recapture stage during production is an attractive proposition.

Chapter 7 - Screen Printed Bio-Catalyst GDEs for PEM Fuel Cell Use

Previous studies have shown the recovery of PGM nanoparticles through the use of planktonic cell by burning the supporting biomass from the nanoparticles and then reprocessing the catalyst.³¹ As previously stated, the work was brought to an end due to the unreliable technique used to produce GDEs from the nanoparticles. To overcome this issue the screen printing method for the production of GDEs was developed and demonstrated. The same method of burning the biomass was used and the catalysts re-supported on carbon. The supported catalysts and commercial catalysts were then fabricated into GDEs and the characteristics of the catalyst layer produced were compared.

7.1 Development of Screen Printing Technique

Initial experiments were conducted into the volume of ink required to create a completely covered substrate using the supplied screen printer ink (Dek). It was found that an initial volume of 0.8 mL of ink needed to be introduced for the first print. For subsequent prints, the amount of ink required was less due to residual ink on the surface of the screen and squeegees. The cost of the PEM fuel cell catalyst ink is extremely high and as such the amount of ink used was kept to a minimum. However, to keep experimental rigour, after each layer was printed, the screen printer was cleaned and fresh ink administered.

To gain information on maximum amounts of mass deposited, a 'mock' ink was made up using the same activated carbon but without Pt. Figure 40 shows that the concentration of ink has relatively little effect on the mass of the printed layer and that only at the extreme upper and lower

concentrations deviations are seen. It was shown that the mass printed consistently remained within the upper boundary and lower boundary (between 0.00015 and 0.0003 g.cm⁻²). These results indicate that the desired loading required 0.0025 g.cm⁻² Pt/C or 0.002 g.cm⁻² C cannot be achieved with one print and that subsequent prints on the same substrate are required to achieve the desired loading. It was also seen that sweeping the squeegees in one direction led to an uneven ink distribution across the surface. For this reason, each layer was printed in one direction then removed turned 90° and printed over to achieve an even distribution.

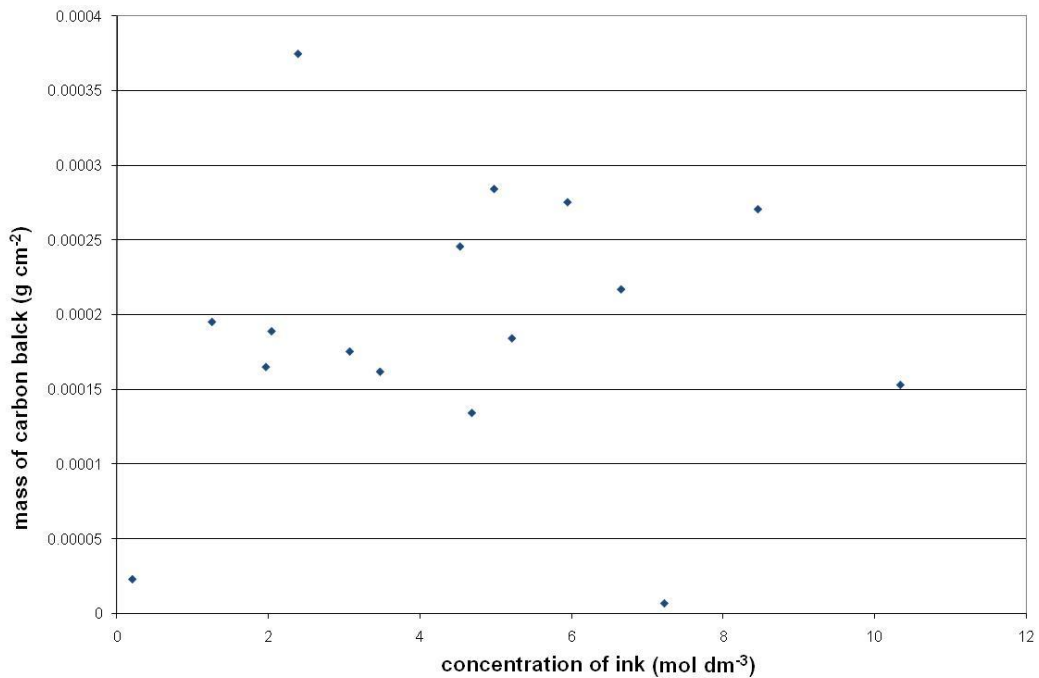


Figure 40 - Concentration of Mock ink Vs mass deposited per centimetre.

It was also found that the vacuum level as supplied on the vacuum bed caused a much higher effective vacuum at the surface of the substrate than was required and had a tendency to pull the Ink from the surface of the GDL into the substrate. Unfortunately, this setting was not adjustable as it is a preset parameter on the screen printing device. To overcome this issue, filter paper was used to

reduce the effective vacuum of the table. Using this method, catalyst layers were produced that 'sat' on the top of the GDL substrate (Figure 41).

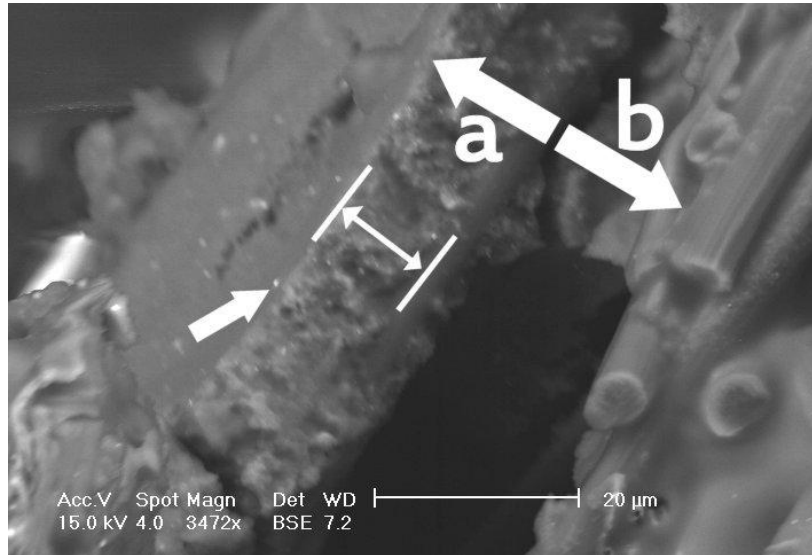


Figure 41 - ESEM image of cut commercial catalyst GDE. Showing catalysts layer (a) and GDL substrate (b)

7.2 Commercial Catalyst Screen Printed GDE

Having developed the screen printing technique, inks were fabricated from commercial fuel cell catalyst, 20 %wt Pt supported on carbon black (Vulcan XC-72R). The screen printing technique was used to prepare GDEs on Toray paper (h-060). Various layers of filter papers were used to determine the amount required to achieve the desired effective vacuum on the surface of the substrate. The ESEM was then used to analyse the GDEs produced and Figure 41 shows the ESEM images of the successful GDEs.

Figure 41 shows that a layer sitting on top of the GDL substrate was achieved with a thickness of approximately 5-10 μm. The image was obtained by cutting through a prepared GDE and positioning the GDE perpendicular to the SEM stub, images were then taken across the cut surface and the catalyst layer was observed on top of the GDL substrate below.

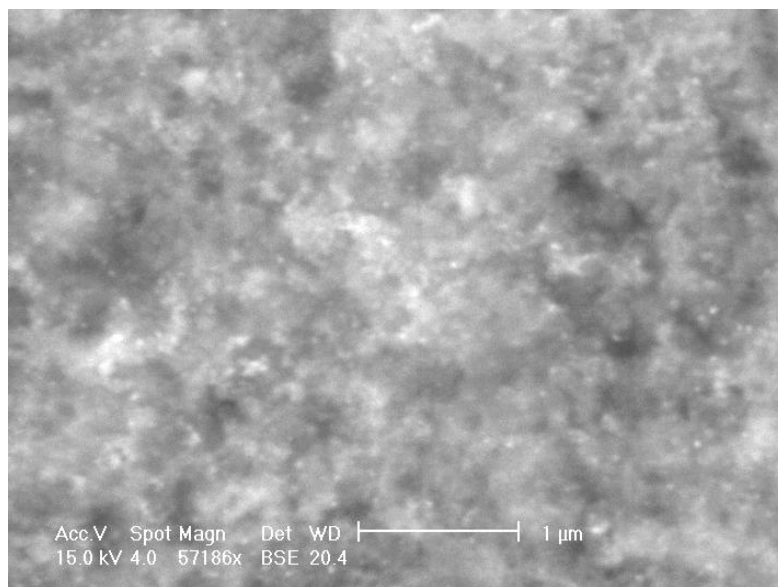


Figure 42 - BSE ESEM image of commercial catalyst GDE showing dispersion of Pt particles across catalyst layer surface.

Figure 42 is a BSE ESEM image and clearly shows an even distribution of nanoparticles was achieved throughout the layer. Figure 43 shows the surface structure of the catalysts and demonstrates the porous nature of the carbon particles forming the support for the Pt nanoparticles. It also shows that each carbon particle is approximately 200 nm in diameter.

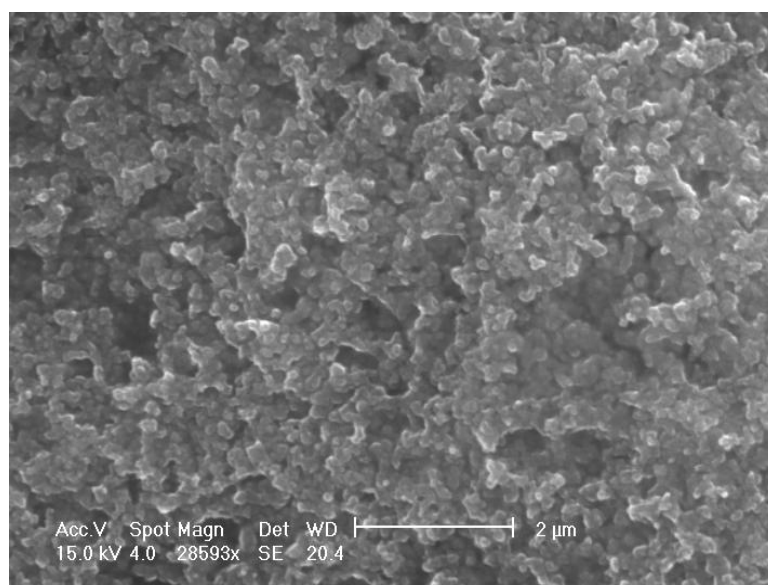


Figure 43 - ESEM image of commercial catalyst GDE catalyst layer surface.

7.3 Bio-Catalyst Screen Printed GDEs

After screen printing the commercial fuel cell catalyst, Bio-Pd based GDEs were fabricated. Bio-Pd was produced supported on planktonic cell bacteria as in prior investigation. To remove the biomass of the planktonic cell support, the powder was ground (as described in the methodology section) and the biomass (principally carbon) was burned at 700°C in an oven open to the atmosphere. The metallic particles produced were supported on the same activated carbon as the commercial catalyst (Vulcan XC-72R) as described in the methodology section. An ink was then formulated in an identical manner as the commercial catalyst and the same preparation via the screen printing technique produced Bio-Pd GDEs.

The Bio-Pd GDEs were examined identically to the commercial catalyst GDEs using ESEM. It is shown that a catalyst layer is printed on top of the GDL substrate, approximately 5-10 µm in thickness (Figure 44). It can be observed that it is of the same thickness as shown with the commercial catalyst GDE (Figure 41), however, these values were difficult to determine, varying slightly across the cut.

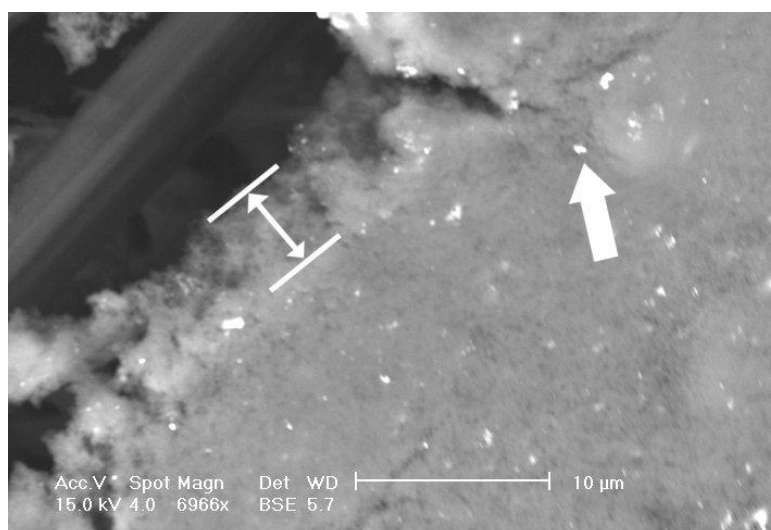


Figure 44 BSE ESEM image of a cut Bio-Pd GDE showing the side view of the catalyst layer and GDL. Showing thickness and white arrow shows Pd Particle.

It is also shown (Figure 45) that an even distribution of nanoparticles could be achieved with the bio-Pd GDE as was demonstrated with the commercial catalyst GDE (Figure 42). Figure 46 shows that the structure of the carbon support is again very similar to that of the commercial catalyst GDE (Figure 43) and that the particle size of the activated carbon was ca. 200nm.

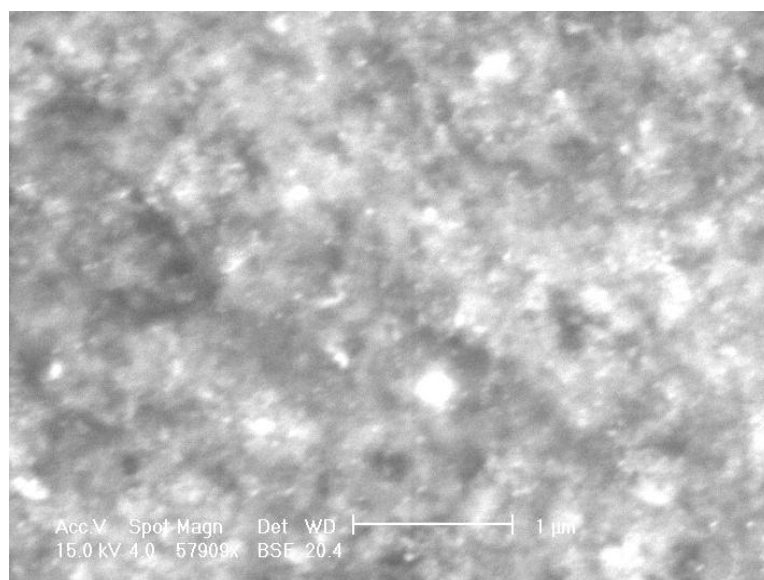


Figure 45 - BSE ESEM image of bio-Pd GDE showing the even distribution of Pd nanoparticles

However, the particle size of the commercial and bio catalyst was different with the biologically produced particles being much larger. The particle size seen was also larger than that observed when the particles were supported on planktonic cell bacterial cells. This indicates that the particle size may have increased during the processing after the biomineralisation process.

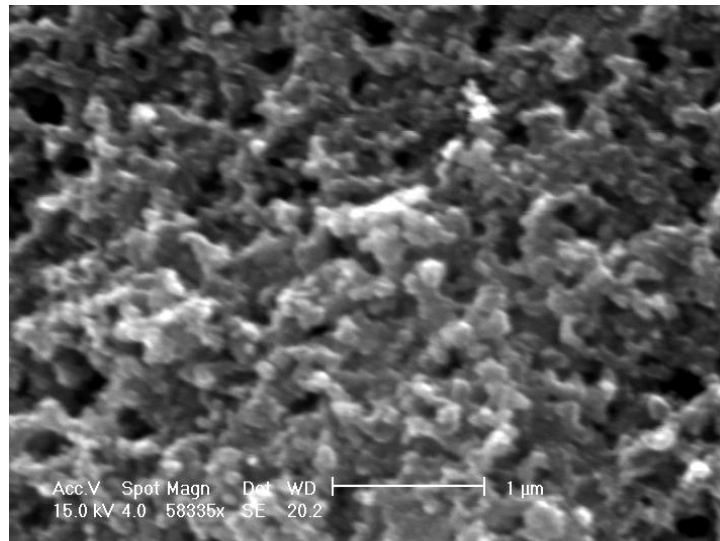


Figure 46 - ESEM image of bio-Pd GDE showing surface of catalyst layer

There are two key areas where this increase in particle size could occur. The removal of the bacterial biomass or the energy introduced to the system and the removal of support in the burning step could cause the particles to aggregate or sinter together causing enlarging of the particle size, as has been seen in previous studies.^{119,120} The second possible reason for the enlargement could occur during the re-supporting of the catalyst particles on the activated carbon. It is a common problem with PEM Fuel Cell catalysts as they tend to aggregate during this process and thereafter whilst on the carbon surface.¹²¹ This problem is largely overcome with the use of steric stabilisers. It has previously been proposed that the bio-catalysts are sterically stabilised by residual carbon traces on the surface of the particles. However, here an enlargement of the particle size is observed. Further analysis is required to precisely measure the change in particle size at each step of the fabrication process.

7.4 GDE Testing

A commercial catalyst GDE was tested in a single cell test rig and generated I/V curves as shown in Figure 47. The single cell test showed that the screen printed commercial catalyst GDE produced an open circuit voltage (OCV) of 0.6 V (Figure 47) compared to the 0.9 V (Figure 48) produced by the commercially produced GDE. The MEA suffered significant activation losses only achieving 0.02 W.cm^{-2} at a current density of 0.08 A.cm^{-2} compared to the 0.6 W.cm^{-2} at 1.4 A.cm^{-2} produced by the commercial GDE. This shows that the screen printed GDE did not function electrochemically to produce a significant current density.

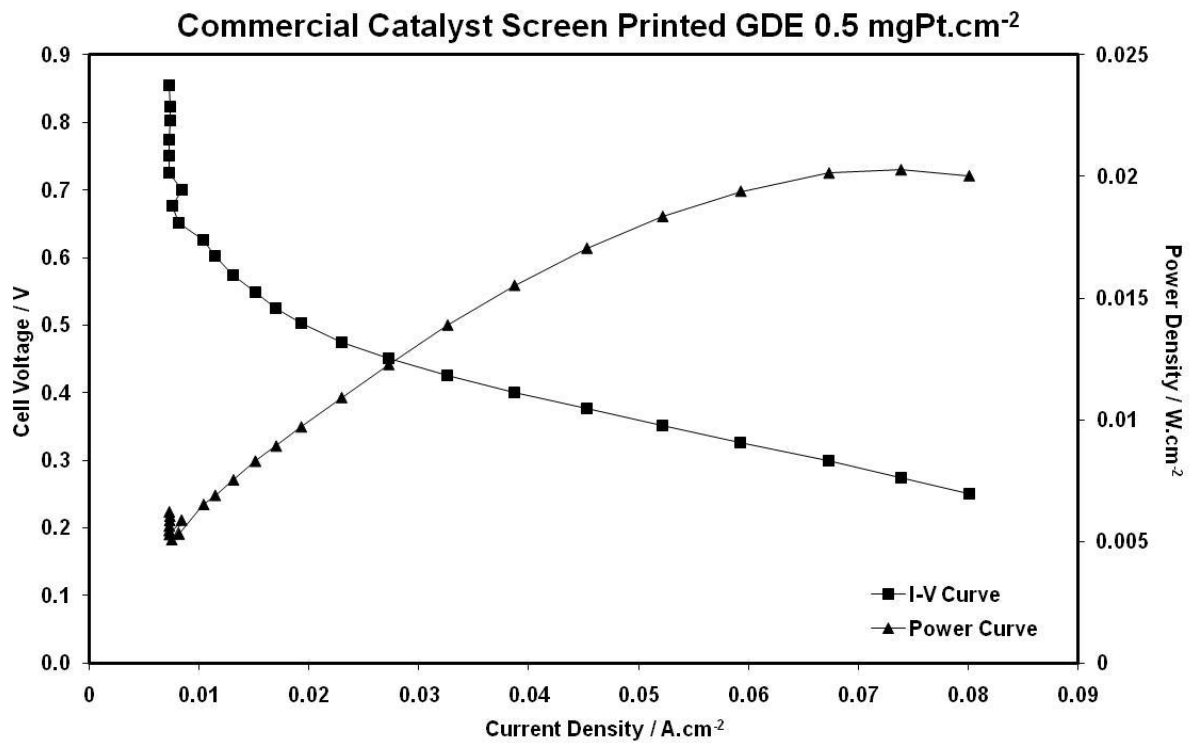


Figure 47 - I/V curve and Power curve for screen printed commercial catalyst GDE

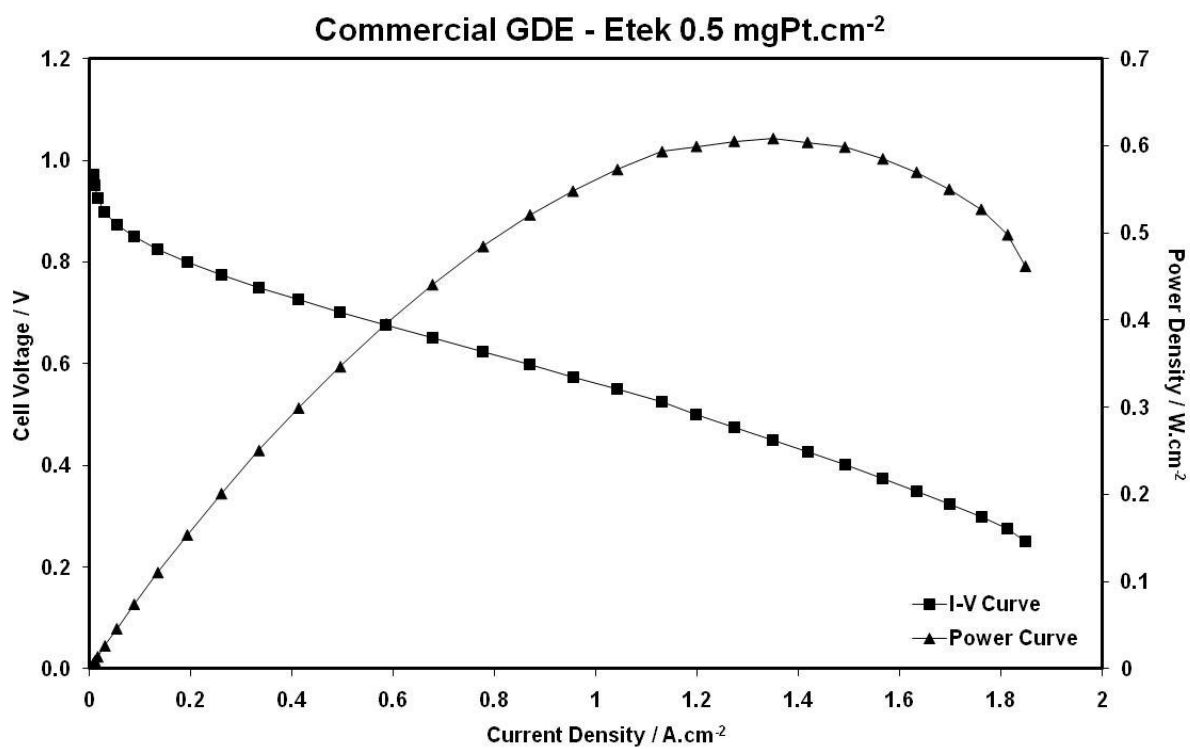


Figure 48 - I/V curve and power curve for commercially obtained GDE.

There are several reasons that could be attributed to the failure of the GDE produced and the repetition shown in Figure 49 confirms that the screen printed GDEs do not function as working fuel cell electrodes.

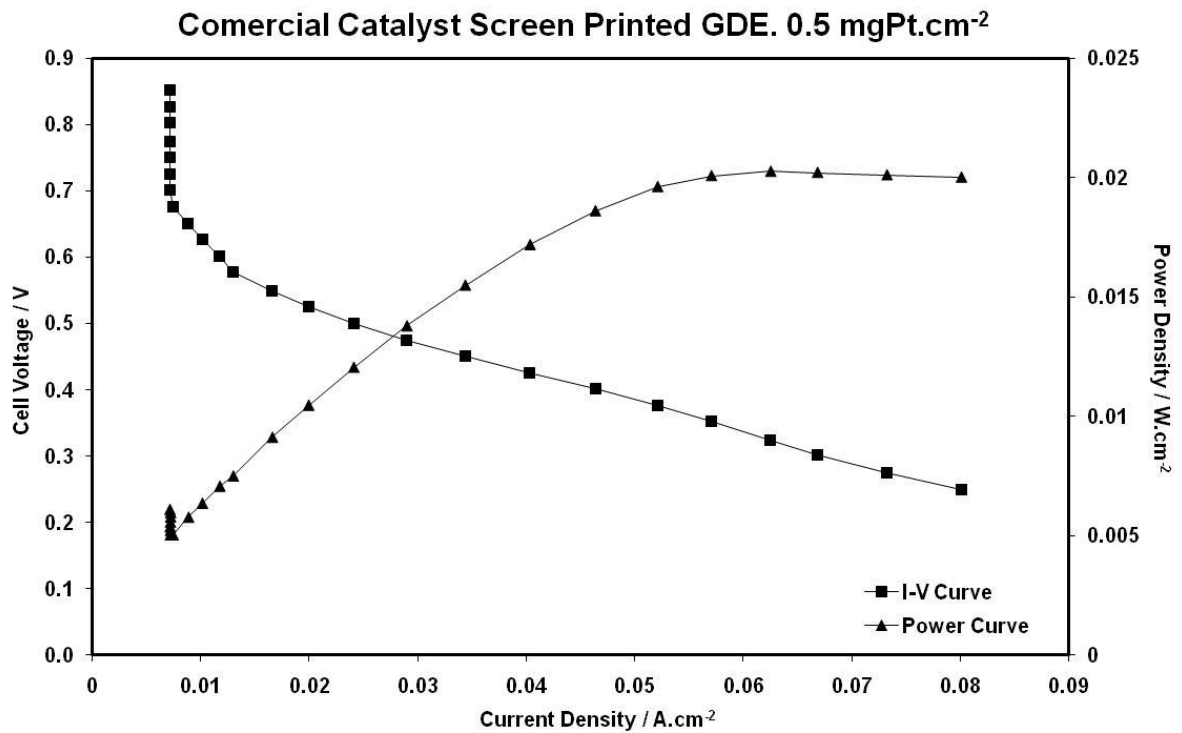


Figure 49 - I/V curve and power curve for screen printed commercial catalyst GDE repeat 2.

Firstly, the GDL chosen (Toray H-060) has a low Teflon content which may lead to poor water management in the PEM Fuel Cell supplied with high humidity gas such as with the single cell test stand. Secondly, the drying temperature of 120⁰C may be too close to the glass transition temperature (T_g) of Nafion and may deform the ionomer matrix within the catalyst layer inhibiting proton conduction throughout the layer. The third is the possibility of not fully removing trapped glycerol within the pores of the catalyst layer.

Chapter 8 – Conclusions and Further Work

It has been shown that the spin coated biofilms produced by the method of Tsoligkas *et al.* can be reproduced. A method for the metallisation of the biofilms was developed and demonstrated. It was shown that an even dispersion of Pt or Pd nanoparticles can be produced within the biofilms at varying concentrations of Pt and Pd. It was also shown that the biofilms retain the characteristic interconnected flow channels throughout the process. However, work is still required to understand factors such as time on the biomineralisation process. As such, the effect that time of biomineralisation has on particle size is suggested for further study.

It has been shown that the films are non-conductive and without alterations are not suitable for direct PEM Fuel Cell use. It was demonstrated that the biofilm can accept additives and that the mineralisation of the films is unaffected by the addition of carbon particles within the film. It was shown that the addition of carbon particles had no effect on the conductivity of the films. However, there are many potential additives. As such, it is suggested that further additives such as conducting polymers are investigated to increase the conductivity of biofilms.

It was also observed that both the planktonic cell and biofilm supported Bio-Pd are suitable to catalyse the hydrogenation of Dimethyl Itaconate. The particles retain their catalytic activity within the films, however, there are significant mass transport issues resulting in diffusion limited reaction kinetics. Despite this, the durability and the advantages posed by biofilm catalysts mean that further investigation into reactors and other possible catalysed reactions is suggested.

The screen printing technique for GDE fabrication was investigated and it was shown that the recapture of bio-catalysts and processing of the catalyst into GDE is comparable with using commercial catalysts. However, it was also observed that the screen printing protocol currently used

does not produce active PEM Fuel Cell electrodes and that the technique needs further work. Therefore, it is suggested that the protocol is investigated for improvement varying such parameters such as the solvent used for ink formulation, drying temperature and type of substrate. It is also suggested that the effect of 'burning' on the particle size of planktonic cell produced biocatalysts is studied.

References

1. Bockris, J. O. Hydrogen Economy. *Environment* **1971**, *13* (10), 51-&.
2. The history of hydrogen. www.HydrogenAssociation.org . 7-5-2010.
3. Jones, L. W. *Toward a liquid Hydrogen Fuel Economy*. University of Michigan Environmental Action for Survival Teach. University of Michigan. Mar 13, 70.
4. Biondi, L. Question of Hydrogen As Energy Carrier. *Energia Nucleare* **1975**, *22* (4), 185-190.
5. Hagenmuller, P. Hydrogen As An Energy Carrier. *Abstracts of Papers of the American Chemical Society* **1976**, 11.
6. Keller, C. Hydrogen - Potential-Energy Carrier of Future. *Chemiker-Zeitung* **1977**, *101* (5), 223-240.
7. Zegers, P. Fuel cell commercialization: The key to a hydrogen economy. *Journal of Power Sources* **2006**, *154* (2), 497-502.
8. Canadian Hydrogen and Fuel Cell Association . About Fuel cells. www.h2fcc.ca . 2010. 11-9-2010.
9. Department of Energy and Climate Change . Energy Flow Chart 2008. 2009. 11-9-2010.
10. Moore, K. First Cell. professional Engineering , 50. 2010.
11. History of Hydrogen. www.getenergysmart.org Hydrogen Fact Sheet. 2010. 11-9-0210.
12. Moore, B. John Deere Green II. www.evworld.com . 2010. 11-9-2010.
13. Bar-On, I.; Kirchain, R.; Roth, R. Technical cost analysis for PEM fuel cells. *Journal of Power Sources* **2002**, *109* (1), 71-75.
14. Vision revealed for German, European hydrogen infrastructures. *Fuel Cells Bulletin* **2005**, *2005* (4), 7-8.
15. Grant, I. Business rates stifle investment on broadband infrastructure. www.computerweekly.com. 2009. 11-9-2010.
16. Steinburger-Wilkins, R. T. S. C. European Hydrogen Infrastructure and Production. www.roads2hy.com . 2010. 11-9-2010.
17. Landucci, G.; Tugnoli, A.; Cozzani, V. Safety assessment of envisaged systems for automotive hydrogen supply and utilization. *International Journal of Hydrogen Energy* **2010**, *35* (3), 1493-1505.
18. Schjølberg, I.; +stdahl, A. B. Security and tolerable risk for hydrogen service stations. *Technology in Society* **2008**, *30* (1), 64-70.

19. Karlström, M. Local environmental benefits of fuel cell buses--a case study. *Journal of Cleaner Production* **2005**, *13* (7), 679-685.
20. El-Sharkh, M. Y.; Tanrioven, M.; Rahman, A.; Alam, M. S. Cost related sensitivity analysis for optimal operation of a grid-parallel PEM fuel cell power plant. *Journal of Power Sources* **2006**, *161* (2), 1198-1207.
21. Teagan, W. P.; Bentley, J.; Barnett, B. Cost reductions of fuel cells for transport applications: fuel processing options. *Journal of Power Sources* **1998**, *71* (1-2), 80-85.
22. Offer, G. J.; Howey, D.; Contestabile, M.; Clague, R.; Brandon, N. P. Comparative analysis of battery electric, hydrogen fuel cell and hybrid vehicles in a future sustainable road transport system. *Energy Policy* **2010**, *38* (1), 24-29.
23. Lee, G. y.; Jung, M. k.; Ryoo, S. n.; Park, M. s.; Ha, S. c.; Kim, S. Development of cost innovative BPs for a PEMFC stack for a 1ákW-class residential power generator (RPG) system. *International Journal of Hydrogen Energy In Press, Corrected Proof*.
24. Garland, N. L. US DOE Fuel Cell Activities. www.electricdrive.org . 2008. 12-9-2010.
25. George, M. W. *Platinum Group Metal*. U.S. Geological Survey. Mineral Commodity Summaries. 2007.
26. Johnson matthey. Price charts. www.platinum.matthey.com/pgm-prices/price-charts 2010. 12-9-2010.
27. Platinum in South Africa. www.mining.com , 26-27. 2008.
28. Hydrometallurgy - definition. Encyclopedia Britannica . 2010.
29. Pyrometallurgy - definition. Encyclopedia Britannica . 2010.
30. Macaskie, L. E.; Mikheenko, I. P.; Yong, P.; Deplanche, K.; Murray, A. J.; Paterson-Beedle, M.; Coker, V. S.; Pearce, C. I.; Cutting, R.; Patrick, R. A. D.; Vaughan, D.; van der Laan, G.; Lloyd, J. R. Today's wastes, tomorrow's materials for environmental protection. *Hydrometallurgy In Press, Corrected Proof*.
31. Yong, P.; Paterson-Beedle, M.; Mikheenko, I. P.; Macaskie, L. E. From bio-mineralisation to fuel cells: biomanufacture of Pt and Pd nanocrystals for fuel cell electrode catalyst. *Biotechnology Letters* **2007**, *29* (4), 539-544.
32. Tsofigkas.A.N, E. Al. A New Approach to Generating Biocatalytic Biofilms: Mapping To Topographty and biocatalytic Capabilities of This Man-made Landscape. *Angewandte Chemie* **2010**.
33. Gillet, A. C. From water to water. Hydrogen as a renewable energy vector for the future. World Renewable Energy Congress '99 Malaysia. 1999. pp 513-517.
34. Kazim, A. Exergy analysis of a PEM fuel cell at variable operating conditions. *Energy Conversion and Management* **2004**, *45* (11-12), 1949-1961.

35. Barbir, F.; Gómez, T. Efficiency and economics of proton exchange membrane (PEM) fuel cells. *International Journal of Hydrogen Energy* **1996**, *21* (10), 891-901.
36. Semelsberger, T. A.; Borup, R. L. Fuel effects on start-up energy and efficiency for automotive PEM fuel cell systems. *International Journal of Hydrogen Energy* **2005**, *30* (4), 425-435.
37. Imai, H. In situ Real-time structural characterisation of Platinum-based Electrocatalysts: Hard X-ray diffraction and time-resolved X-ray absorption spectroscopy. The 1st International Fuel Cell Summer Seminar Yamanashi 2010. 2010; pp 146-160.
38. Bezerra, C. W. B.; Zhang, L.; Lee, K.; Liu, H.; Zhang, J.; Shi, Z.; Marques, A. L. B.; Marques, E. P.; Wu, S.; Zhang, J. Novel carbon-supported Fe-N electrocatalysts synthesized through heat treatment of iron tripyridyl triazine complexes for the PEM fuel cell oxygen reduction reaction. *Electrochimica Acta* **2008**, *53* (26), 7703-7710.
39. Lv, H.; Mu, S.; Cheng, N.; Pan, M. Nano-silicon carbide supported catalysts for PEM fuel cells with high electrochemical stability and improved performance by addition of carbon. *Applied Catalysis B: Environmental In Press, Corrected Proof*.
40. Trongchuankij, W.; Poochinda, K.; Pruksathorn, K.; Hunsom, M. A study on novel combined processes for preparation of high performance Pt-Co/C electrocatalyst for oxygen reduction in PEM fuel cell. *Renewable Energy* **2010**, *35* (12), 2839-2843.
41. Kim, J. Y.; Oh, T. K.; Shin, Y.; Bonnett, J.; Weil, K. S. A novel non-platinum group electrocatalyst for PEM fuel cell application. *International Journal of Hydrogen Energy In Press, Corrected Proof*.
42. Crawley, G. Opening doors to fuel cell commercialisation. www.fuelcelltoday.com . 2006.
43. Banerjee, S.; Curtin, D. E. Nafion[®] perfluorinated membranes in fuel cells. *Journal of Fluorine Chemistry* **2004**, *125* (8), 1211-1216.
44. Mehta, V.; Cooper, J. S. Review and analysis of PEM fuel cell design and manufacturing. *Journal of Power Sources* **2003**, *114* (1), 32-53.
45. Ralph, T. R.; Hards, G. A.; Keating, J. E.; Campbell, S. A.; Wilkinson, D. P.; Davis, M.; St-Pierre, J.; Johnson, M. C. Low Cost Electrodes for Proton Exchange Membrane Fuel cells. *Electrochem Soc.* **1997**, *144* (11), 3845-3857.
46. Gasteiger, H. A.; Kocah, S. S.; Sompalli, B.; Wagner, F. T. Activity benchmarks and requirements for Pt, Pt-alloy and non-pt oxygen reduction catalysts for PEMFC's. *Applied Catalysis B: Environmental* **2005**, *56*, 9-35.
47. Chu, H. S.; Wang, C. P.; Liao, W. C.; Yan, W. M. Transient behavior of CO poisoning of the anode catalyst layer of a PEM fuel cell. *Journal of Power Sources* **2006**, *159* (2), 1071-1077.
48. Qi, Z.; Kaufman, A. CO-tolerance of low-loaded Pt/Ru anodes for PEM fuel cells. *Journal of Power Sources* **2003**, *113* (1), 115-123.

49. Davies, J. C.; Tsoitridis, G.; Varlam, M.; Valkiers, S.; Berglund, M.; Taylor, P. SSITKA investigation of CO and H₂ competitive adsorption at PEM fuel cell anode catalysts. *International Journal of Mass Spectrometry* **2010**, *291* (3), 152-158.
50. Grigoriev, S. A.; Lyutikova, E. K.; Martemianov, S.; Fateev, V. N. On the possibility of replacement of Pt by Pd in a hydrogen electrode of PEM fuel cells. *International Journal of Hydrogen Energy* **2007**, *32* (17), 4438-4442.
51. Alcaide, F.; Alvarez, G. e.; Cabot, P. L.; Miguel, O.; Querejeta, A. Performance of carbon-supported PtPd as catalyst for hydrogen oxidation in the anodes of proton exchange membrane fuel cells. *International Journal of Hydrogen Energy In Press, Corrected Proof*.
52. Moreira, J.; del Angel, P.; Ocampo, A. L.; Sebastián, P. J.; Montoya, J. A.; Castellanos, R. H. Synthesis, characterization and application of a Pd/Vulcan and Pd/C catalyst in a PEM fuel cell. *International Journal of Hydrogen Energy* **2004**, *29* (9), 915-920.
53. Cho, Y. H.; Choi, B.; Cho, Y. H.; Park, H. S.; Sung, Y. E. Pd-based PdPt(19:1)/C electrocatalyst as an electrode in PEM fuel cell. *Electrochemistry Communications* **2007**, *9* (3), 378-381.
54. Zhang, L.; Lee, K.; Zhang, J. Effect of synthetic reducing agents on morphology and ORR activity of carbon-supported nano-Pd-Co alloy electrocatalysts. *Electrochimica Acta* **2007**, *52* (28), 7964-7971.
55. Fouda-Onana, F.; Bah, S.; Savadogo, O. Palladium-copper alloys as catalysts for the oxygen reduction reaction in an acidic media I: Correlation between the ORR kinetic parameters and intrinsic physical properties of the alloys. *Journal of Electroanalytical Chemistry* **2009**, *636* (1-2), 1-9.
56. Thanasilp, S.; Hunsom, M. Effect of MEA fabrication techniques on the cell performance of Pt-Pd/C electrocatalyst for oxygen reduction in PEM fuel cell. *Fuel In Press, Corrected Proof*.
57. Tang, H.; Wang, S.; Jiang, S. P.; Pan, M. A comparative study of CCM and hot-pressed MEAs for PEM fuel cells. *Journal of Power Sources* **2007**, *170* (1), 140-144.
58. Taylor, A. D.; Kim, E. Y.; Humes, V. P.; Kizuka, J.; Thompson, L. T. Inkjet printing of carbon supported platinum 3-D catalyst layers for use in fuel cells. *Journal of Power Sources* **2007**, *171* (1), 101-106.
59. Towne, S.; Viswanathan, V.; Holbery, J.; Rieke, P. Fabrication of polymer electrolyte membrane fuel cell MEAs utilizing inkjet print technology. *Journal of Power Sources* **2007**, *171* (2), 575-584.
60. Cho, J. H.; Kim, J. M.; Prabhuram, J.; Hwang, S. Y.; Ahn, D. J.; Ha, H. Y.; Kim, S. K. Fabrication and evaluation of membrane electrode assemblies by low-temperature decal methods for direct methanol fuel cells. *Journal of Power Sources* **2009**, *187* (2), 378-386.

61. Saha, M. S.; Paul, D. K.; Peppley, B. A.; Karan, K. Fabrication of catalyst-coated membrane by modified decal transfer technique. *Electrochemistry Communications* **2010**, *12* (3), 410-413.
62. Park, I. S.; Li, W.; Manthiram, A. Fabrication of catalyst-coated membrane-electrode assemblies by doctor blade method and their performance in fuel cells. *Journal of Power Sources* **2010**, *195* (20), 7078-7082.
63. Billy, E.; Maillard, F.; Morin, A.; Guetaz, L.; Emieux, F.; Thurier, C.; Doppelt, P.; Donet, S.; Mailley, S. Impact of ultra-low Pt loadings on the performance of anode/cathode in a proton-exchange membrane fuel cell. *Journal of Power Sources* **2010**, *195* (9), 2737-2746.
64. Boyer, C.; Gamburgzev, S.; Velez, O.; Srinivasan, S.; Appleby, A. J. Measurements of proton conductivity in the active layer of PEM fuel cell gas diffusion electrodes. *Electrochimica Acta* **1998**, *43* (24), 3703-3709.
65. Taylor, A. D.; Sekol, R. C.; Kizuka, J. M.; D'Cunha, S.; Comisar, C. M. Fuel cell performance and characterization of 1-D carbon-supported platinum nanocomposites synthesized in supercritical fluids. *Journal of Catalysis* **2008**, *259* (1), 5-16.
66. Ihm, J. W.; Ryu, H.; Bae, J. S.; Choo, W. K.; Choi, D. K. High performance of electrode with low Pt loading prepared by simplified direct screen printing process in PEM fuel cells. *Journal of Materials Science* **2004**, *39* (14), 4647-4649.
67. Brown, D. screen printing in the dawn of fuel cells. www.smtmag.com . 2006. 12-3-2010.
68. Henry, T. C. B. P. D. P. R. Development of low cost MEA Manufacturing Process. www.confex.com , 1-4. 2010. 12-9-2010.
69. Bender, G.; Zawodzinski, T. A.; Saab, A. P. Fabrication of high precision PEFC membrane electrode assemblies. *Journal of Power Sources* **2003**, *124* (1), 114-117.
70. Tashima, D.; Sakaguchi, Y.; Hidaka, H.; Otsubo, M. Estimating the optimal number of membrane electrode assembly catalyst layers for proton exchange membrane fuel cell by considering open circuit voltage and polarization. *Materials Chemistry and Physics* **2010**, *122* (2-3), 544-547.
71. Wan, C. H.; Zhuang, Q. H. Novel layer wise anode structure with improved CO-tolerance capability for PEM fuel cell. *Electrochimica Acta* **2007**, *52* (12), 4111-4123.
72. Choi, H. J.; Kim, J.; Kwon, Y.; Han, J. Comparative study of three different catalyst coating methods for direct methanol fuel cells. *Journal of Power Sources* **2010**, *195* (1), 160-164.
73. Rajalakshmi, N.; Dhathathreyan, K. S. Catalyst layer in PEMFC electrodes--Fabrication, characterisation and analysis. *Chemical Engineering Journal* **2007**, *129* (1-3), 31-40.
74. Xiao, Z.; Laplante, A. R. Characterizing and recovering the platinum group minerals--a review. *Minerals Engineering* **2009**, *17* (9-10), 961-979.

75. Loferski, P. J. Platinum-Group Metals. U.S.geological Survey. Mineral Commodity Summaries. 2010.
76. Murata, K. J. Spectrochemical Analysis for trace elements in geological Materials. www.astm.org , 67-78. 1958.
77. Koeberl, C. Identification of meteoritic componenets in impactites. Geological Society. London. Special Publications 1998. [140], 133-153.
78. Environmental industrial catalysis: an emerging subdiscipline. *Catalysis Today* **1993**, 17 (1-2), 3-4.
79. Bierley, J. A. G. D. L. Biooxidation process for recovery of metal values from sulfur-conating ore materials. www.freepatentsonline.com/6383458. pat no. 6383458, 2002.
80. Benson, M.; Bennett, C. R.; Harry, J. E.; Patel, M. K.; Cross, M. The recovery mechanism of platinum group metals from catalytic converters in spent automotive exhaust systems. *Resources, Conservation and Recycling* **2000**, 31 (1), 1-7.
81. Saville, J. Process for the extraction of platinum group metals. Texasgulf Mineral and metals inc. pat no. 3304169/1841207. 1987.
82. Han, K. N.; Kim, P. N. Recovery of platinum group metals. South Dakota School of Mines and technology. pat no. 7067090. 2006.
83. Zanjani, A.; Baghalha, M. Factors affecting platinum extraction from used reforming catalysts in iodine solutions at temperatures up to 95°C. *Hydrometallurgy* **2009**, 97 (1-2), 119-125.
84. Shams, K.; Beiggy, M. R.; Gholamipour Shirazi, A. Platinum recovery from a spent industrial dehydrogenation catalyst using cyanide leaching followed by ion exchange. *Applied Catalysis A: General* **2004**, 258 (2), 227-234.
85. Shams, K.; Goodarzi, F. Improved and selective platinum recovery from spent [alpha]-alumina supported catalysts using pretreated anionic ion exchange resin. *Journal of Hazardous Materials* **2006**, 131 (1-3), 229-237.
86. Barakat, M. A.; Mahmoud, M. H. H. Recovery of platinum from spent catalyst. *Hydrometallurgy* **2004**, 72 (3-4), 179-184.
87. Hudson, M. J. An introduction to some aspects of solvent extraction chemistry in hydrometallurgy. *Hydrometallurgy* **1982**, 9 (2), 149-168.
88. Hidalgo, M.; Masana, A.; Salvadè, V.; Freiser, H.; Al-Bazi, S. J.; Valiente, M. Accelerated mass transfer of palladium(II) through a selective solid-supported liquid membrane containing Cyanex 471. *Analytica Chimica Acta* **1991**, 251 (1-2), 233-239.
89. Lee, J. Y.; Raju, B.; Kumar, B. N.; Kumar, J. R.; Park, H. K.; Reddy, B. R. Solvent extraction separation and recovery of palladium and platinum from chloride leach liquors of spent automobile catalyst. *Separation and Purification Technology* **2010**, 73 (2), 213-218.

90. de Sβ Pinheiro, A. A.; de Lima, T. S.; Campos, P. C.; Afonso, J. I. C. Recovery of platinum from spent catalysts in a fluoride-containing medium. *Hydrometallurgy* **2004**, *74* (1-2), 77-84.
91. Recovery of Precious Metal Catalysts with Supercritical Water Oxidation. *Filtration & Separation* **2003**, *40* (5), 16-18.
92. Duyvesteyn, W. D. C. L. H. D. S. Dissolution of Platinum group metals from materials from containing said metals. pat no. 845068. 1994.
93. Baghalha, M.; Khosravian, G.; Mortaheb, H. R. Kinetics of platinum extraction from spent reforming catalysts in aqua-regia solutions. *Hydrometallurgy* **2009**, *95* (3-4), 247-253.
94. Brierley, J. A. A perspective on developments in biohydrometallurgy. *Hydrometallurgy* **2008**, *94* (1-4), 2-7.
95. Brierley, J. A.; Brierley, C. L. Present and future commercial applications of biohydrometallurgy. In *Process Metallurgy Biohydrometallurgy and the Environment Toward the Mining of the 21st Century, Proceedings of the International Biohydrometallurgy Symposium*, Volume 9, Part 1 ed.; and, R. A., Ed.; Elsevier: 1999; pp 81-89.
96. Poulin, R.; Lawrence, R. W. Economic and environmental niches of biohydrometallurgy. *Minerals Engineering* **1996**, *9* (8), 799-810.
97. Bosecker, K. Bioleaching: metal solubilization by microorganisms. *FEMS Microbiology Reviews* **1997**, *20* (3-4), 591-604.
98. Krebs, W.; Brombacher, C.; Bosshard, P. P.; Bachofen, R.; Brandl, H. Microbial recovery of metals from solids. *FEMS Microbiology Reviews* **1997**, *20* (3-4), 605-617.
99. Rossi, G. The design of bioreactors. *Hydrometallurgy* **2001**, *59* (2-3), 217-231.
100. Johnson, D. B. Biohydrometallurgy and the environment: Intimate and important interplay. *Hydrometallurgy* **2006**, *83* (1-4), 153-166.
101. Das, N. Recovery of precious metals through biosorption -- A review. *Hydrometallurgy* **2010**, *103* (1-4), 180-189.
102. Dobson, R. S.; Burgess, J. E. Biological treatment of precious metal refinery wastewater: A review. *Minerals Engineering* **2007**, *20* (6), 519-532.
103. De vargos, I.; Macaskie, L. E.; Guibal, E. Biosorption of palladium and platinum by sulfate-reducing bacteria. *Journal of chemical technology and biotechnology* **79**[1], 49-56. 2004.
104. Lloyd, J. R.; Yong, P.; Macaskie, L. E. Enzymatic Recovery of Elemental Palladium by using Sulfate-reducing bacteria. *Applied and Environmental Microbiology* **64**[11], 4607-4609. 1998.

105. Yong, P.; Rowson, N. A.; Farr, J. P. G.; Harris, L. R.; Macaskie, L. E. A novel electrobiotechnology for the recovery of precious metals from spent automotive catalysts. *Environmental Technology* **24**[3], 289-297. 2003.
106. Creamer, N. J.; Baxter-Plant, V. S.; Henderson, J.; Potter, M.; Macaskie, L. E. Palladium and gold removal and recovery from precious metal solutions and electronic scrap leachates. *Biotechnology Letters* **28**[18], 1475-1484. 2006.
107. Riddin, T. L.; Govender, Y.; Gericke, M.; Whiteley, C. G. Two different hydrogenase enzymes from sulphate-reducing bacteria are responsible for the bioreductive mechanism of platinum into nanoparticles. *Enzyme and Microbial Technology* **2009**, *45* (4), 267-273.
108. Mikheenko, I. P.; Bennett, J. A.; Shannon, I. J.; Wood, J.; Macaskie, L. E. *Biominedalised palladium is an effective hydrogenation catalyst*; TRANS TECH PUBLICATIONS LTD: STAFA-ZURICH, 2009.pp. 725-728.
109. Wood, J.; Bodenes, L.; Bennett, J.; Deplanche, K.; Macaskie, L. E. Hydrogenation of 2-Butyne-1,4-diol Using Novel Bio-Palladium Catalysts. *Industrial & Engineering Chemistry Research* **2010**, *49* (3), 980-988.
110. Bennett, J. A.; Creamer, N. J.; Deplanche, K.; Macaskie, L. E.; Shannon, I. J.; Wood, J. Palladium supported on bacterial biomass as a novel heterogeneous catalyst: A comparison of Pd/Al₂O₃ and bio-Pd in the hydrogenation of 2-pentyne. *Chemical Engineering Science* **2010**, *65* (1), 282-290.
111. Fischer, A.; Jindra, J.; Wendt, H. Porosity and catalyst utilization of thin layer cathodes in air operated PEM-fuel cells. *Journal of Applied Electrochemistry* **1998**, *28* (3), 277-282.
112. Monroe, D. Looking for Chinks in the Armor of Bacterial Biofilms. *PLoS Biol* **2007**, *5* (11), e307.
113. Vidal, O.; Longin, R.; Prigent-Combaret, C.; Dorel, C.; Hooreman, M.; Lejeune, P. Isolation of an Escherichia coli K-12 mutant strain able to form biofilms on inert surfaces: Involvement of a new ompR allele that increases curli expression. *Journal of Bacteriology* **1998**, *180* (9), 2442-2449.
114. Charlot, G. Dosages Absorptometrique des elements mineraux. Editions Masson. Paris. 1978.
115. Flemming, H. C.; Neu, T. R.; Wozniak, D. J. The EPS matrix: The "House of Biofilm cells". *Journal of Bacteriology* **2007**, *189* (22), 7945-7947.
116. An, D.; Parsek, M. R. The promise and peril of transcriptional profiling in biofilm communities. *Current Opinion in Microbiology* **2007**, *10* (3), 292-296.
117. Gruber, D.; Ponath, N.; Mlller, J.; Lindstaedt, F. Sputter-deposited ultra-low catalyst loadings for PEM fuel cells. *Journal of Power Sources* **2005**, *150*, 67-72.
118. Peng, L.; You, S. J.; Wang, J. Y. Carbon nanotubes as electrode modifier promoting direct electron transfer from Shewanella oneidensis. *Biosensors and Bioelectronics* **2010**, *25* (5), 1248-1251.

119. myoung-Ki, M.; Jihoon, C.; kyuwoong, C.; Hasuck, K. Particle size and the alloying effects of Pt-based alloy catalysts for fuel cell applications. *Electrochimica Acta* **2000**, *45*, 4211-4217.
120. Min, K. J.; Ki, R. L.; Hee, J. J.; Seong, I. W. Effect of heat treatment on PtRu/C catalyst for methanol electro-oxidation. *Journal of Applied Electrochemistry* **2009**, *39* (9), 1503-1508.
121. Wu, Y. N.; Liao, S. J.; Zeng, J. H. Investigating the addition of silicon oxide to carbon: Effects of amount and heat treatment on anti-aggregation and electrochemical performance of Pt catalysts. *Journal of Power Sources In Press, Corrected Proof*.
122. Toray Industries, I. Toray Carbon Fiber paper "TGP-H". www.fuelcell.com . 2010. 11-9-2010.
123. Freudenberg FCCT. Freudenburg Gas Diffusion Layers for PEMFC and DMFC. www.freudenbergfcct.com . 2010. 11-9-2009.
124. SGL Group The Carbon Company . Sigracet GDL 10 series Gas Diffusion Layer. www.fuelcellmarkets.com . 2010. 11-9-2010.

Chapter 10 - Appendix

10.1 - supplementary images to Chapter 1

10.1.1 - supplementary images to Chapter 1.4.1

Bio-Engineered Catalyst Layers for PEMFC – From Waste to Riches

J.M. Courtney^a, A.Tsoligkas^a, K. Deplanche^b, L.M. Macaskie^b & B.G. Pollet^a

^aPEM Research Group, Centre for Hydrogen and Fuel Cell research, School of Chemical Engineering,
^bFBU, School of Biosciences, The University of Birmingham, Edgbaston, B15 2TT, U.K.

*Jmc991@bham.ac.uk
www.polletresearch.com

The high cost, price fluctuation and finite nature of platinum reserves still proves a significant barrier to the successful commercialization of PEM fuel cells for worldwide energy production. Several methods have been demonstrated for the recovery of PGM's (Platinum Group Metals) from liquid waste streams for use in PEMFCs. Here we highlight a novel method by using Engineered Biofilms for direct recovery and production of GDEs (Gas Diffusion Electrodes) for PEMFCs.

PGM Recovery Via Bacteria

The recovery method used couples the oxidation of Hydrogen to the reduction of soluble metallic species (e.g. Pd(II), Pt(IV)) via hydrogenase enzymes as previously demonstrated by Yong et al. (2002, 2003). The process produces Metallic Nanoparticles 'scaffolded' to bacterial membranes.

Screen Printed Commercial Catalyst GDEs

To provide controls, the screen printing fabrication technique was developed. Using Commercial 20%wtPd/C and glycerol based inks GDEs were produced. The ESEM images show the catalyst layer on the GDL, the thickness of the catalyst layer, the surface and the distribution of nanoparticles across the surface.

Screen Printed Biocatalyst GDEs

After recovery, the biomass is incinerated from the sample leaving just the metallic nanoparticles. These are then processed to produce carbon supported catalysts (e.g. 20%wtPd/C as shown). The catalyst was then processed identically to the control to produce GDEs.

Biofilm Fabrication

Engineered Biofilms potentially provide a method to produce GDE from recovered Biocatalysts whilst avoiding the need for sintering, burning or acid treatment. It has been shown that both Pt and Pd metallic nanoparticles can still be produced when the bacteria have been manipulated into the biofilm. It has also been shown that the Engineered Biofilm possesses interconnected flow channel and pores similar to those in regular PEMFC catalyst layers. However the layers produced are non-conductive. Several methods were trialled such as the carbonation shown, however the films remain non-conductive. The technique still provides potential due to the long term durability of catalytic activity exhibited by the layers for other catalytic processes. The fabrication method still remains a strong candidate to successfully produce a 'one pot' production technique for recovered bio-catalyst GDEs for PEMFCs.

Future Work

The screen printed bio-catalyst GDEs need to be fully characterised: (Electrochemical and physical characterisation). New methods for increasing the conductivity of the Engineered Biofilms will be attempted and full characterisation inc. performance testing will be conducted.

Figure 50 - Poster presented at the 1st International Fuel Cell Seminar, Yamanashi, Japan, 2010. Courtney, J., Tsoligkas, A.N., Deplanche, K., Macaskie, L.E., 2010

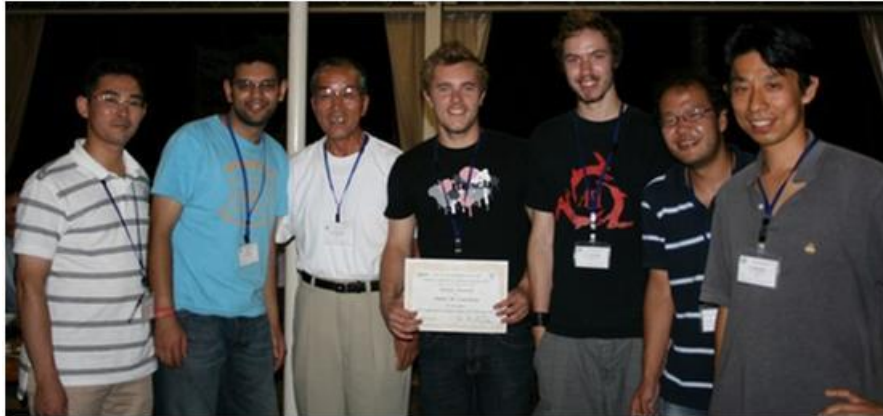


Figure 51 - James Courtney receiving poster presentation award at the 1st international Fuel Cell summer seminar, Japan, 2010

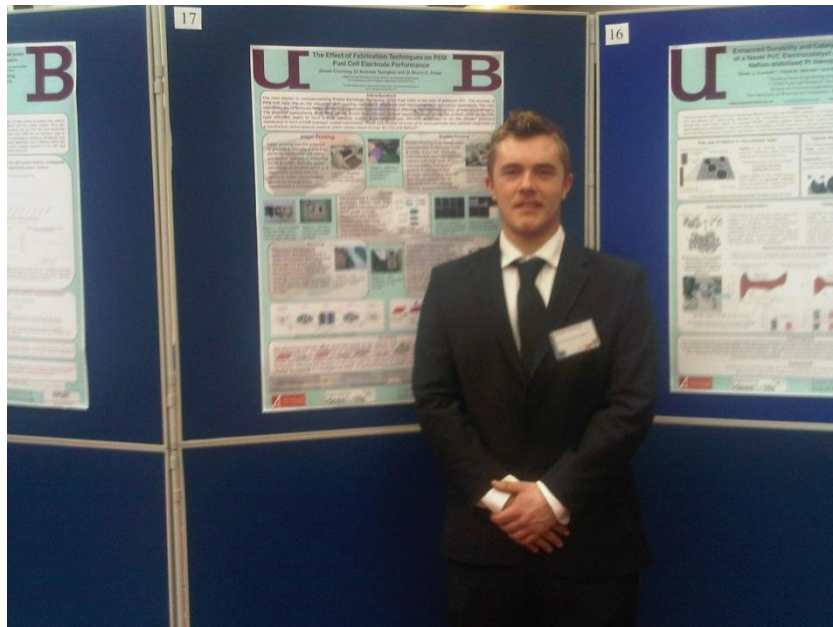


Figure 52 - Presented Poster at the 6th Annual International Conference and Exhibition, Hydrogen & Fuel Cell for Clean Cities



Figure 53 - Alan Johnson MP, Lab tour, 2009

10.2 Supplementary Images to Chapter 2

10.2.1 Supplementary images to section 2.2 Current PEM Fuel Cell Design

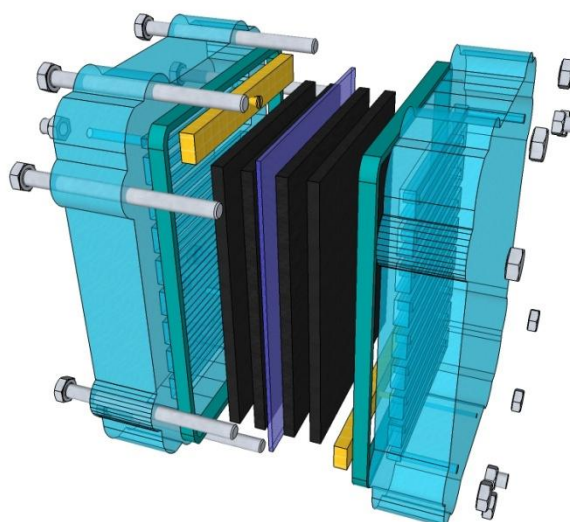


Figure 54 - Example PEMFC design. James Courtney©

10.2.2 – Supplementary images to section 2.4 GDE Fabrication Techniques

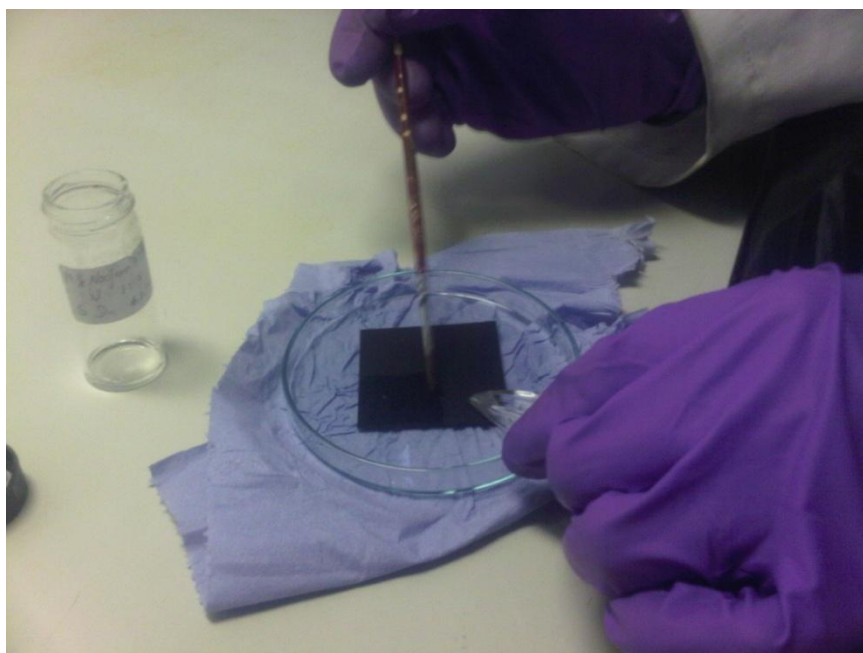


Figure 55 - Image of painting method for fabrication of GDEs.

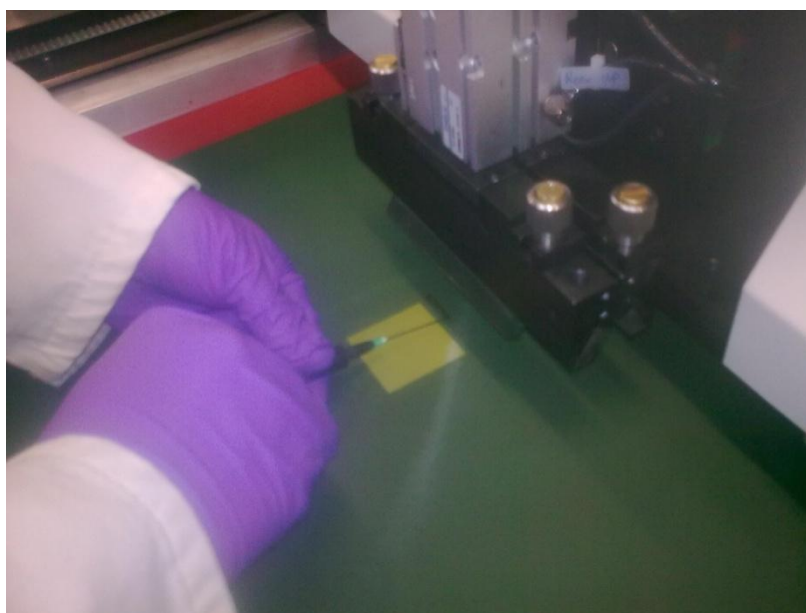


Figure 56 - Image of the introduction of ink to the screen printer for the fabrication of a GDE.

10.3 – Supplementary images and tables to chapter 3

10.3.1 Supplementary images and tables to section 3.6

Company	Number	Type	Microporous layer	Thickness (µm)	Area Weight g/cm ²	PTFE content/Hydrophobic treatment
Freudenburg	H2315c2	Carbon Cloth (unwoven)	yes	252	132	Hydrophobic treatment
Freudenburg	h2315I6	Carbon Cloth (unwoven)	no	210	115	hydrophobic treatment
SGL	10BC	Carbon Paper	Yes	415	135	5% PTFE
SGL	10AA	Carbon Paper	No	390	85	None
Toray	H-060	Carboin Paper	No	190		5% PTFE

Figure 57 - Table of GDL details.¹²²⁻¹²⁴



Figure 58 - Image of Dek 258 screen printer

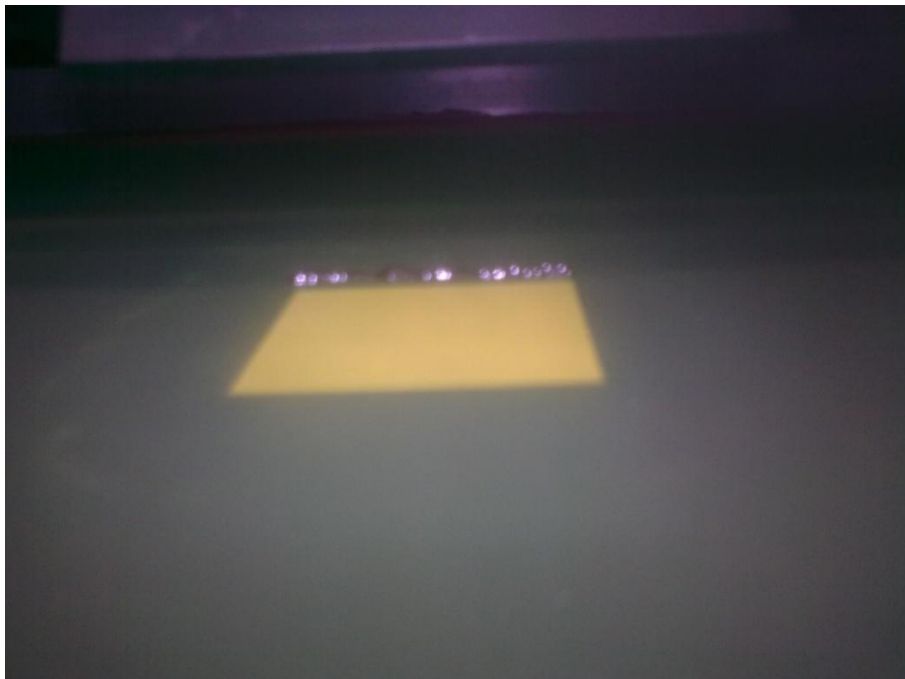


Figure 59 - Image of deposited ink within screen printer.

10.3.2 – Supplementary images to section 3.7.6.2



Figure 60 - Paxitech FCT - 50s Test station

10.4 Supplementary Images and Tables to Chapter 6

10.4.1 Supplementary Images and Tables to Section 6.1

Biofilm	weights (mg)		% weight change from initial		% weight change from last reaction		% weight change from initial		% weight change from last reaction		% weight change from initial		% weight change from last reaction		Average % weight change per reaction	
	rp1	rp2			rp3				rp4							
5%w/v	18.5	16.4	11.35135	11.35135	14.5	21.62162	11.58537	12.8	30.81081	11.72414	11.55362					
2.5w/v	37	26.3	28.91892	28.91892	23.2	37.2973	11.78707	9.1	75.40541	60.77586	33.82728					

Figure 61 - Table of planktonic cell catalyst mass loss during repeated reactions.